# The effects of molecular architecture and conformational asymmetry on block copolymer morphology.

# THE EFFECTS OF MOLECULAR ARCHITECTURE AND CONFORMATIONAL ASYMMETRY ON BLOCK COPOLYMER MORPHOLOGY

A Dissertation Presented

by

DARRIN J. POCHAN

Submitted to the Graduate School of the
University of Massachusetts Amherst in partial fulfillment
of the requirements for the degree of

DOCTOR OF PHILOSOPHY

September 1997

Polymer Science and Engineering

# THE EFFECTS OF MOLECULAR ARCHITECTURE AND CONFORMATIONAL ASYMMETRY ON BLOCK COPOLYMER MORPHOLOGY

A Dissertation Presented

by

DARRIN J. POCHAN

Approved as to style and content by:

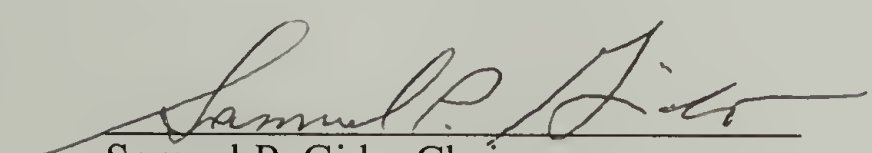

Samuel P. Gido, Chair

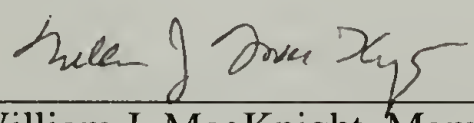

William J. MacKnight, Member

Murugappan Muthukumar, Member

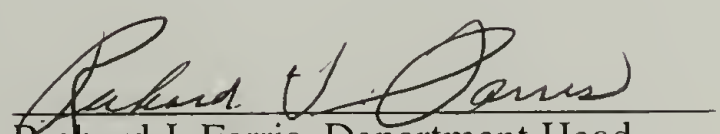

Richard J. Farris, Department Head
Polymer Science and Engineering

# ACKNOWLEDGMENTS

My personality dictates me to surround myself with many interpersonal relationships in order to constantly interact, learn, and, most importantly, enjoy both the grand and frivolous things in life. I have always been happier experiencing all of these things in the company of others and discussing issues and events with companions. During my higher education I consider myself most fortunate to have been given the opportunity to form relationships with a crew of intriguing and imaginative people.

The core of any success that I may encounter is built upon the endless support, love, and fun that I reap from my family. They are people who bring happiness to many people's lives, especially mine, each in their own way.

In undergraduate school I encountered first-hand what it means to be a dedicated and careful scientist through my adivisor Prof. Hyuk Yu. The only motive of his aggressive and passionate style in the classroom and laboratory was his students' success. I think even the most successful scientists could learn a thing or two about successful scientific research, and themselves, from Prof. Yu's research skills and overall philosophies.

In graduate school I've seen the energy, dedication, and unbelievable hard work it requires to become a successful assistant professor through my advisor Sam Gido. I have learned a great deal from Sam's example and only hope to be as successful in my career. I've also benefitted from the wisdom and seemingly boundless knowledge of my committee members Prof. MacKnight and Muthu. Their advice has been crucial and their foresight 20/20 over the past year when mulling over career possibilities and options.

My friends and labmates have helped make the most frustrating times enlightenting, the most successful times celebratory, and the most happy times the greatest possible. My undergraduate friends Larry and Aaron are the direct cause of the crinkles around my eyes from smiling and laughing much more than is good for the skin. The friendships I have developed in graduate school have made me much smarter, much

wiser, and a much richer person. My sweet girlfriend Beth has made me about as happy as a person can be before actually exploding. My roomate Bert and his exemplary (and mostly faux) cynicism, Mike and his runway style, Shalabh and his endless energy and enthusiasm, Wendy and her endless generosity and sincerity, as well as Rick, Chin, Meredith, Darius and others have provided daily excitement and enrichment as well as important lessons for me which one can't encounter in any textbook or classroom.

I'm immensely proud to call all of these people my friends and companions. My relationships with all of these people defines for me what it truly means to have a fortunate and successful life.

ABSTRACT

THE EFFECTS OF MOLECULAR ARCHITECTURE
AND CONFORMATIONAL ASYMMETRY ON
BLOCK COPOLYMER MORPHOLOGY

SEPTEMBER 1997

DARRIN J. POCHAN

B.S., UNIVERSITY OF WISCONSIN MADISON
M.S., UNIVERSITY OF MASSACHUSETTS AMHERST
PH.D., UNIVERSITY OF MASSACHUSETTS AMHERST
DIRECTED BY: PROFESSOR SAMUEL P. GIDO

The effects of molecular architecture and block conformational asymmetry on the equilibrium bulk morphological behavior of strongly phase-separated, amorphous block copolymers have been studied. Transmission electron microscopy techniques and small angle x-ray scattering, as well as small angle neutron scattering, were primarily utilized to characterize the block copolymer morphologies. Both architecture and block conformational characteristics are found to be molecular parameters, in addition to the relative volume fractions of the constituent blocks, with which one can controllably manipulate the bulk morphological behavior.

The effects of novel molecular architecture were discerned via a systematic morphological study of a series of simple graft $A_2B$, or "Y", block copolymers where A=polyisoprene (PI) and B=polystyrene (PS). In the microphase separated state a 2:1 A to B arm number asymmetry is introduced across the AB interface due to the simple graft architecture. This arm number asymmetry causes significant deviations in the volume fraction dependence of the morphologies formed by the $A_2B$ series as compared to the

volume fraction dependence of linear diblock morphology. In addition, at a unique volume fraction in the $A_2B$ series where the two PI arms per molecule are first forced to the concave side of the interface, a new morphology in neat block copolymers is observed which has not been predicted by theory.

The bulk morphological behavior of a series of poly(isoprene-*block* -tert-butylmethacrylate) linear block copolymers was characterized. The larger unperturbed dimension of PtBMA, due to its larger statistical segment length relative to PI, provides for a lower PtBMA entropic chain stretching penalty in the microphase separated state. This also causes the relative volume fraction windows in which morphologies are observed to shift to higher relative volume fractions of the more easily stretched PtBMA block than found in conformationally symmetric AB linear diblocks.

In addition, initial morphology studies on more complicated graft architectures and linear diblocks with tunable conformational asymmetry are presented.

TABLE OF CONTENTS

# LIST OF TABLES

LIST OF FIGURES

# CHAPTER 1

# REVIEW OF MORPHOLOGICAL STUDIES ON UNIQUE BLOCK COPOLYMERS FOCUSING ON ARCHITECTURAL EFFECTS AND GRAFT COPOLYMERS

## 1.1 Historical Background

Block copolymers have been subject to an amazing amount of research in the fields of polymer chemistry, physics, and engineering for over the past 30 years. The covalent coupling of chemically different chains into a single molecule leads to an inherent amphiphilic character in block copolymers which, in turn, provides for unique behavior in thin films, the bulk, and as modifiers in multicomponent solutions, blends, and composites. Due to significant synthetic advances scientists and engineers are now able to study a vast and quickly growing number of types of block copolymers. While the array of possible chemical constituents which can be incorporated as blocks is seemingly becoming limitless, the ability to precisely control the connectivity of constituent blocks, and the ultimate architecture of the block molecule, has only recently been developed. The purpose of this chapter is to consolidate the experimental and, to a lesser extent, the theoretical developments in the area of block copolymers with unique architectures and, in particular, graft copolymers. The first half of the chapter provides a historical perspective on block copolymer research in general and its progression from simple, model systems to more chemically diverse and architecturally complicated molecules. The second half emphasizes very recent developments in the synthesis and experimental morphological characterization of block copolymers with unique graft molecular architectures.

While the primary focus of this thesis is the bulk phase behavior of block copolymers with unique architectures, the underlying thermodynamic principles defining the bulk phase behavior are the same as found in model AB linear diblocks. The phase behavior is determined by the magnitude of the segment-segment interaction parameter, $\chi$, the total number of statistical segments, N, and the relative volume fractions of the

constituent blocks. The combined parameter $\chi N$ defines the strength of segregation in a block copolymer melt. Since $\chi$ is inversely proportional to temperature, at high temperatures and low molecular weights the diblock comprises a homogeneous melt. However, by raising $\chi N$ (lowering the temperature, increasing molecular weight, or removal of a nonselective solvent) a linear AB diblock melt, which is considered a one component system from a colligative point of view, exhibits UCST-type phase behavior similar to polymer solutions and blends. In stark contrast to two component polymer solutions and blends, when a block copolymer phase separates from the homogeneous melt the separation of component A from B is limited to the dimensions of the respective A and B block chains due to the covalent junction point between them. Hence, upon undergoing what is termed microphase separation from each other the blocks form a wide array of lattice symmetries and domain shapes depending on the relative volume fractions of the respective blocks and the magnitude of $\chi N$. At high degrees of phase segregation, or large $\chi N$, one finds what are termed the traditional block copolymer phases: cubic arrays of spheres, hexagonally packed cylinders, and alternating lamellar systems depending on the relative volume fractions of the respective blocks in the molecules.[1]

A vast majority of the experimental and theoretical literature concerning block copolymers involves research performed on bulk block copolymer systems and their microphase separation behavior. In order to elucidate the fundamental characteristics of the microphase separation transition and basic block copolymer morphological behavior, model systems have primarily been studied. These model systems consist of linear AB diblocks and, to a lesser extent, ABA triblocks of two amorphous, conformationally similar blocks lacking any specific enthalpic interactions between them such as hydrogen bonding or dipole-dipole interactions. The reader is directed to earlier reviews which deal predominantly with the morphological behavior of these types of model systems.[2-5] The solid foundation of research on model systems as well as refinement of anionic and development of new block synthetic techniques have allowed researchers to focus on

linear block copolymer systems with more inherent complexity. These more complex, linear block copolymer systems include, but are not limited to,[6] linear amorphous ABC triblocks,[7-11] AB amorphous diblocks in which there is a degree of conformational dissimilarity between blocks (chapter 5 specifically addresses system of linear diblocks containing conformational asymmetry),[12-14] AB diblocks in which one block is crystallizable,[15-18] and AB rod-coil diblocks.[19,20]

## 1.2 Early Complex Architecture Syntheses via Coupling Chemistry

Regardless of the actual chemical monomers used in the above more complex block copolymer studies, the blocks are all covalently linked in series creating linear polymer chains. An intuitive step to take in block copolymer research is to utilize the chemical constituents of the model linear diblock copolymer research (amorphous, conformationally symmetric blocks) and focus on the effects of the actual molecular architecture on the phase behavior. The study of new architectures in block copolymer morphology research had to wait for the development of the synthetic capability to produce well defined molecules with novel connectivity between blocks. The earliest manifestations of the concept to study architectural effects was to utilize chlorosilane and divinyl benzene (DVB) coupling chemistry to make $(AB)_n$ starblocks in which every arm is an identical diblock copolymer. In the microphase separated state the $(AB)_n$ star architecture was found to behave almost identically as linear diblocks with the same relative volume fractions of A and B.[6,21] Only at large arm molecular weights and high number of arms did the architecture slightly shift the relative volume fraction dependence of the observed morphologies from that found in linear diblocks. More recently, similar coupling chemistry has been used in other systems to study cyclic block copolymers[22] and $A_8B_8$ "Vergina" star block copolymers where an equal number of A and B arms are connected to a common junction point.[23,24] These two types of architectures qualitatively displayed the same morphological behavior as found in linear blocks with the same

relative volume fractions of block species although the domain spacings had different scaling behavior than found in diblocks. While the $(AB)_n$, cyclic blocks, and $A_8B_8$ Vergina stars all consist of novel molecular architectures, there is no inherent asymmetry in the architectures to produce new phase behavior in the microphase separated state. In other words, after microphase separating there are an equal number of A and B arms per molecule across the AB interface, an analogous situation to what is found in linear diblocks.

An intriguing possibility afforded by the well-controlled chlorosilane coupling method utilized in the $(AB)_n$ star synthesis is the possibility of introducing architectural asymmetry into block copolymer molecules and directly observing its effect on morphology. One is not limited to a symmetric number of A and B arms. Nor is one limited to just two types of block arms per molecule. A whole new realm of morphological possibilities is opened with the silane coupling chemistry through which model $A_nB_m$ graft copolymers and ABC terpolymers, which have been termed miktoarm star copolymers from the greek word μικτοσ meaning "mixed", and "comb" copolymers with multiple grafts can be synthesized and studied. The remainder of the chapter is concerned with the experimental work, morphology characterization in particular, which has been carried out very recently on such unique graft copolymer systems as well as touching on some important theoretical studies concerning the phase behavior of such systems.

## 1.3 Graft Copolymers: Practical Uses and Predicted Phase Behavior

One of the motivations behind morphological work on model graft copolymers is their promise in helping to model and rationalize the pronounced modification ability that more complicated, multigraft copolymers have in polymer blends. These AB multigraft, or comb, polymers usually have an A backbone from which an ill-defined number of B teeth are connected at random positions. Due to their inherent amphiphilic character they

have important industrial uses as modifiers in multicomponent polymer systems such as composites, solutions, and, in particular, to compatibilize blends.[25-27] Linear block copolymers have also been found to greatly affect the miscibility and morphologies of blends although only within very restrictive limits in terms of their relative size and chemical composition.[28,29] These shortcomings are in addition to the high cost of synthesizing well-defined, linear block copolymers which greatly limits any industrial applications. Multigraft copolymers with varying numbers, sizes, and placements of B grafts onto an A backbone have been found to modify the miscibility of blends as well as, or better than, linear block copolymers in addition to being relatively simple to produce.[28,30,31] Other recent uses of easily produced, ill-defined amphiphilic grafts include increased impact resistance in glassy polymer matrices,[32] permselective microphase separated membranes,[33] and as oil/water system emulsifiers.[34] In order to begin to understand the phase behavior of these complicated and ill-defined multiple graft, or comb, copolymers several theoretical studies have focused on model systems in the melt and the criterion required for instability of the homogeneous phase preceding the microphase separated state. In particular, Olvera de la Cruz and Sanchez[35] extended the mean-field theory of Leibler[36] to study the phase stability criteria and static structure factors for homogeneous melts of increasing complexity in molecular architecture, from linear diblocks to $A_2B$ simple grafts (two identical arms of A and a single B arm all emanating from a common junction point) to $A_nB_n$ and $(AB)_n$ starblocks. It was found that slightly higher values of $\chi N$ (slightly lower temperatures) are required for phase separation of the more complex graft molecules. Benoit and Hadziioannou[37] calculated phase stability for three types of multiblock copolymers; linear $-(A-B)_n-$ multiblock block copolymers, AB comb copolymers with evenly spaced, identical B teeth emanating from an A backbone, and $(AB)_n$ starblock copolymers; and found that above a relatively low N the microphase separation temperature of a melt no longer changes as N increases. Shinozaki, *et al.*[38] extended the architectural complexity even further with calculations

concerning AB comb polymers at the AB interface of immiscible A and B homopolymers with a number of B grafts placed at specific integrals along the A backbone, as well as placed randomly, in an attempt to model more realistic systems used in blend modification. This later study has recently been extended to systems which varied the number of teeth and, therefore, the molecular weight of the comb molecules.[39] It was found that symmetric combs with equal volume fractions of A and B caused the greatest reduction in the interfacial tension between A and B. With the successful synthesis of simple graft and miktoarm terpolymers the mean field predictions of Olvera de la Cruz and Sanchez were recently borne out in the high temperature, homogeneous state via small angle x-ray scattering experiments although deviations were found in the regions close to, but above, the microphase separation temperature due to fluctuations.[40] However, experiments addressing more complex architectures such as comb copolymers have had to wait until recently for the controlled syntheses of model systems and are currently being investigated.[41,42]

## 1.4 Recent Complex Architecture Syntheses

Laboratory efforts to synthetically introduce controllable and precise architectural asymmetry into block copolymers have utilized various linking agents[6] such as 1,1-diphenylethylenes[43] and the DVB linking method[44] in order to produce AnBn stars where A and B are of differing molecular weights, cationic polymerization,[45] and end-functionalized polymers such as naphthalene-terminated polymers to produce $A_2B$, or simple graft, molecules.[46] However, these techniques generally lead to relatively high polydispersities and imperfections in arm numbers which make precise experimental morphology and phase transition studies difficult. Conversely, as in the synthesis of $(AB)_n$ starblocks, chlorosilane coupling chemistry has been recently used to produce asymmetric graft molecules with high precision in arm number in addition to the extreme precision in molecular weight afforded by the anionic syntheses of the incorporated arms.

The first attempt at an asymmetric graft copolymer utilizing the chlorosilane coupling method by Pennisi and Fetters produced narrow molecular weight distribution of three-arm polystyrene (PS) and polyisoprene (PI) stars where one arm differs in molecular weight.[47] This approach was utilized by Mays in order to produce the first well-defined "simple graft" $A_2B$ system consisting of two identical arms of PI both connected with a single PS graft at a single trifunctional silane coupling point.[48] The trifunctional coupling scheme was extended to form ABC miktoarm terpolymer stars of PS, PI, and polybutadiene (PB).[49] These syntheses were the first to produce model asymmetric block copolymer systems with completely controlled architectures and molecular weight.

## 1.5 Recent Developments in $A_2B$ and $A_3B$ Simple Graft Morphology

Well controlled and precise syntheses of graft copolymers have opened the door to experimental and theoretical study of these unique molecules which serve as model systems for more complicated branched or multi-grafted molecular architectures. The simple graft architecture, along with its inherent amphiphilic character, provides for complicated solution behavior. While the remainder of the chapter is concerned with the morphological behavior of graft copolymers, much research is being done on the solution viscosity and rheology of polymer molecules with unique graft and star architectures. The interested reader is directed to several recent publications and reviews concerning solution viscosity and rheology research.[26,50,51] While a foundation of knowledge on the behavior of simple and multiple graft molecules in the region of the microphase separation transition exists,[35,40] only recently has the microphase separated, morphological behavior of the simplest of the graft architectures, the $A_2B$ simple graft, been addressed theoretically in the large $\chi N$, strongly segregated regime. Interestingly, while the behavior of graft copolymers in the region of the microphase separation transition was calculated and experimentally determined to be almost identical to that of linear AB diblocks, the strongly phase separated bulk behavior was found to be highly altered.

Milner utilized calculations developed for strongly stretched polymer brushes in his calculation of the phase behavior of $A_2B$ and $A_3B$ simple graft systems.[52] The phase behavior at the entire range of relative volume fraction of B graft block was calculated. Since all of the systems are assumed to be strongly segregated and, therefore, independent of $\chi N$, the normal block copolymer thermodynamic parameter of $\chi N$ on the abscissa of the phase diagram vs. relative volume fraction on the ordinate is replaced by $\varepsilon = n_A/n_B(l_A/l_B)^{1/2}$ where $n_i$ is the number of arms of species i and $l_i = b_i^2/v_{o,i}$ where b is the statistical segment length and $v_o$ is the segmental volume. The ratio of $(l_A/l_B)^{1/2}$ accounts for any conformational asymmetry between the constituent blocks due to differing chain statistics.(For a complete study of the effect of conformational asymmetry between blocks please see chapter 4) The species with the smaller value of $l_i$ is more difficult to stretch and, therefore, is favored on the convex side of the AB interface. Due to the arm number asymmetry introduced by the graft molecular architecture there is a crowding of multiple A arms on the same side of the AB interface joined at a common junction point with a single B arm. In order to alleviate the crowding of the A blocks the volume fraction windows of stability of the various microphases found in linear diblock copolymers is shifted towards significantly higher volume fractions of the single B graft block. The experimental motivation for the above calculations can be found in the first morphological study of model graft miktoarm molecules in the bulk performed by Hadjichristidis, *et al.*[53] They synthesized several samples, two of which, an $A_2B$ simple graft where A=PI and B=PS and an ABC miktoarm terpolymer of PS and miscible PI and PB arms, formed microphase separated cylindrical microstructures at relative volume fractions which one would find a bicontinuous and lamellar morphology in a linear diblock architecture. This shift in the volume fraction window of stability relative to linear diblock architecture is in quantitative accordance with the calculations of Milner. The Milner theory was rigorously tested for the first time in two works, by Pochan, Gido *et al.*[54] which dealt exclusively with a series of $A_2B$ molecules consisting of A = PI and B = PS (the reader is directed to

Chapter 2) and by Tselikas *et al.*[55] which studied several $A_2B$ and $A_3B$ samples of A = PI and B = PS and several $A_2B$ with A = PS and B = PI. In Pochan *et al.* the phase behavior was in good quantitative agreement with Milner's calculations except for one region of the phase diagram with low relative volume fraction of PI where the two arms of PI are first forced to the concave side of the PI/PS interface in the microphase separated state, i.e. the lamellar to bicontinuous boundary.[56] This novel phase behavior, which consists of worm-like domains of PI randomly oriented in a PS matrix and is not found in neat linear or $(AB)_n$ star block copolymers, was attributed to lattice frustration as a result of initially packing the two PI arms on the concave interface. This frustration seems to prevent an underlying lattice of the PI domains. Tselikas *et al.* also found good quantitative agreement between experiment and theory except for some minor discrepancies close to order-order boundaries. Since the theoretical model only addresses interactions and stretching from a single AB interface these minor discrepancies are ascribed to possible "multiple domain effects" due to the chains from an AB interface overlapping with those from a neighboring interface causing contributions to the configurations and free energy of those chains.

The remainder of the thesis involves morphological work on architecturally unique block copolymers; a series of $A_2B$ simple graft block copolymers in chapters 2 and 3, an initial study of their copolymer/copolymer blends in chapter 5, part 5.2, and the initial morphological characterization of a couple of more complex graft architectures in chapter 5, part 5.1. Chapter 4 and Chapter 5, part 5.3 are departures from simple graft block copolymers and focus on linear AB diblocks containing conformational asymmetry. The thesis is complete with conclusions and proposed future work in Chapter 6.

## 1.6 References


(1) Frederickson, G. H.; Bates, F. S. "Dynamics of Block Copolymers: Theory and Experiment." *Annu. Rev. Mater. Sci.*, **26**, 501 (1996).

(2) Aggarwal, S. L., Ed. *Block Copolymers*; Plenum Press: New York, 1970.

(3) Molau, G. E., Ed. *Colloidal and Morphological Behavior of Block and Graft Copolymers*; Plenum Press: New York, 1971.

(4) Goodman, I., Ed. *Developments in Block Copolymers*; Applied Science: New York, 1982; Vol. 1.

(5) Bates, F. S.; Frederickson, G. H. "Block Copolymer Thermodynamics: Theory and Experiment." *Annu. Rev. Phys. Chem.*, **41**, 525 (1990).

(6) Quirk, R. P.; Kinning, D. J.; Fetters, L. J. In: *Comprehensive Polymer Science: The Synthesis, Characterization, Reactions, and Applications of Polymers. Specialty Polymers & Polymer Processing*; S. L. Aggarwal, Ed.; Pergamon: Oxford, 1989; Vol. 7; 1.

(7) Jung, K.; Abetz, V.; Stadler, R. "Thermodynamically Controlled Morphological Disorder in a Mircophase-Separated Cylindrical Block Copolymer." *Macromolecules*, **29**, 1076 (1996).

(8) Matsushita, Y.; Choshi, H.; Fujimoto, T.; Hasagawa, N. "Preparation and Morphological Properties of a Triblock Copolymer of the ABC Type." *Macromolecules*, **13**, 1053 (1980).

(9) Mogi, Y.; Mori, K.; Kotsuyi, H.; Matsushita, Y.; Noda, I. "Molecular Weight Dependence of the Lamellar Domain Spacing of ABC Triblock Copolymers and Their Chain Conformations in Lamellar Domains." *Macromolecules*, **26**, 5169 (1993).

(10) Riess, G.; Schlienger, M.; Marti, S. "New Morphologies in Rubber Modified Polymers." *J. Macromol. Sci., Phys.*, **B17**, 355 (1980).

(11) Shibayama, M.; Hasegawa, H.; Hashimoto, T.; Kawai, H. "Microdomain Structure of an ABC Type Triblock Polymer of Polystyrene-Poly-(4-vinylbenzyl)-di-methylamine-)-Polyisoprene Cast from Solutions." *Macromolecules*, **15**, 274 (1982).

(12) Pochan, D. J.; Gido, S. P.; Zhou, J.; Mays, J. W.; Whitmore, M. D.; Ryan, A. J. "Microphase Separated Morphology of a Conformationally Asymmetric Block Copolymer." *J. Polym. Sci. Polym. Phys.*, in press, (1997).

(13) Bates, F. S.; Schulz, M. F.; Khandpur, A. K.; Førster, S.; Rosedale, J. H.; Almdal, K.; Mortensen, K. "Fluctuations, Conformational Asymmetry, and Block Copolymer Phase Behavior." *Faraday Discuss. Chem. Soc.*, **98**, 7 (1994).

(14) Gehlsen, M. D.; Bates, F. S. "Conformational Asymmetry in Poly(vinylcyclohexane) Containing Diblock Copolymers." *Macromolecules*, **27**, 3611 (1994).

(15) Ryan, A. J.; Hamley, I. W.; Bras, W.; Bates, F. S. "Structure Development in Semicrystalline Diblock Copolymers Crystallizing from the Melt." *Macromolecules*, **28**, 3860 (1995).

(16) Cohen, R. E.; Cheng, P. L.; Douzinas, K.; Kofinas, P.; Berney, C. V. "Path Dependent Morphologies of a Diblock Copolymer of Polystyrene and Hydrogenated Polybutadiene." *Macromolecules*, **23**, 324 (1990).

(17) Rangarajan, P.; Register, R. A.; Fetters, L. J.; Bras, W.; Naylor, S.; Ryan, A. J. "Crystallization of a Weakly Segregated Polyolefin Diblock Copolymer." *Macromolecules*, **28**, 4932 (1995).

(18) Khandpur, A. K.; Macosko, C. W.; Bates, F. S. "Transmission Electron Microscopy of Saturated Hydrocarbon Block Copolymers." *J. Polym. Sci., B: Polym. Phys.*, **33**, 247 (1995).

(19) Chen, J. T.; Thomas, E. L.; Ober, C. K.; Mao, G.-p. "Self-Assembled Semectic Phases in Rod-Coil Block Copolymers." *Science*, **273**, 343 (1996).

(20) Radzilowski, L. H.; Wu, J. L.; Stupp, S. I. "Self-Assembly of Rod-Coil Diblock Copolymers." *Macromolecules*, **26**, 879 (1993).

(21) Alward, D. B.; Kinning, D. J.; Thomas, E. L.; Fetters, L. J. "Effect of Arm Number and Arm Molecular Weight on the Solid-State Morphology of Poly(styrene-isoprene) Star Block Copolymers." *Macromolecules*, **19**, 215 (1986).

(22) Lescanec, R. L.; Hajduk, D. A.; Kim, G. Y.; Gan, Y.; Yin, R.; Gruner, S. M.; Hogen-Esch, T. E.; Thomas, E. L. "Comparison of the Lamellar Morphology of Microphase-Separated Cyclic Block Copolymers and Their Linear Precursors." *Macromolecules*, **28**, 3485 (1995).

(23) Avgeropoulos, A.; Poulos, Y.; Hadjichristidis, N.; Roovers, J. "Synthesis of 16-Arm Vergina Star Block Copolymers." *Macromolecles*, **29**, 6076 (1996).

(24) Beyer, F. L.; Gido, S. P.; Poulos, Y.; Hadjichristidis, N. "Morphology of Vergina Star 16-Arm Block Copolymers and Scaling Behavior of Interfacial Area with Graft Point Functionality." *Macromolecules*, **30**, 2373 (1997).

(25) Dreyfuss, P.; Quirk, R. P. In: *Encyclopedia of Polymer Science and Engineering*; H. F. Mark, N. M. Bikales, C. G. Overberger, G. Menges and J. I. Kroschwitz, Eds.; Wiley-Interscience: New York, 1987; Vol. 7; 551.

(26) Pitsikalis, M.; Pispas, S.; Mays, J. W.; Hadjichristidis, N. "Nonlinear Block Copolymer Architectures." *Adv. Polym. Sci.*, in press (1997).

(27) Cowie, J. M. G. In: *Comprehensive Polymer Science: The Synthesis, Characterization, Reactions, and Applications of Polymers. Chain Polymerization I*; C. J. Eastmond, A. Ledwith, S. Russo, P. Sigwalt, Eds.; Pergamon: Oxford, 1989; Vol. 3; 33.

(28) Braun, D.; Fischer, M.; Hellmann, G. P. "Block-Graft Copolymers as Compatibilizers in Polymer Blends." *Polymer*, **37**, 3871 (1996).

(29) Löwenhaupt, B.; Steurer, A.; Hellmann, G. P.; Gallot, Y. "Microphases and Macrophases in Polymer Blends with a Diblock Copolymer." *Macromolecules*, **27**, 908 (1994).

(30) Amorim, M. C. V.; Oliveira, C. M. F.; Tavares, M. I. B. "Investigation of PMMA/Polyoxide Blends Containing Graft-Copolymer Compatibilizers by Using NMR, SEM, and Thermal Analysis." *J. Appl. Polym. Sci.*, **61**, 2245 (1996).

(31) Feng, H.; Tian, J.; Ye, C. "Compatibilization Effect of Graft Copolymer on Immiscible Polymer Blends. II. LLDPE/PS/LLDPE-*g*-PS Systems." *J. Appl. Polym. Sci.*, **61**, 2265 (1996).

(32) Yanagase, A.; Ito, M.; Yamamoto, N.; Ishikawa, M. "Mechanism of Enhanced Impact Strength of Poly(vinylchloride) Modified by Acrylic Graft Copolymer." *J. Appl. Polym. Sci.*, **60**, 87 (1996).

(33) Miyata, T.; Takagi, T.; Uragami, T. "Microphase Separation in Graft Copolymer Membranes with Pendant Oligodimethylsiloxanes and Their Permselectivity for Aqueous Ethanol Solutions." *Macromolecules*, **29**, 7787 (1996).

(34) Holmberg, A.; Piculell, L.; Wesslén, B. "Viscosity Effects of a Graft Copolymer with a Hydrophobic Backbone and Hydrophilic Side Chains in a Water/Cyclohexane Oil-Continuous Microemulsion." *J. Phys. Chem.*, **100**, 462, (1996).

(35) Olvera de la Cruz; Sanchez, I. C. "Theory of Microphase Separation in Graft and Star Copolymers." *Macromolecules*, **19**, 2501 (1986).

(36) Leibler, L. "Theory of Microphase Separation in Block Copolymers." *Macromolecules*, **13**, 1602 (1980).

(37) Benoit, H.; Hadziioannou, G. "Scattering Theory and Properties of Block Copolymers with Various Architectures in the Homogeneous Bulk State." *Macromolecules*, **21**, 1449 (1988).

(38) Shinozaki, A.; Jasnow, D.; Balazs, A. C. "Microphase Separation in Comb Copolymers." *Macromolecules*, **27**, 2496 (1994).

(39) Lyatskaya, Y.; Jacobson, S. H.; Balazs, A. C. "Effect of Composition on the Compatibilizing Activity of Comb Copolymers." *Macromolecules*, **29**, (1996).

(40) Floudas, G.; Hadjichristidis, N.; Iatrou, H.; Pakula, T.; Fischer, E. W. "Microphase Separation in Model 3-Miktoarm Star Copolymers (Simple Graft) and Terpolymers. 1. Statics and Kinetics." *Macromolecules*, **27**, 7735 (1994).

(41) Beyer, F. L.; Gido, S. P.; Hadjichristidis, N. "Microphase-Separated Morphologies of Comb-Block Copolymers" *Macromolecules*, in preparation (1997).

(42) Hasegawa, H.; Hashimoto, T.; Hyde, S. T. "Microdomain Structures with Hyberbolic Interfaces in Block and Graft Copolymer Systems." *Polymer*, **37**, 3825 (1996).

(43) Quirk, R. P.; Ignatz-Hoover, F. "Living Coupling Agents. Rational Synthesis of Heteroarm Star-Branched Polymers." In: *Recent Advances in Anionic Polymerization*; T. E. Hogen-Esch and J. Smid, Eds.; Elsevier: New York, 1987; 393.

(44) Tsitsilianis, C.; Ghaumont, P.; Rempp, P. "Synthesis and Characterization of Hetero-Arm Star Copolymers." *Makromol. Chem.*, 191, 2319 (1990).

(45) Storey, R. F.; Chisholm, B. J.; Masse, M. A. "Morphology and Physical Properties of Poly(styrene-*b*-isobutylene-*b*-styrene) Block Copolymers." *Polymer*, **37**, 2925 (1996).

(46) Huynh, B.-G.; Jérome, R.; Teyssié, P. "Star-Shaped Block Copolymers. I. Synthesis of New A(B)2 Starshaped Block Copolymers Based on Vinyl or Diene Hydrocarbons (A) and Oxirane (B)*J. Polym. Sci., Polym. Chem. Ed.*, **18**, 3483 (1980).

(47) Pennisi, R. W.; Fetters, L. J. "Preparation of Asymmetric Three-Arm Polybutadiene and Polystyrene Stars." *Macromolecules*, **21**, 1094 (1988).

(48) Mays, J. W. "Synthesis of 'Simple Graft' Poly(isoprene-*g*-styrene) by Anionic Polymerization." *Polym. Bull.*, **23**, 247 (1990).

(49) Iatrou, H.; Hadjichristidis, N. "Synthesis of a Model Three-Miktoarm Star Terpolymer." *Macromolecules*, **25**, 4649 (1992).

(50) Vlahos, C.; Tselikas, Y.; Hadjichristidis, N.; Roovers, J.; Rey, A.; Freire, J. "Conformation of $A_2B$ and $A_3B$ Miktoarm Star Copolymers in Dilute Solutions." *Macromolecules*, **29**, 5599 (1996).

(51) Vlahos, C.; Horta, A.; Hadjichristidis, N.; Freire, J. "Monte Carlo Simulations of the Conformations of $A_2B$ and $A_3B$ Miktoarm Star Copolymers in Dilute Solution." *Macromolecules*, **28**, 1500 (1995).

(52) Milner, S. T. "Chain Architecture and Asymmetry in Copolymer Microphases." *Macromolecules*, **27**, 2333 (1994).

(53) Hadjichristidis, N.; Iatrou, H.; Behal, S. K.; Chludzinski, J. J.; Disko, M. M.; Garner, R. T.; Liang, K. S.; Lohse, D. J.; Milner, S. T. "Morphology and Miscibility of Miktoarm Styrene-Diene Copolymers and Terpolymers." *Macromolecules*, **26**, 5812 (1993).

(54) Pochan, D. J.; Gido, S. P.; Pispas, S.; Mays, J. W.; Ryan, A. J.; Fairclough, J. P. A.; Hamley, I. W.; Terrill, N. J. "Morphologies of Microphase-Separated $A_2B$ Simple Graft Copolymers." *Macromolecules*, **29**, 5091 (1996).

(55) Tselikas, Y.; Iatrou, H.; Hadjichristidis, N.; Liang, K. S.; Mohanty, K.; Lohse, D. J. "Morphology of Miktoarm Star Block Copolymers of Styrene and Isoprene." *J. Chem. Phys.*, **105**, 2456 (1996).

(56) Pochan, D. J.; Gido, S. P.; Pispas, S.; Mays, J. W. "Morphological Transitions in an $I_2S$ Simple Graft Block Copolymer: From Folded Sheets to Folded Lace to Randomly Oriented Worms at Equilibrium." *Macromolecules*, **29**, 5099 (1996).

# CHAPTER 2

# MORPHOLOGIES OF MICROPHASE SEPARATED $A_2B$ SIMPLE GRAFT COPOLYMERS

## 2.1 Abstract

The morphological behavior of a series of well defined $A_2B$ simple graft or "Y" architecture block copolymers is characterized via small-angle x-ray scattering (SAXS) and transmission electron microscopy (TEM). This model architecture is formed by grafting a poly(styrene) block onto the center of a poly(isoprene) backbone. The volume fraction windows in which specific strongly segregated microphase separated morphologies are observed are shifted to higher volume fractions of the PS graft material than in the corresponding linear diblock copolymers. These findings are in good agreement with recently calculated theoretical phase behavior for simple graft, $A_2B$, block copolymers. However, a new morphology, not found in neat linear diblock copolymers, is also observed. This $A_2B$ material is microphase separated into worm-like micelles but not ordered on a lattice. This morphology is found at high PS graft volume fraction ($\phi_s$=0.81) where the two PI chains per molecule are initially forced to the concave side of the PS/PI interface.

## 2.2 Introduction

### 2.2.1 Linear Diblock vs. $A_2B$ Simple Graft

For linear diblock copolymers in the strong segregation limit (large $\chi N$) the morphology formed is solely dictated by the relative volume fractions of the respective blocks. Changing molecular architecture, making graft block copolymers for instance, can allow control of the morphology independent of the volume fraction, thus providing an additional variable for control of structure. $A_2B$ simple graft block copolymers are systems in which strong segregation limit (SSL) microphase separated morphologies are

expected to occur in volume fraction ranges which are higher in the B block than for AB linear diblocks. These simple graft block copolymers are models for more complex multiple graft block copolymers typically used as compatibilizing and toughening agents in polymer blends. In the work reported here a poly(styrene) (PS) block is utilized as the graft chain while polyisoprene (PI) forms the backbone in a range of relative volume fractions.

In the strong segregation limit (SSL) the interphase region between domains has been measured and theoretically modeled to be only about 20 to 50Å.[1-3] By comparison, to the length scale of the microphase separated domains, typically hundreds of Ångstroms, the interphase region can be considered a two dimensional surface. This interface, which has been called an intermaterial dividing surface[4] has curvature properties which can be approximately correlated to the volume filling characteristics of the opposing blocks of the copolymer. The volume available to a polymer chain increases as one moves from the concave to the convex side of a curved interface in a block copolymer, and the disparity in the relative volumes available to the two blocks is proportional to the magnitude of the interfacial curvature. Thus the highest curvature interface geometry, spheres, occurs for the most asymmetric block volume fractions. As the volume fraction difference decreases so does the interfacial curvature across the sequence of observed morphologies: spheres, cylinders, cubic bicontinuous, and lamellar. The two A chains are more highly stretched and experience more lateral crowding than the single B chain. Therefore, the A phase will favor the convex side of the interface at volume fractions ($\phi_A$ from about 0.34 to 0.50) where a simple AB diblock would prefer a flat, lamellar interface.

### 2.2.2 $A_2B$ Simple Graft Theory

The SSL behavior of simple graft architecture studied in this paper was recently explored in the mean-field calculations of Milner[5] and the ground breaking synthesis

and subsequent initial morphological studies of Hadjichristidis.[6] Both works reveal intriguing results introduced by the simplest case of an architectural asymmetry in the form of an $A_2B$ simple graft or "Y" block copolymer. As a way to reveal bulk morphological effects of grafting the chains in this manner Milner used a simple calculation to reveal the center of the lamellar phase in a melt of "Y" polymers. It was found that the B graft component volume fraction is $\phi_B = 2/3$ in an $A_2B$ graft block copolymer to produce a flat preferred interfacial curvature. The analogous absence of a preferred curvature for symmetric diblock architecture occurs at $\phi_B = 1/2$ revealing the shift of the center of the phase diagram due to architecture alone. The possible morphologies were modeled with round unit cells for the cylindrical and spherical phases and utilized an approximation based on "Gaussian wedges"[7] to describe a generic bicontinuous phase. The morphology phase diagram was calculated by minimizing the sums of the free energies associated with the interfacial tension between phases and the stretching of the blocks away from the interface. The latter was calculated with methods developed for polymer brushes.[8] The crossings of the free energy curves for the differing geometries vs. graft volume fraction determines the equilibrium SSL phase behavior as shown in Figure 2.1. The diagram is generic in that within the parameter $\varepsilon = (n_a/n_b)(l_a/l_b)^{1/2}$ different architectures and chain statistics are accounted for. The number of arms one chooses, $n_a$ of A or $n_b$ of B, can be varied. Also, differing chain statistics between blocks are represented in the square root ratios of $l_a$ and $l_b$ with $l_i = V_i/R_i^2 = v_i / b_i^2$ where $V_i$ and $R_i$ are the molecular volume and radius of gyration of the respective blocks and $v_i$ and $b_i$ are the segment volume and Kuhn length of the respective blocks. If the constituent blocks are conformationally symmetric then $\varepsilon$ is simply the ratio of the number of A and B arms in the molecule.

At $\varepsilon = 1$ the phase diagram models linear, AB diblock phase behavior with the phases being symmetric around $\phi_b = 0.5$. However, as one increases arm number of one species relative to the other or varies the relative chain statistics of A and B, the phase

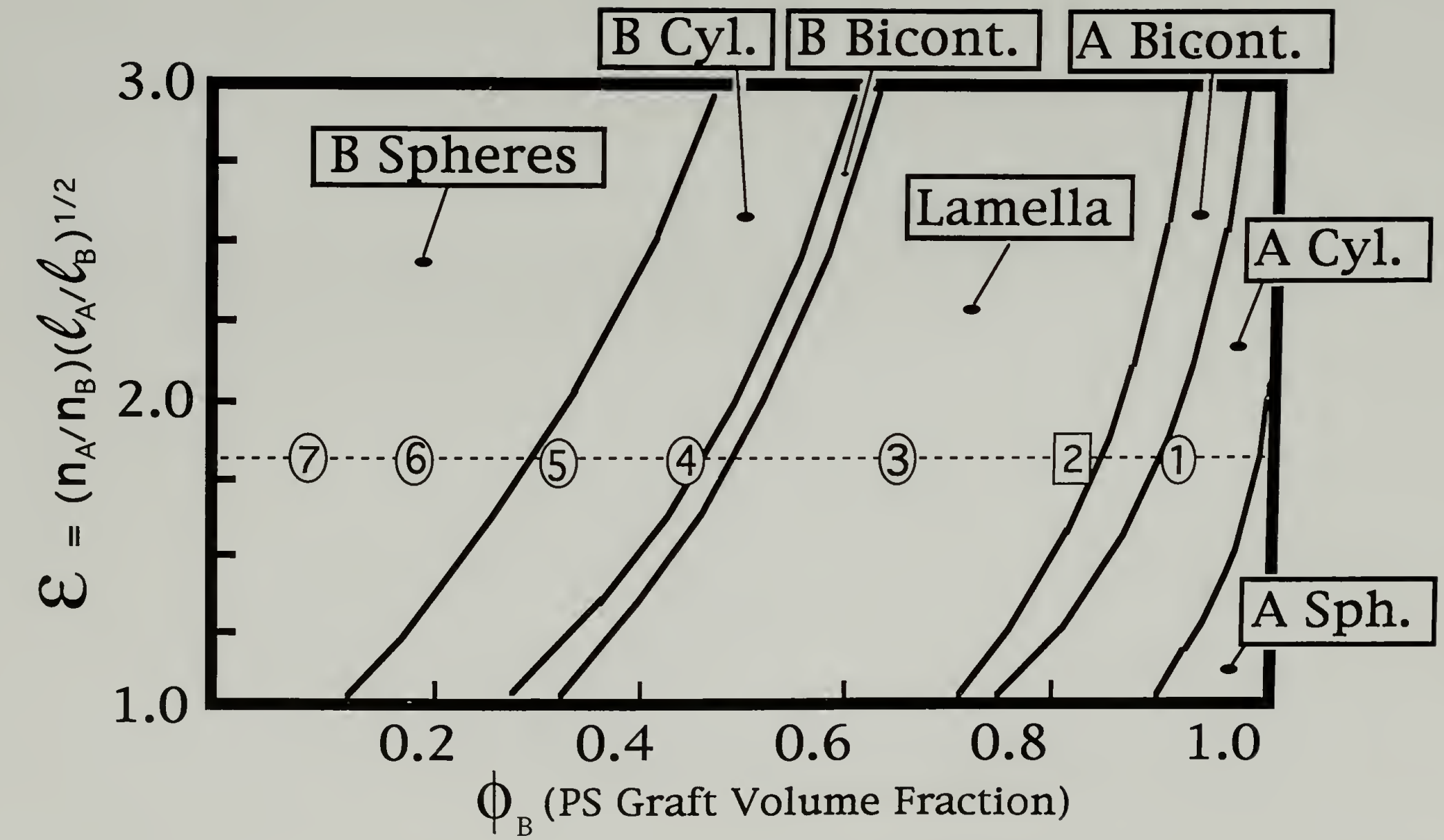


Figure 2.1: Theoretical phase diagram calculated by Milner. The ovals along the dashed line where $\varepsilon = 1.78$ each represent a specific $I_2S$ sample corresponding to the number within the oval. $I_2S$-2 is represented by a square due to its unusual morphology not found in linear diblocks or accounted for theoretically in this phase diagram.

behavior becomes extremely asymmetric with volume fraction. Hadjichristidis *et al.*.[6] recently characterized the bulk phases behavior of three $A_2B$ block copolymers or "miktoarm" star copolymers. The asymmetry of the graft architecture forced two of the samples to shift the observed morphology away from that which would be formed by diblock architecture analogs with the same component volume fractions: A 37 vol. % polystyrene "$I_2S$" graft (polyisoprene backbone and a single polystyrene graft emanating from the middle of that backbone) and a 40 vol. % styrene SIB graft (the rubbery phase consists of mixed isoprene and butadiene blocks) were observed to form cylindrical phases where diblocks of the same compositions would be bicontinuous or lamellar respectively. The $I_2S$ blocks studied in this work confirm the strong asymmetry in the phase behavior vs. volume fraction for $\varepsilon > 1$ shown in Figure 2.1. However, in addition to simply shifting the volume fractions at which the standard diblock phases are found, the architecture also introduces a novel morphological behavior unique to the simple graft architecture. A new phase is observed at a volume fraction at which the two PI arms per molecule are first forced to the concave side of the PS/PI interface in the microphase separated state. This phase consists of microphase separated worm-like micelles which are not ordered on a lattice. A worm-like micelle phase has been previously observed in blends of diblock copolymers with homopolymers,[9] but, to our knowledge, this phase has not been previously observed in neat block copolymers.

## 2.3 Experimental

### 2.3.1 Simple Graft Synthesis

$I_2S$ simple graft block copolymers were prepared under high-vacuum conditions in all-glass reactors which had been washed with n-BuLi and rinsed with solvent. Additions of reagents were made through breakseals and removals of samples were made through heat sealing of constrictions. The benzene solvent, styrene-$d_8$

(Cambridge Isotopes, halogen free) and isoprene monomers, $CH_3SiCl_3$ linking agent, and $CH_3OH$ terminating agent were purified using standard anionic polymerization techniques.[10,11] *s*-BuLi, purified by sublimation under high vacuum, was used as the initiator throughout the synthesis. The reaction scheme followed for the preparation of the $(PI)_2PS\text{-}d_8$ miktoarm stars can be represented by the following reactions:[12,13]

$$PS\text{-}d_8Li + \text{excess } CH_3SiCl_3 \longrightarrow PS\text{-}d_8SiCH_3Cl_2 + LiCl + CH_3SiCl_3\uparrow$$

$$PS\text{-}d_8SiCH_3Cl_2 + \text{excess } PILi \longrightarrow (PI)_2SiCH_3PS\text{-}d_8 + 2LiCl$$

In the first step a dilute solution of the living polystyrene-$d_8$ (d-8 labeling of the PS graft in this work was used to facilitate subsequent analysis of these materials via neutron scattering techniques) was added into a large excess of methyl trichlorosilane (Si-Cl/Li=100). Excess methyltrichlorosilane was removed by continuous pumping on the vacuum line followed by redisolution of the polymer with purified benzene and removal of the solvent. This process was repeated twice. In the second step excess living polyisoprene chains were added to the macromolecular linking agent. When the coupling of the polyisoprene chains was completed excess polyisoprenyllithium was deactivated with degreased methanol.

Fractionation of the samples was performed by addition of methanol to a 1% solution of the polymers in a 60/40 volume benzene/hexane mixture. Usually three fractionations were enough to remove any unlinked poly(isoprene) arms. All stages of polymer synthesis were monitored by size exclusion chromatography (SEC). A Waters Model 510 pump, Model 410 differential refractometer, and a LDC/Milton Roy variable wavelength UV detector in series with three Waters Ultrastyragel linear column set were used. Tetrahydrofuran was the elution solvent at a flow rate of 1ml/min at 35°C.

Composition of the samples was measured by SEC-UV at 260 nm after calibration with several concentrations of polystyrene standards.

Number-average molecular weights, $M_n$ and second virial coefficients, $A_2$, for the copolymers and the arms were determined with a Wescan Model 231 membrane osmometer at 37°C. RC-51 membranes were used with $CaH_2$ distilled toluene as the solvent. In all cases $M_n$ and $A_2$ values were obtained from the $(\pi/c)^{1/2}$ vs. c plots where $\pi$ is the osmotic pressure and c is the concentration. For molecular weights lower than 10,000 a UIC Model 070 vapor pressure osmometer was used. HPLC grade benzene was the solvent at 40°C. The instrument was calibrated with benzil.

As an additional check, apparent weight-average molecular weights, $M_w$, and $A_2$ for the copolymers were measured with a Chromatix KMX-6 low-angle laser light scattering photometer equipped with a helium-neon laser. The $M_w$ values were obtained from the $(Kc/\Delta R_0)^{1/2}$ vs. c plots where $\Delta R_0$ is the excess Rayleigh ratio, c is the concentration, and K is a combination of known optical constants including the refractive index increments *dn/dc*. Values of *dn/dc* were also measured in THF at 25°C with an Otsuka DRM-1020 differential refractometer at 633 nm calibrated with NaCl solutions. Within experimental uncertainty the light scattering data are consistent with results from membrane osmometry. The molecular characteristics of the samples are given in Table 2.1.

### 2.3.2 Morphology Characterization

Solid films approximately 2 mm. thick were cast from toluene solutions of 5 weight % polymer in 30 ml Pyrex beakers. The evaporation of solvent was controlled to form a solid film after 10-14 days. The films were given several more days at room temperature and atmospheric pressure and an additional several days under high vacuum at room temperature to allow residual solvent to evaporate. The vacuum oven temperature was ramped to 120°C over a period of three days and kept there for one

Table 2.1

$I_2S$ Molecular Characteristics: (a) by membrane osmometry, (b) by SEC, (c) by LALLS, (d) by SEC-UV, (e) by VPO, (f) calculated utilizing ρ(d-PS) = 1.14 g/ml$^3$ @ 25°C and ρ(PI) = 0.91 g/ml$^3$ @ 25°C along with the wt.% compositions from SEC-UV)

| Sample | Vol.% d-PS[f] | $M_n$ PS arm[a] (g/mol) ($x10^{-3}$) | $M_n$ PI arm[a] (g/mol) ($x10^{-3}$) | $M_n$ total[a] (g/mol) ($x10^{-3}$) | $M_w/M_n$[b] | $M_w$ total[c] (g/mol) ($x10^{-3}$) | Wt.% d-PS[d] |
|---|---|---|---|---|---|---|---|
| $I_2S$-1 | 89 | 87.3 | 4.6[e] | 97.1 | 1.04 | 106.0 | 91 |
| $I_2S$-2 | 81 | 79.1 | 9.6 | 89.4 | 1.04 | 90.8 | 84 |
| $I_2S$-3 | 62 | 61.2 | 14.8 | 83.0 | 1.04 | 87.4 | 67 |
| $I_2S$-4 | 44 | 44.4 | 21.3 | 82.5 | 1.04 | 92.0 | 49 |
| $I_2S$-5 | 31 | 31.6 | 26.5 | 82.6 | 1.04 | 89.8 | 35 |
| $I_2S$-6 | 17 | 21.1 | 34.7 | 92.3 | 1.04 | 100.1 | 20 |
| $I_2S$-7 | 8 | 9.4[e] | 39.1 | 84.3 | 1.06 | 91.3 | 10 |

week. After annealing the temperature was slowly ramped down to 80°C over two days and then quickly lowered to room temperature. This casting and annealing procedure was designed to promote the development of equilibrium strong segregation morphologies. After the oven temperature exceeded approximately 110°C sample $I_2S$-7 began to creep indicating a loss of microphase separated order at the order-disorder transition (ODT). A second film of $I_2S$-7 was annealed at 108°C, below the ODT of the system but high enough for significant annealing.[15,16]

All samples for electron microscopy were microtomed in a Reichert-Jung cryoultramicrotome. Sections approximately 300-800 Å thick were cut with a Diatome cryo diamond knife at a sample temperature of -110°C and a knife temperature of -90°C. The sections were stained in 4 wt. % aqueous $OsO_4$ vapors for four hours. Transmission electron microscopy experiments (TEM) were performed on a JEOL 100CX electron microscope operated at 100kV accelerating voltage.

Synchrotron SAXS experiments were performed on beamline 2.1 of the Synchrotron Radiation Source (SRS) at the Daresbury Laboratory, Warrington, U. K. Details of the electron storage ring, radiation, camera geometry, and data collection electronics have been given elsewhere[17]. White radiation from the electron ring was collimated using a cylindrically bent Ge(111) crystal to isolate an intense beam of $\lambda = 1.50 \pm 0.01$ Å X-rays. At 2 GeV and 200 mA the SRS generates a flux of $4 \times 10^{10}$ photons $s^{-1}$ at the sample/focal plane. The instrument is equipped with a multiwire quadrant SAXS detector five meters from the sample position with a vacuum chamber placed in between to reduce air scattering and absorption. The spatial resolution of the detector is 500 μm, and it is able to process up to approximately 250,000 counts/s. The bulk polymer films were mounted in the beam after being sandwiched between two pieces of Kapton (polyimide) tape in a desired orientation. An oriented specimen of wet collagen (rat tail tendon) was used to calibrate the SAXS detector. A parallel-plate ionization detector placed before the sample cell recorded the incident intensities. The

experimental data were corrected for Kapton and camera background scattering, sample absorption, and the positional alinearity of the detector.

Birefringence observations were performed on bulk films at room temperature with a Leitz optical microscope under cross polars.

## 2.4 Results and Discussion

For the sake of comparison with the calculated phase behavior of the simple graft architecture, an approximate ε, as described in the Introduction, is assigned to the $I_2S$ system. If PS and PI blocks were conformationally symmetric then ε would simply be the ratio of PI arms to PS or ε = 2. However, the slight asymmetry inherent in the different chemical species slightly lowers the ε parameter. We assign segmental volumes, $v_i$, as 132 $Å^3$ and 176 $Å^3$ for PI and PS respectively.[18] Statistical segment lengths, $b_i$, are assigned as 6.8 Å and 6.9 Å for PI and PS respectively.[19] These values produce an ε of 1.78. While these values were measured at different temperatures (123°C for the segment volumes and 150°C for the segment lengths) they are adequate in revealing the slight effect the small conformational asymmetry between PS and PI has within the framework of the theoretical phase diagram. Any changes in the values due to temperature or isotope effects would have only a slight effect on ε and are accounted for via the size of the symbols on the phase diagram in Figure 2.1.

Table 2.2 contains tabulated d-spacings and birefringence information as well as the resulting morphology assignments as described in the remainder of the paper. Birefringence observations were performed on the annealed films as a preliminary measure on the degree of microphase separation. The form birefringence, a result of non-cubic symmetry, is evidence of either a cylindrical or a lamellar microstructure.[20,21] The most fundamental facet to this work is the confirmation of asymmetry in the phase behavior vs. volume fraction in the simple graft block copolymer architectures. For the simple graft architecture each particular morphology (spheres, cylinders, lamella, etc.)

Table 2.2

$I_2S$ Morphology Characteristics: (a) $d_1 = 2\pi/q_1$ where $q_1 = 4\pi/\lambda(\sin\theta_1)$ and $2\theta_1$ is the scattering angle for the lowest angle Bragg peak; corresponds to $d_{(10)}$ for hex. cylinders, $d_{(001)}$ for lamellae, and either $d_{(100)}$ or $d_{(110)}$ for simple cubic or body-centered cubic respectively

| Sample | $\phi_s$ | $d_1$(Å)[(a)] | Morphology | Optical Birefringence |
|---|---|---|---|---|
| $I_2S$-1 | 0.89 | 310±5 | hex. packed PI cylinders in PS matrix | Yes |
| $I_2S$-2 | 0.81 | NA | disordered PI micelles | No |
| $I_2S$-3 | 0.62 | 390±5 | alternating PS and PI lamellae | Yes |
| $I_2S$-4 | 0.44 | 429±5 | hex. packed PS cylinders in PI matrix | Yes |
| $I_2S$-5 | 0.31 | 380±5 | hex. packed PS cylinders in PI matrix | Yes |
| $I_2S$-6 | 0.17 | 289±5 | cubic array PS spheres in PI matrix | No |
| $I_2S$-7 | 0.08 | 235±5 | cubic array PS spheres in PI matrix | No |

occurs at a higher PS graft volume fraction than would be expected in a simple diblock architecture. This results in a morphology diagram which is asymmetric about 0.5 volume fraction and which is in good qualitative agreement with the calculations of Milner.[5] However, in addition to simply shifting normal diblock phase behavior to higher PS volume fractions, the $A_2B$ simple graft architecture also introduces a new morphology in sample $I_2S$-2 not yet anticipated theoretically or observed experimentally in neat diblock copolymers. Our experimental data are plotted on Milner's morphology diagram in Figure 2.1.

Based on the TEM image in Figure 2.2 and the SAXS data in Figure 2.3 we assign sample $I_2S$-1 ($\phi_s = 0.89$) a morphology of hexagonally packed PI cylinders in a PS matrix. A linear diblock copolymer of the same composition would form PI spheres in a PS matrix. The observation of optical birefringence in $I_2S$-1 is consistent with a

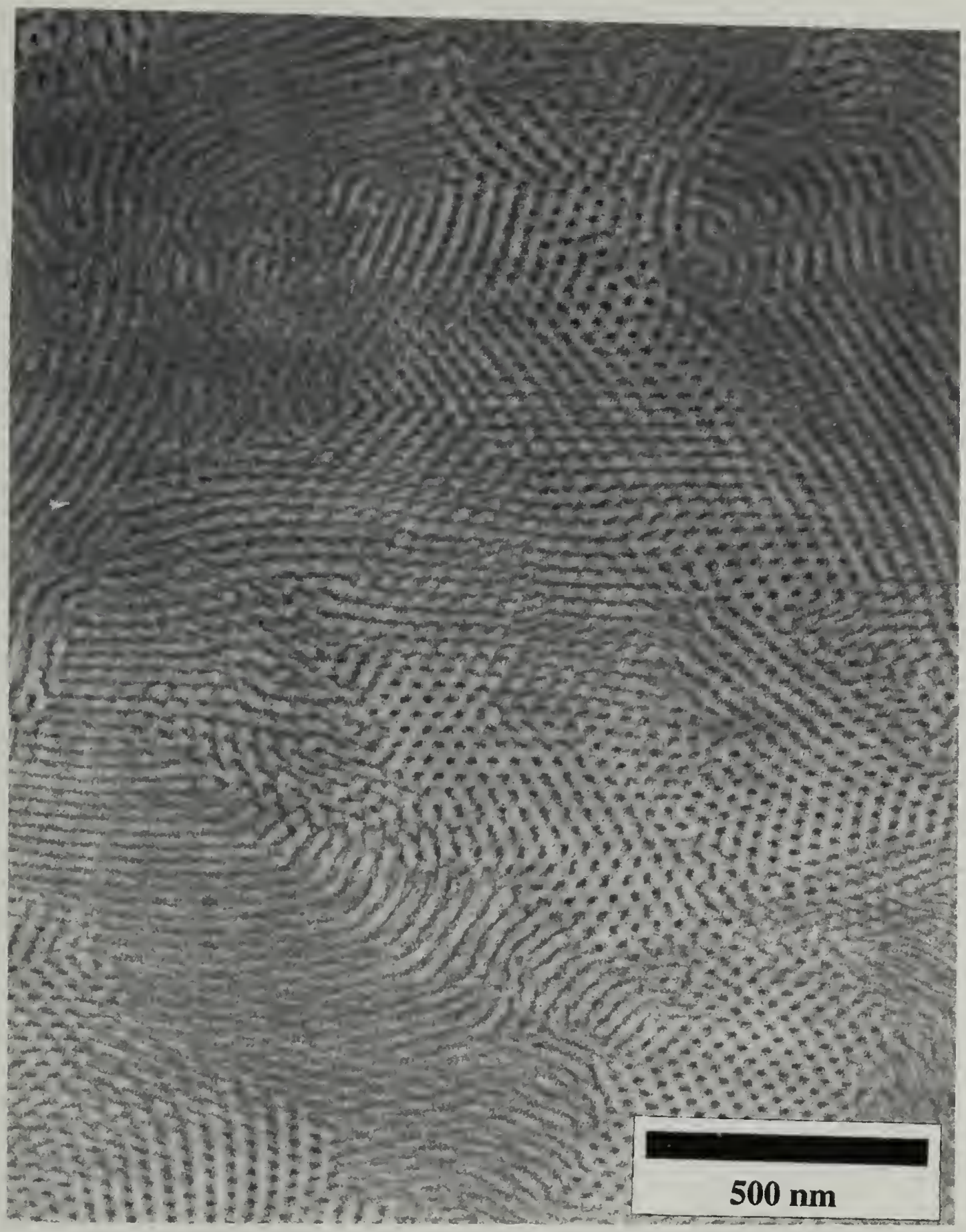


Figure 2.2: TEM micrograph of $I_2S$-1 ($\phi_s = 0.89$) showing projections both parallel and perpendicular to the PI cylinders as well as revealing a small average grain size.

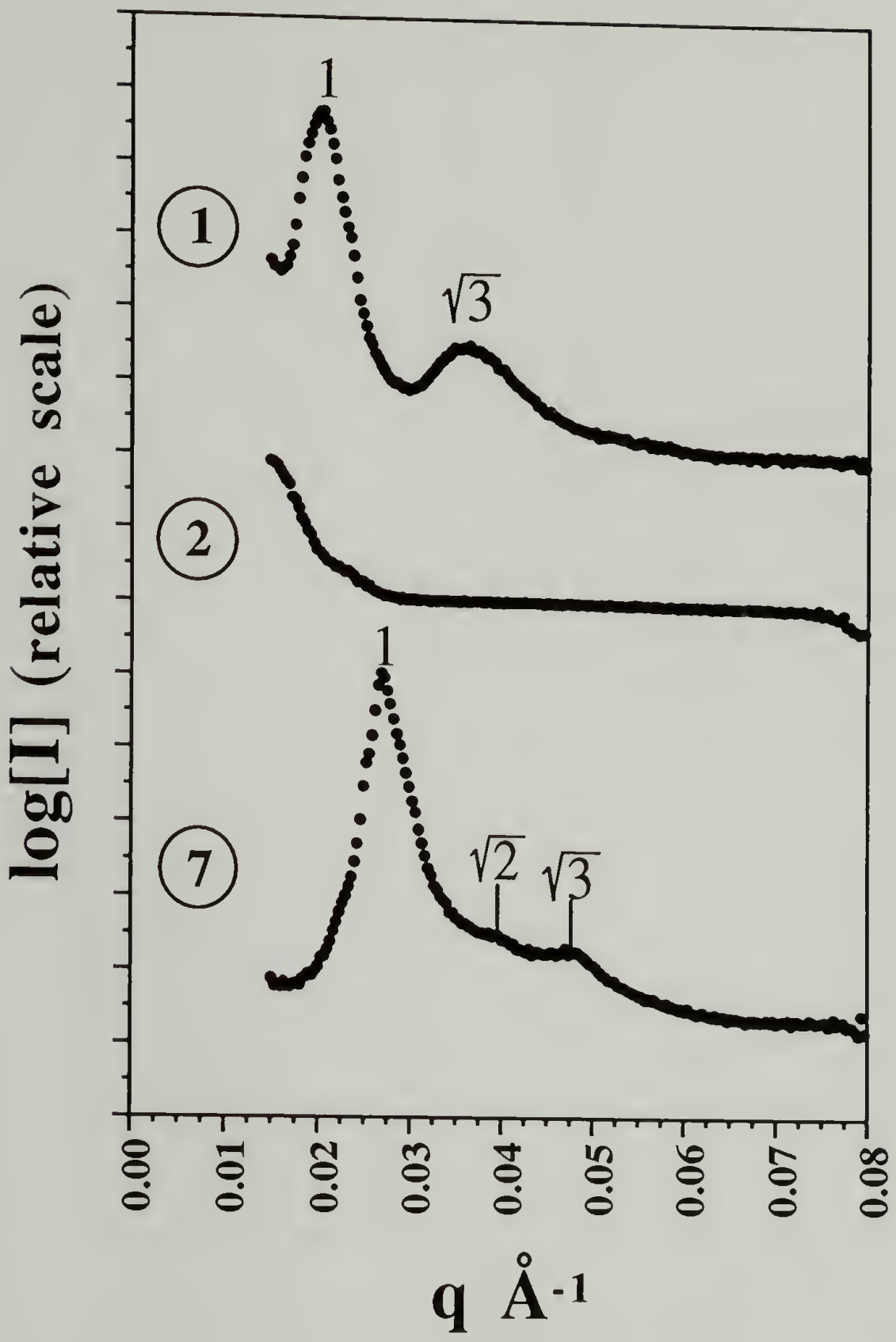


Figure 2.3: Isotropic SAXS patterns azimuthally integrated into one dimensional plots of log[intensity] vs. q. The intensities are offset for clarity of representation. The circled numbers represent the respective $I_2S$ sample. 1) $I_2S$-1 ($\phi_s = 0.89$) containing the first two reflections of hexagonally packed cylinders. 2) $I_2S$-2 ($\phi_s = 0.81$) lack of any discrete interference peaks indicative of the absence of an underlying lattice in the microstructure. 7) $I_2S$-7 ($\phi_s = 0.09$) containing the first three reflections of a cubic array of spheres.

cylindrical structure. The SAXS pattern contains no preferential orientation of the microphase separated structure, and thus we display only a one dimensional plot of intensity vs. scattering vector, I vs. q. We define q* as the scattering vector of the lowest scattering angle Bragg peak and $q_n$ as the series of Bragg peaks beginning with q* and including subsequent higher scattering angle peaks. The SAXS pattern for $I_2S$-1 contains two isotropic rings with $q_n/q^*$ ratios of 1 and $\sqrt{3}$ corresponding to the {10} and {11} sets of planes respectively in the hexagonal structure. The TEM images reveal a predominant grain size within the bulk of only several hundred nanometers to a few microns in diameter. The lack of a preferential grain orientation, also evident in the TEM images, is consistent with the isotropic character of the SAXS pattern and the lack of higher order reflections.

The TEM image in Figure 2.4 and the SAXS pattern in Figure 2.3, indicate why sample $I_2S$-2 ($\phi_s = 0.81$) is of particular interest. This sample appears to be microphase separated but not ordered on a lattice. The TEM images indicate a microphase separated state due to the discrete dark (PI) and light (PS) domains. The pattern of dark dots and short, curved segments is characteristic of a microtomed section through a phase of disordered cylindrical or worm-like micelles.[9] The inset schematic in Figure 2.4 indicates how a thin section of such a structure produces the resultant image in a 2-D projection. The lack of an underlying lattice is obvious in the micrograph as well as in the lack of any discrete Bragg peaks in the SAXS pattern. Additionally, $I_2S$-2 displays no optical birefringence which is consistent with the observation of worm-like micelles distributed isotropically in space.

The lack of any long range order in this sample immediately made us suspect sample contamination or degradation during the casting and annealing process. However, comparison of GPC traces of the material before casting (as obtained from the original synthesis and purification procedure) and after annealing indicate a pure sample with an extremely narrow molecular weight distribution which undergoes no

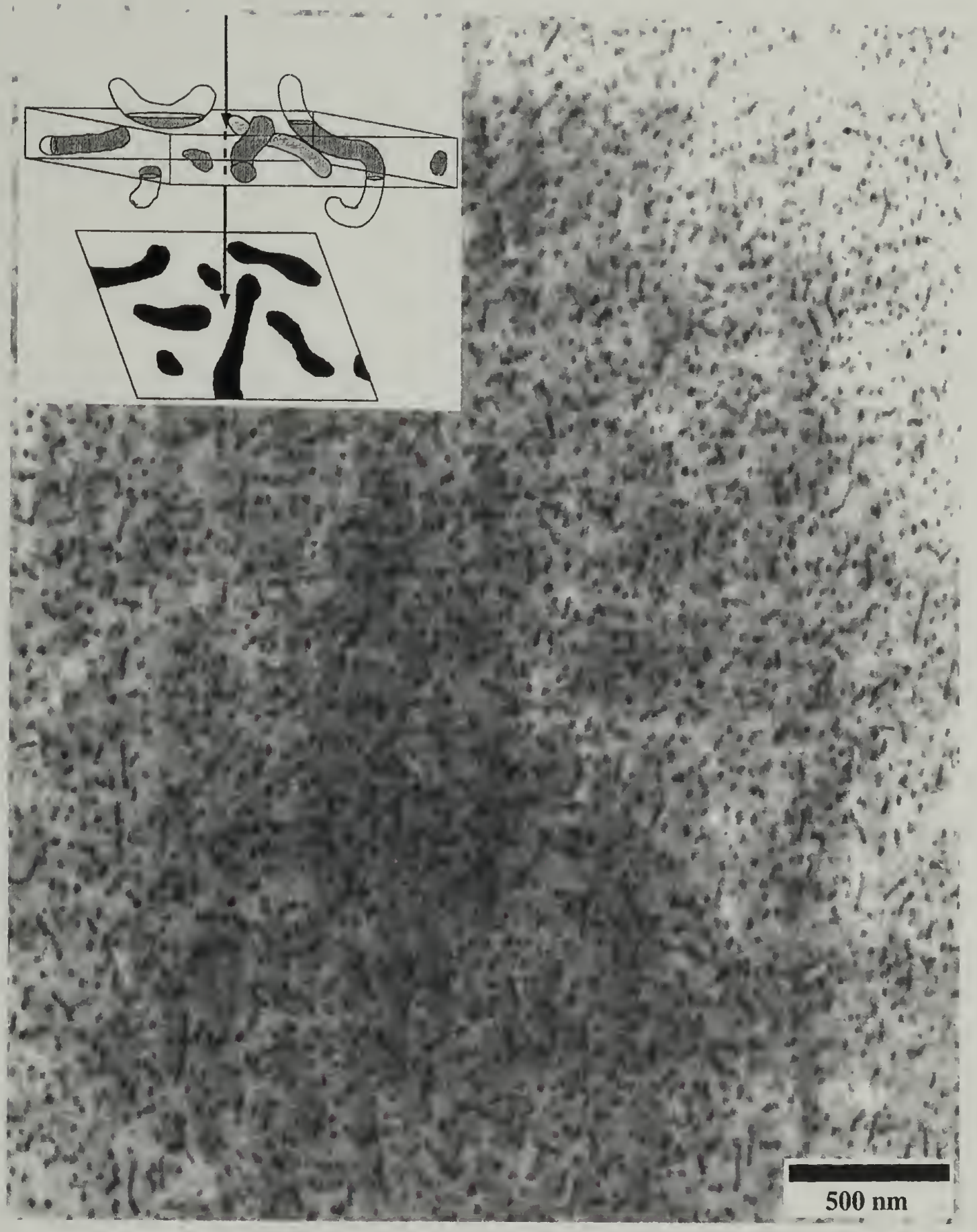


Figure 2.4: TEM micrograph of $I_2S$-2 ($\phi_s = 0.81$) showing dark PI worm-like micelles embedded in the PS graft matrix. Inset in the micrograph is a schematic showing how a projection through a microtomed section of the disordered, worm-like micelles appears in a 2-dimensional representation as observed in the micrograph.

degradation during sample preparation. The sample casting and annealing procedure for sample $I_2S$-2 was repeated, and the same worm-like micelle morphology was again observed for the neat graft block copolymer. We are thus led to the conclusion that a simple graft block copolymer with the composition of $I_2S$-2 is unable to form an ordered lattice at this composition. It does, however, microphase separate and display a clear preference for a specific micelle structure. If we look at our series of seven graft copolymers in reverse order (from $I_2S$-7 to $I_2S$-1), and compare to Milner's morphology diagram (Figure 2.1), we see that sample $I_2S$-2 is the first sample for which the PS graft block is large enough to force the two PI blocks onto the concave side of the interface. This observation is supported by Figure 2.4 in which it is evident that the PI material (stained to appear dark with $OsO_4$) is on the concave side of the interface of the microphase separated, but disordered, domain structures. We hypothesize that frustration inherent in packing the two PI chains on the concave side of the interface inhibits the formation of a morphology with an ordered lattice. However, the reproducible observation of disordered worm-like micelles of constant diameter indicates the approximate selection of a preferred interfacial curvature. Sample $I_2S$-1, which has even shorter PI chains than $I_2S$-2, may experience less packing frustration enabling it to form the hexagonally packed cylindrical structure that we observe. It appears that the inability to form an ordered lattice is confined to a narrow volume fraction range near the transition at which the two PI chains per molecule are initially forced to the concave side of the interface.

If this hypothesis about the lack of long range order in the $I_2S$-2 structure is correct then we should be able to transform this disordered structure into an ordered structure by slightly perturbing the volume fractions in one direction or the other. This can be achieved by casting samples of $I_2S$-2 from a selective solvent. Casting from cyclohexane, a selective solvent for PI, results in a lamellar morphology as shown in Figure 2.5. Casting $I_2S$-2 from dioxane, a selective solvent for PS enhanced the ability

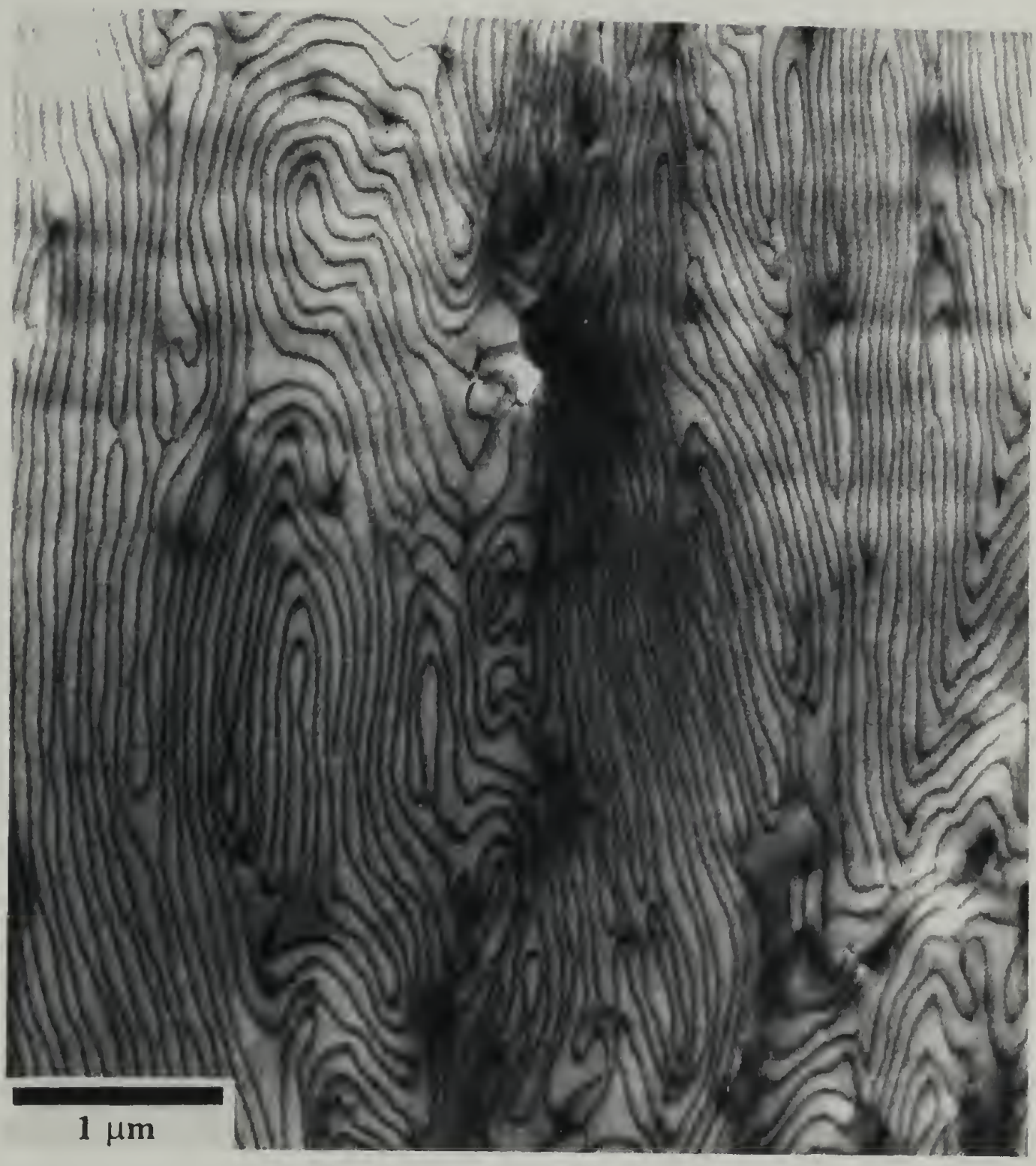


Figure 2.5: TEM micrograph of $I_2S$-2 cast from cyclohexane before annealing displaying a kinetically trapped, non-equilibrium lamellar morphology.

of the single PS graft to force the two PI chains onto the concave side of a highly curved interface resulting in PI spheres in a PS matrix. After complete removal of the selective solvent these morphologies are no longer at equilibrium, but are kinetically trapped. Annealing above $T_g$ of the PS block may allow these samples to return to the disordered worm-like micelle structure. Selective solvent casting followed by annealing has been used to demonstrate the equilibrium nature of the structure formed on annealing.[22] Annealing the lamellar interfaces of the cyclohexane cast sample caused them to become perforated in a mesh-like morphology[23] which eventually disintegrated back into the disordered worm-like micelle morphology. These selective solvent casting and annealing experiments are described in detail elsewhere.[24]

Sample $I_2S$-3 ($\phi_s = 0.62$) contains a lamellar microstructure with well developed, large grains as is evident in the TEM micrograph in Figure 2.6a. Figure 2.7a shows an oriented SAXS pattern containing four orders of reflection at q*, 2q*, 3q*, and 4q* due to scattering from a cross section of the film placed vertically into the SAXS camera. The concentration of scattered intensity along the equator with arcs extending azimuthally indicates that the lamellar layers are predominantly parallel with the surface of the film. Optical birefringence was observed in sample $I_2S$-3 consistent with our structural identification of lamella.

Both samples $I_2S$-4 ($\phi_s = 0.44$) and $I_2S$-5 ($\phi_s = 0.31$) yield hexagonally packed PS cylinders in a PI matrix and contain regions displaying a remarkable degree of long range order, especially considering that no special efforts, such as shearing, were employed to induce alignment. Figure 2.7b and c displays two dimensional SAXS patterns from $I_2S$-4 and $I_2S$-5 with six-fold symmetry suggestive of a [001] zone axis of a hexagonally packed array of cylinders. The $q_n/q^*$ ratios of 1, $\sqrt{3}$, $\sqrt{4}$, $\sqrt{7}$, $\sim\sqrt{9}$, and $\sim\sqrt{12}$ correspond to the {10}, {11}, {20}, {21}, {30}, and {22} families of planes respectively. These hexagonal patterns were taken with X-rays incident through a cross section of the film indicating that the cylinder axes lie predominantly in the plane of the

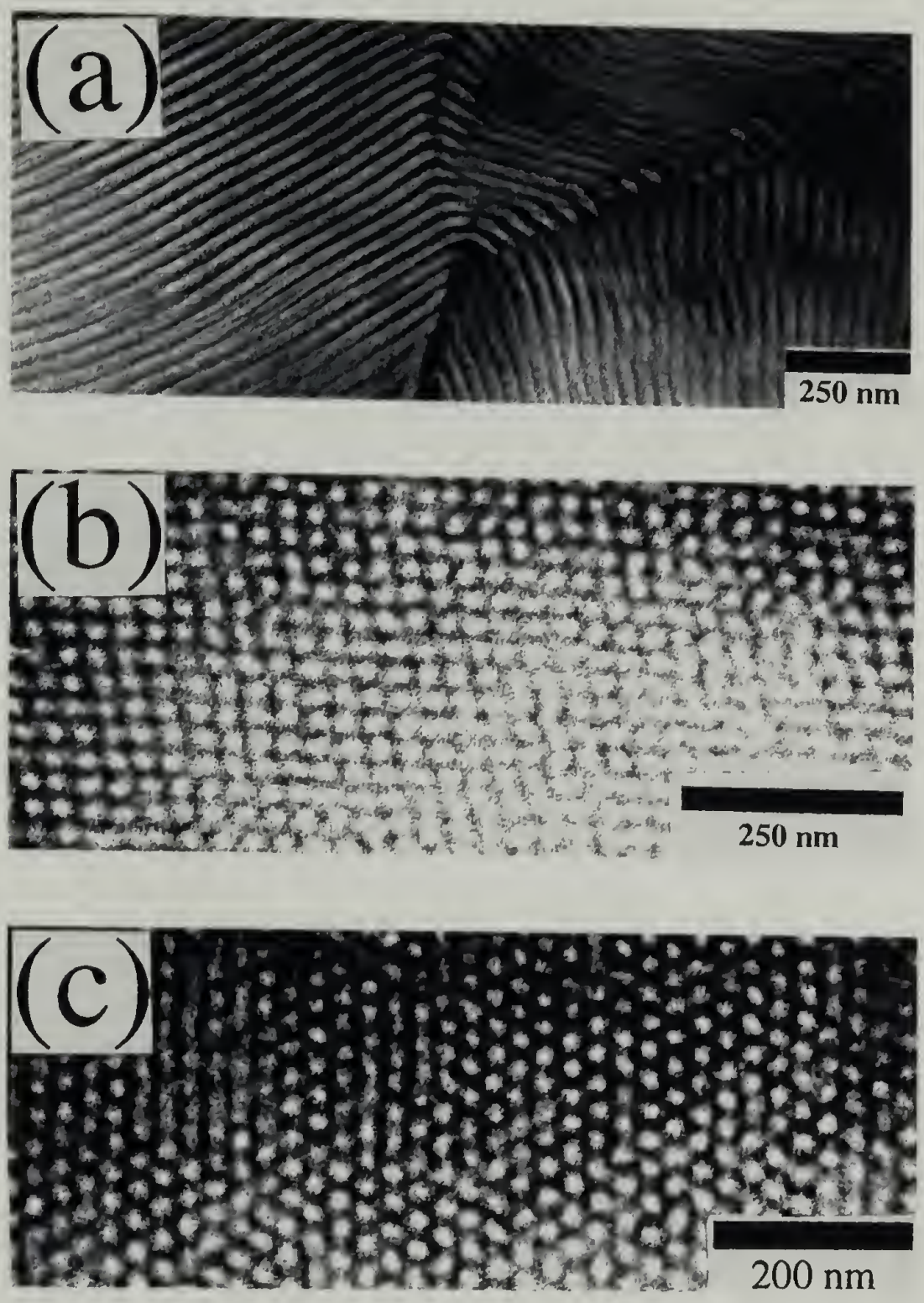


Figure 2.6: a) TEM micrograph of $I_2S$-3 ($\phi_s = 0.62$) showing a lamellar phase. b) TEM micrograph of $I_2S$-6 ($\phi_s = 0.17$) showing 4-fold symmetry due to a [100] projection of the cubic array of PS spheres. c) TEM micrograph of $I_2S$-6 ($\phi_s = 0.17$) containing 3-fold hexagonal symmetry due to a [111] projection of the cubic array of spheres.

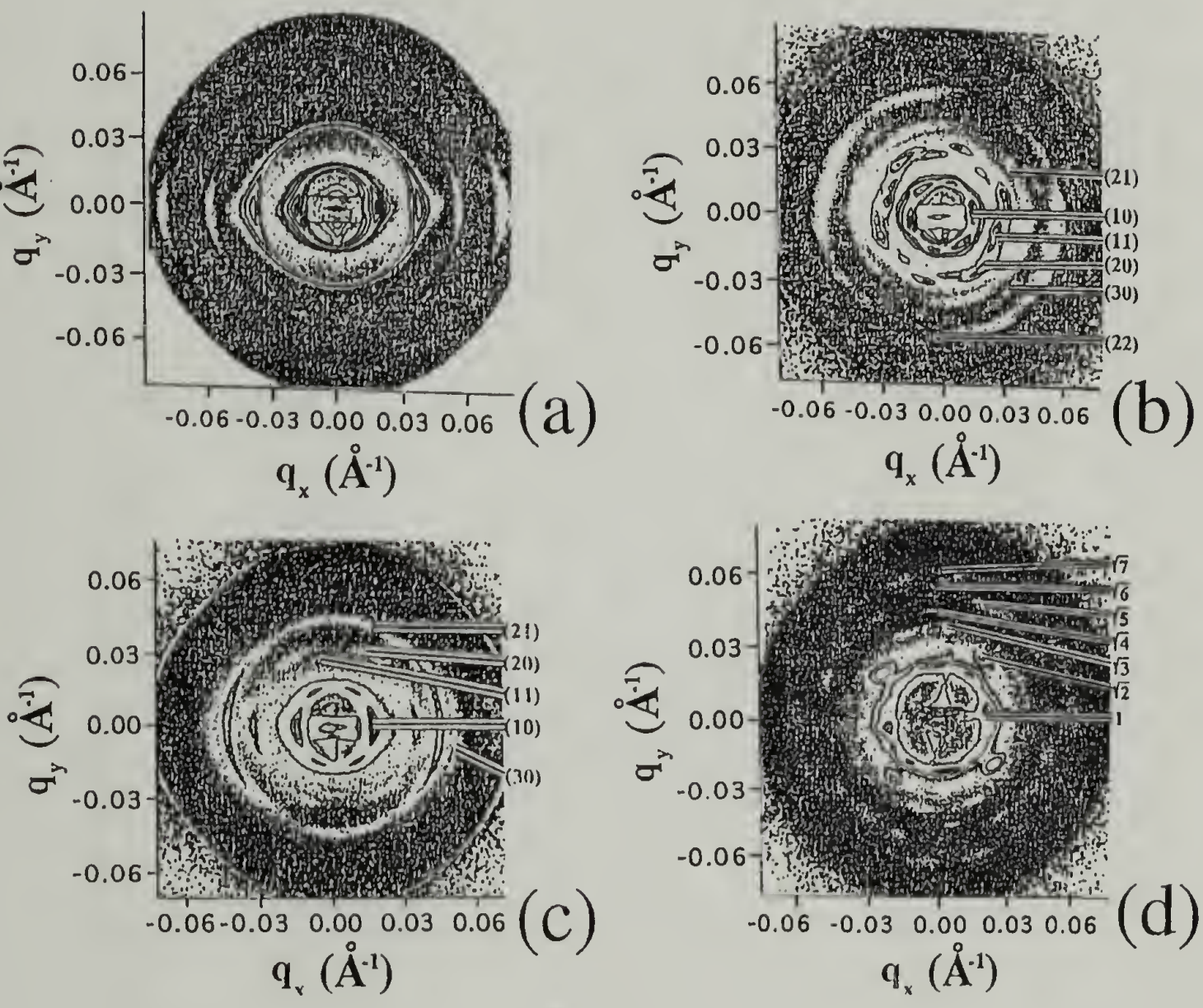


Figure 2.7: 2-D SAXS data of samples containing a high degree of long range order of their respective microstructures which produces highly anisotropic scattering patterns. a) $I_2S$-3 ($\phi_s = 0.62$) showing the first four orders of the lamellar long period. b) $I_2S$-4 ($\phi_s = 0.44$) showing an approximate [100] zone axis of hexagonally packed cylinders c) $I_2S$-5 ($\phi_s = 0.36$) also showing the [100] hexagonal zone axis d) $I_2S$-6 ($\phi_s = 0.17$) 4-fold symmetry of an approximate [100] zone axis of the bcc array of spheres.

film. A hexagonally packed cylindrical structure with a remarkable degree of long range order is clearly evident in TEM micrographs of $I_2S$-4 and $I_2S$-5. Figure 2.8a is a TEM image taken from sections microtomed perpendicular to the surface of the $I_2S$-4 film. Figure 2.8b is a projection through a section microtomed parallel with the surface of the same film yielding a projection perpendicular to the cylinder axes which appear as long stripes. SAXS data collected with the sample film surfaces perpendicular to the incident beam produced uniaxial arc patterns with the same $q_n/q^*$ ratio obtained in Figure 2.7b and 2.7c indicative of scattering perpendicular to aligned, hexagonally packed cylinder axes. Strong optical birefringence was observed in the sample films consistent with the assigned cylindrical morphology.

Note the marked difference in degree of long range order between cylinderforming samples with PS (graft blocks) forming the cylindrical domains, samples $I_2S$-4 and $I_2S$-5, and PI (two chains per molecule) forming the cylindrical domains, sample $I_2S$-1. We stress that all these samples were cast, annealed, and observed in exactly the same way, so differences in the observed long range order are not likely to be due to different sample histories. This difference in the quality of long range order for cylinder forming simple graft samples on opposite sides of the morphology diagram (Figure 2.1) is a result of the asymmetry in morphological behavior vs. volume fraction for $\varepsilon$ near 2. Samples $I_2S$-4, $I_2S$-5 and $I_2S$-1 all have higher PS volume fractions than linear PS-PI diblocks forming the same type of morphology. In the cases of $I_2S$-4 and $I_2S$-5 this results in relatively short PI chains forming the coronas covering the outsides of the PS cylinders. Not only is the PI volume fraction of these corona blocks smaller than the PI volume fraction in a linear PS-PI diblock forming PS cylinders, but the reduced PI volume is divided between two chains per molecule. On the other side of the morphology diagram, the greater volume fraction of the PS graft results in a corona of long PS blocks, much longer than the PS block of a

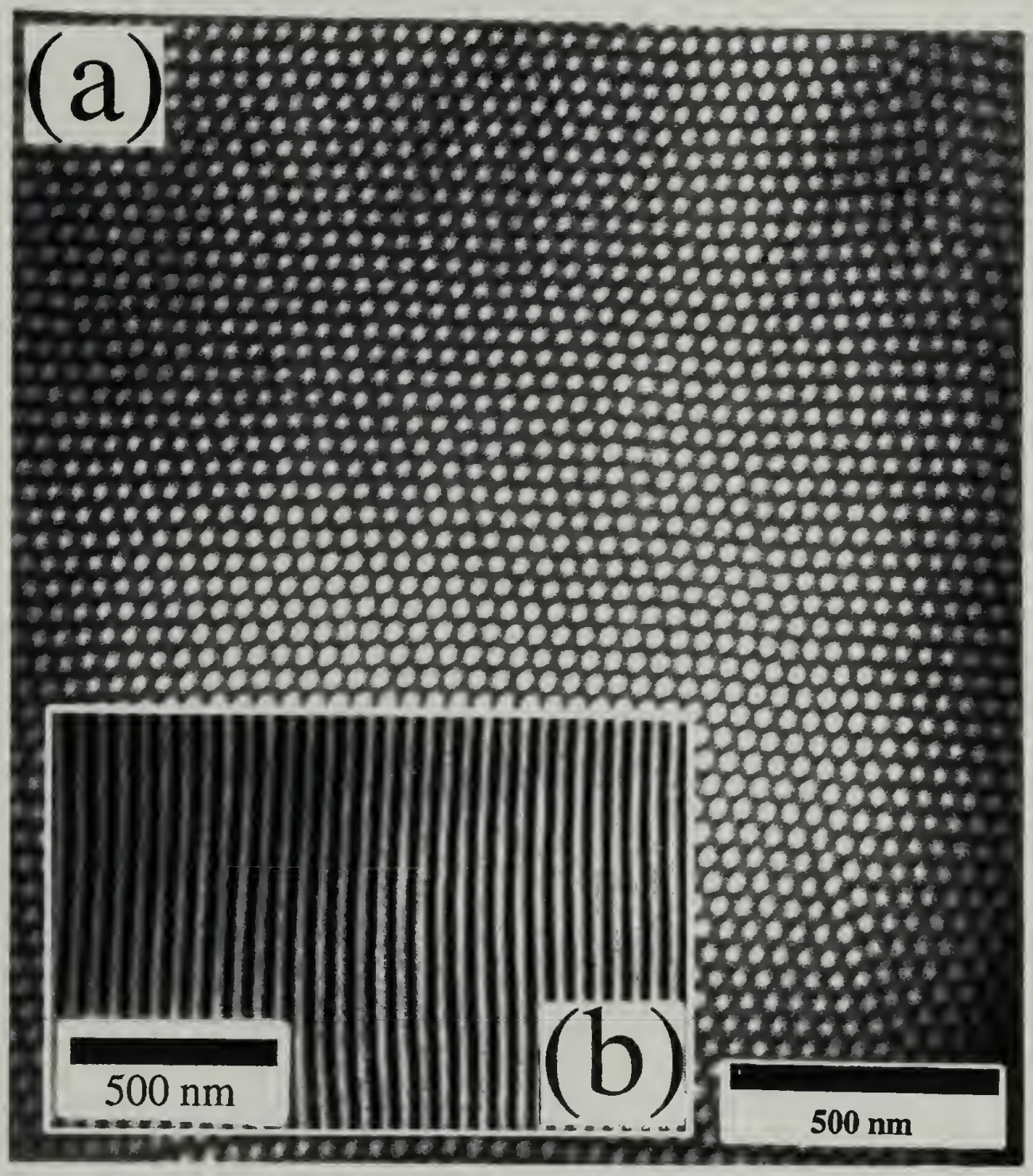


Figure 2.8: TEM micrographs of $I_2S$-4 ($\phi_s = 0.44$) a) taken from sections microtomed perpendicular to the film surface containing an end-on, hexagonal projection of the cylindrical microstructure. b) taken from sections microtomed parallel with the film surface contain a projection perpendicular to the cylinder axes.

PS-PI diblock of the same molecular weight forming PI cylinders. The packing of the cylindrical micelles onto a hexagonal lattice with long range order must be controlled by the interaction of neighboring cylinders through their outer, corona blocks. The cylinders in samples $I_2S$-4 and $I_2S$-5 interact through coronas of relatively short and highly stretched PI chains. This is a much stiffer and more precise interaction than that between the longer and less stretched PS corona chains in $I_2S$-1, resulting in greater long range order for $I_2S$-4 and $I_2S$-5.

The simple graft copolymer series is completed by samples $I_2S$-6 ($\phi_s = 0.17$) and $I_2S$-7 ($\phi_s = 0.08$) which both formed a cubic array of PS spheres in a matrix of PI. The cast and annealed films displayed no optical birefringence, consistent with a cubic symmetry having no form birefringence. Both the 4-fold [100] projection and the hexagonal [111] projection of the $I_2S$-6 cubic unit cell are shown in Figure 2.6b and c. The TEM images for $I_2S$-7 are similar. Figure 2.7d is a SAXS pattern taken from an approximate [100] zone axis of the cubic structure. It displays a characteristic 4-fold symmetry of this projection obtained with the surface of the bulk film perpendicular to the x-ray beam. The $q_n/q^*$ ratios of 1, $\sqrt{2}$, $\sqrt{3}$, and $\sqrt{4}$ for the first four reflections are consistent with both body-centered cubic (110, 200, 211, and 220 for bcc) and simple cubic (100, 110, 111, and 200 for sc) symmetries. However, the long-range order is limited due to unavoidable grain boundaries and dislocations thereby broadening reflections beyond the fourth reflection. The seventh reflection is the first to differ between sc and bcc, producing the *220* at a $q_n/q^*$ of $\sqrt{8}$ for sc and the *321* at $q_n/q^*$ of $\sqrt{7}$ for bcc. To the best of our ability to measure the spacing of the weak seventh reflection, we find a $q_n/q^*$ ratio of approximately $(7.3\pm0.4)^{1/2}$ which seems to favor the bcc structure over sc. Chain packing considerations in the Wigner-Seitz cell around each spherical micelle and previous experimental results for linear diblock and starblock copolymers[7,25,26] suggest a bcc packing of spheres as more likely than sc. Sample $I_2S$-7

did not contain the same degree of long range order in the spherical microstructure giving rise to the isotropic SAXS pattern displayed in Figure 2.3.

## 2.5 Conclusions

Our experimental results confirm that the architectural asymmetry of the $I_2S$ block copolymers results in a large asymmetry relative to volume fraction in the equilibrium phase behavior. The exact shift from what is found in linear AB diblock materials of the same volume fractions can be directly seen in the phase diagram in Figure 2.1. The diagram collapses onto the strong segregation phase behavior of conformationally symmetric linear diblocks at $\varepsilon = 1$. $I_2S$-3 and $I_2S$-7 are the only samples displaying the phase behavior of their diblock analogues exhibiting lamellar and spherical microstructures respectively. However, all other samples are shifted into new phase behavior unobtainable for that volume fraction in a diblock architecture. Theoretically, $I_2S$-2 is shifted from the center of the diblock cylindrical phase very close to the bicontinuous/lamellar phase boundary while experimentally the microstructure is microphase separated into worm-like micelles which are not arranged on a lattice. This microphase separated but disordered morphology occurs at a composition (81 vol. % of the PS graft) which is predicted by Milner's theory to be near the transition to the first structure which requires the two PI chains to be on the concave side of the interface. These results indicate how molecular architecture provides another controllable parameter besides the respective block volume fractions to manipulate the morphology of the bulk.

## 2.6 References


(1) Hashimoto, T.; Todo, A.; Itoi, H.; Kawai, H. "Domain-Boundary Structure of Styrene-Isoprene Block Copolymer Films Cast from Soutions. 2. Quantitative Estimation of the Interfacial Thickness of Lamellar Microphase Systems." *Macromolecules*, **10**, 384 (1977).

(2) Helfand, E.; Wasserman, Z. R. "Strong-Segregation Theory of Microphase Separated Block Copolymers." *Macromolecules*, **9**, 879 (1976).

(3) Bates, F. S.; Berney, C. V.; Cohen, R. E. "Microphase Structure of Solvent-Cast Diblock Copolymers and Copolymer/Homopolymer Blends Containing Spherical Microdomains." *Macromolecules*, **16**, 1101 (1983).

(4) Winey, K. I.; Thomas, E. L.; Fetters, L. J. "Isothermal Morphology Diagrams for Binary Blends of Diblock Copolymer and Homoploymer." *Macromolecules*, **25**, 2645 (1992).

(5) Milner, S. T. "Chain Architecture and Asymmetry in Copolymer Microphases." *Macromolecules*, **27**, 2333 (1994).

(6) Hadjichristidis, N.; Iatrou, H.; Behal, S. K.; Chludzinski, J. J.; Disko, M. M.; Garner, R. T.; Liang, K. S.; Lohse, D. J.; Milner, S. T. "Morphology and Miscibility of Miktoarm Styrene-Diene Copolymers and Terpolymers." *Macromolecules*, **26**, 5812 (1993).

(7) Olmsted, P. D; Milner, S. T. "Strong-Segregation Theory of Bicontinuous Phases in Block Copolymers." *Physical Review Letters*, **72**, 936 (1994).

(8) Milner, S. T.; Witten, T. A.; Cates, M. E. "Theory of the Grafted Polymer Brush." *Macromolecules*, **21**, 2610 (1988).

(9) Kinning, D. J.; Winey, K. I.; Thomas, E. L. "Structural Transitions from Spherical to Nonspherical Micelles in Blends of Poly(styrene-butadiene) Diblock Copolymer and Polystyrene Homopolymers." *Macromolecules*, **21**, 3502 (1988).

(10) Morton, M.; Fetters, L. J. "Anionic Polymerization of Vinyl Monomers." *Rubber Chemistry and Technology*, **48**, 359 (1975).

(11) Roovers, J.; Toporowski, P. "Synthesis of High Molecular Weight Ring Polystyrenes." *Macromolecules*, **16**, 843 (1983).

(12) Mays, J. W. "Synthesis of 'Simple Graft' Poly(isoprene-*g*-styrene) by Anionic Polymerization." *Polym. Bull.*, **23**, 247 (1990).

(13) Iatrou, H.; Siakali-Kioulafa, E.; Hadjichristidis, N.; Roovers, J.; Mays, J. W. "Hydrodynamic Properties of Model Three-Miktoarm Star Copolymers." *J. Polym, Sci., Polym. Phys.*, **33**, 1925 (1995).

(14) Brandrup, J., Immergut, E. H., Eds. *Polymer Handbook*, 3rd ed.; John Wiley & Sons: New York, 1989.

(15) Floudas, G.; Hadjichristidis, N.; Iatrou, H.; Pakula, T.; Fischer, E. W. "Microphase Separation in Model 3-Miktoarm Star Copolymers (Simple Graft) and Terpolymers. 1. Statics and Kinetics." *Macromolecules*, **27**, 7735 (1994).

(16) Pispas, S.; Mays, J. W. unpublished data on glass transition of $A_2B$ copolymers.

(17) Bras, W.; Derbyshire, G. E.; Ryan, A. J.; Mant, G. R.; Felton, R. A.; Lewis, R. A; Hall, C. J.; Greaves, G. N. "Synchrotron X-Ray Camera for Simultaneous Wide-Angle and Small-Angle Scattering." *Nucl. Instrum. Methods Phys. Res.*, **A326**, 587 (1993).

(18) Lin, C. C.; Jonnalagadda, S. V.; Kesani, P. K.; Dai, H. J.; Balsara, N. P. "Effect of Molecular Structure on the Thermodynamics of Block Copolymer Melts." *Macromolecules*, **27**, 7769 (1994).

(19) Gehlsen, M. D.; Bates, F. S. "Conformational Asymmetry in Poly(vinylcyclohexane) Containing Diblock Copolymers." *Macromolecules*, **27**, 3611 (1994).

(20) Folkes, M. J.; Keller, A. "The Birefringence and Mechanical Properties of a 'Single Crystal' from a Three Block Copolymer." *Polymer*, **12**, 222 (1971).

(21) Balsara, N. P.; Perahia, D.; Safinya, C. R.; Tirrell, M.; Lodge, T. P. "Birefringence Detection of the Order-Disorder Transition in Block Copolymer Liquids." *Macromolecules*, **25**, 3896 (1992).

(22) Thomas, E. L.; Alward, D. B.; Kinning, D. J.; Martin, D. C.; Handlin Jr., D. L.; Fetters, L. J. "Ordered Bicontinuous Double-Diamond Structure of Star Block Copolymers: A New Equilibrium Microdomain Morphology." *Macromolecules*, **19**, 2197 (1986).

(23) Hashimoto, T.; Koizumi, S.; Hasegawa, H.; Izumitani, T.; Hyde, S.T. "Observation of 'Mesh' and 'Strut' Structures in Block Copolymer/Homopolymer Mixtures." *Macromolecules*, **25**, 1433 (1992).

(24) Pochan, D. J.; Gido, S. P.; Pispas, S.; Mays, J. W. "Morphological Transitions in an $I_2S$ Simple Graft Block Copolymer: From Folded Sheets to Folded Lace to Randomly Oriented Worms at Equilibrium." *Macromolecules*, **29**, 5099 (1996).

(25) Thomas, E. L.; Kinning, D. J.; Alward, D. B.; Henkee, C. S. "Ordered Packing Arrangements of Spherical Micelles of Diblock Copolymers in Two and Three Dimensions." *Macromolecules*, **20**, 2934 (1987).

(26) Sakurai, S.; Kawada, H.; Hashimoto, T.; Fetters, L. J. "Thermoreversible Morphology Transition between Spherical and Cylindrical Microdomains of Block Copolymers." *Macromolecules*, 26, 5796 (1993).

# CHAPTER 3

# MORPHOLOGICAL TRANSITIONS IN AN $I_2S$ SIMPLE GRAFT BLOCK COPOLYMER: FROM FOLDED SHEETS TO FOLDED LACE TO RANDOMLY ORIENTED WORMS AT EQUILIBRIUM

## 3.1 Abstract

A new equilibrium morphology consisting of randomly oriented worm-like micelles dispersed in a continuous matrix is observed in a neat, strongly segregated $I_2S$ simple graft block copolymer. The equilibrium nature of the worm phase is determined via a set of selective solvent casting and prolonged annealing experiments. Transmission electron microscopy (TEM) experiments on quenched samples allow a unique opportunity to directly observe the transition of a kinetically trapped, non-equilibrium folded-layer morphology, formed by casting the sample with a solvent selective for poly(isoprene) (PI), into the equilibrium, randomly oriented worm phase through an intermediate folded-lace morphology. The folded-lace intermediate is similar to the "mesh" structure previously observed by Hashimoto, *et al.* in starblock/homopolymer blends.[1] The simple graft block copolymer, formed by grafting a single poly(styrene) (PS) chain onto the center of a poly(isoprene) backbone, introduces a 2:1 PI/PS arm number asymmetry in the microphase separated state. The 0.81 volume fraction of the PS graft is theoretically predicted[2] to be the first volume fraction of graft large enough to force the two PI arms per molecule to the concave side of the PI/PS interface in the microphase separated state. This unique volume fraction, coupled with the novel graft architecture, seems to frustrate the system from choosing a lattice during the microphase separation process.

## 3.2 Introduction

By synthetically altering the architecture of block copolymers to form grafts one is able to divorce the strongly segregated phase behavior of amorphous block copolymers from its strict dependence on the relative volume fraction of the respective blocks. While the phase behavior of linear, conformationally symmetric diblocks is solely dependent on the relative volume fractions of the constituent blocks, manipulation of architecture allows additional control of the solid state, equilibrium morphology. By utilizing an $A_2B$, or "Y" shaped, simple graft architecture one is able to produce phase behavior unobtainable with linear diblock architecture at the same volume fractions. The molecules studied here are formed by connecting two poly(isoprene) chains to a terminally difunctional poly(styrene) chain, hence forming an $I_2S$ molecule. The 2:1 arm number asymmetry of PI to PS in the microphase separated state, as shown in Figure 3.1, has been found to skew the volume fraction dependence of the strongly segregated phase behavior to much higher PS volume fractions than found in diblock architecture.[3] In the Pochan, *et al.* $I_2S$ simple graft morphological survey an intriguing structure is observed at one particular composition in which the two PI blocks are just short enough to be confined to the concave side of the interface. This structure, formed by the neat graft block copolymer, consists of randomly oriented worm-like micelles (hereafter named the ROW phase) with PI in the cores and the grafted PS block material forming the continuous matrix. While Kinning, Winey, and Thomas have reported a similar worm-like micelle phase in blends of diblock copolymers with homopolymers,[4] this structure has not been previously observed in neat block copolymers. In ABC triblocks Jung *et al.* have synthesized molecules with designed packing frustrations specifically to suppress the formation of long range order.[5] But the resulting bent cylinder "Banana" morphologies still form small grain-like regions of coherent domain orientation. In contrast, the ROW phase which we

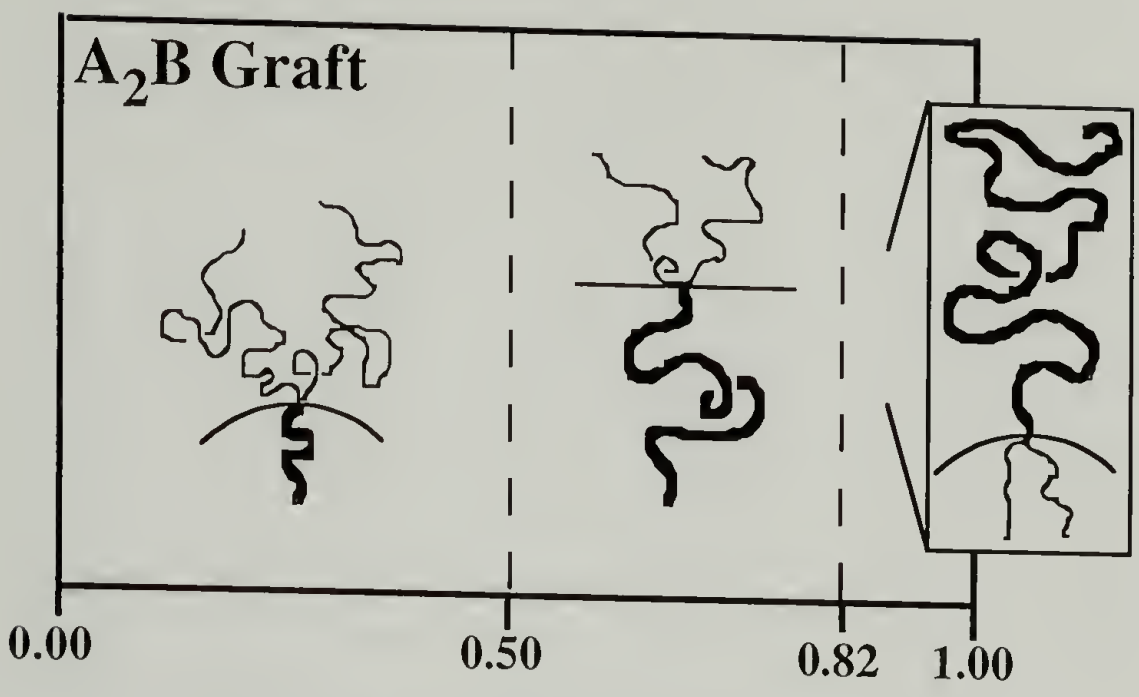


Figure 3.1: Schematic of the $A_2B$, or "Y", molecular architecture in the microphase separated state. The two A chains per molecule are calculated to reside on the convex side of a curved A/B interface until much higher volume fractions than what is experimentally found in diblock architecture. A curved A/B interface generically represents spherical, cylindrical, and bicontinuous morphologies while the flat interface represents a lamellar morphology.

observe in the $I_2S$ system is completely random in orientation. Figure 3.2 shows a Transmission Electron Microscopy (TEM) image of this morphology which appears as a random pattern of dark $OsO_4$ stained PI dots and short, often curved, line segments in a lighter PS matrix. The shape of a worm-like micelle projected in two dimensions is highly dependent on its orientation in three dimensions with respect to the incident electron beam. The inset in Figure 3.2 illustrates how TEM projections from a thin microtomed section of the ROW phase results in this type of image. Figure 3.3a and b is a tilt series at a higher magnification of an ultrathin section of the toluene-cast ROW phase. Spherical shaped projections of the PI micelles in 3.3a, which accompany more elongated worm-like structures, are merely projections perpendicular to thin cross-sections of the worm micelles. After 40° of tilt in 3.3b all of the PI micelles elongate perpendicular to the tilt axis thus revealing the worm-like nature of the entire system.

Figure 3.1 illustrates the chain packing considerations inherent in the microphase separation of $I_2S$ or "Y" shaped block copolymers. In the microphase separated state the two symmetric PI blocks are crowded on the same side of the PS/PI interface which leads to additional PI chain stretching. To compensate for the PI crowding there is an increased tendency for the interface to curve away from the PI blocks. This convexity provides more volume closer to the interface to pack the two PI chains. The two PI chains prefer to be on the convex side of a curved interface to significantly lower PI volume fractions than one observes in the corresponding diblocks. Or, looking at the situation from the point of view of the single PS graft, the windows in which the various morphologies are observed are shifted to higher volume fractions of the PS block.[2] Therefore, the morphology diagram, as shown in Figure 3.4, is markedly asymmetrical with respect to the two component volume fractions.

The diagram is generic in that within the parameter $\varepsilon = (n_a/n_b)(l_a/l_b)^{1/2}$ different architectures and chain statistics are accounted for. The number of arms one chooses, n of $A_a$ or n of $B_b$, can be varied. Also, differing chain statistics between blocks are

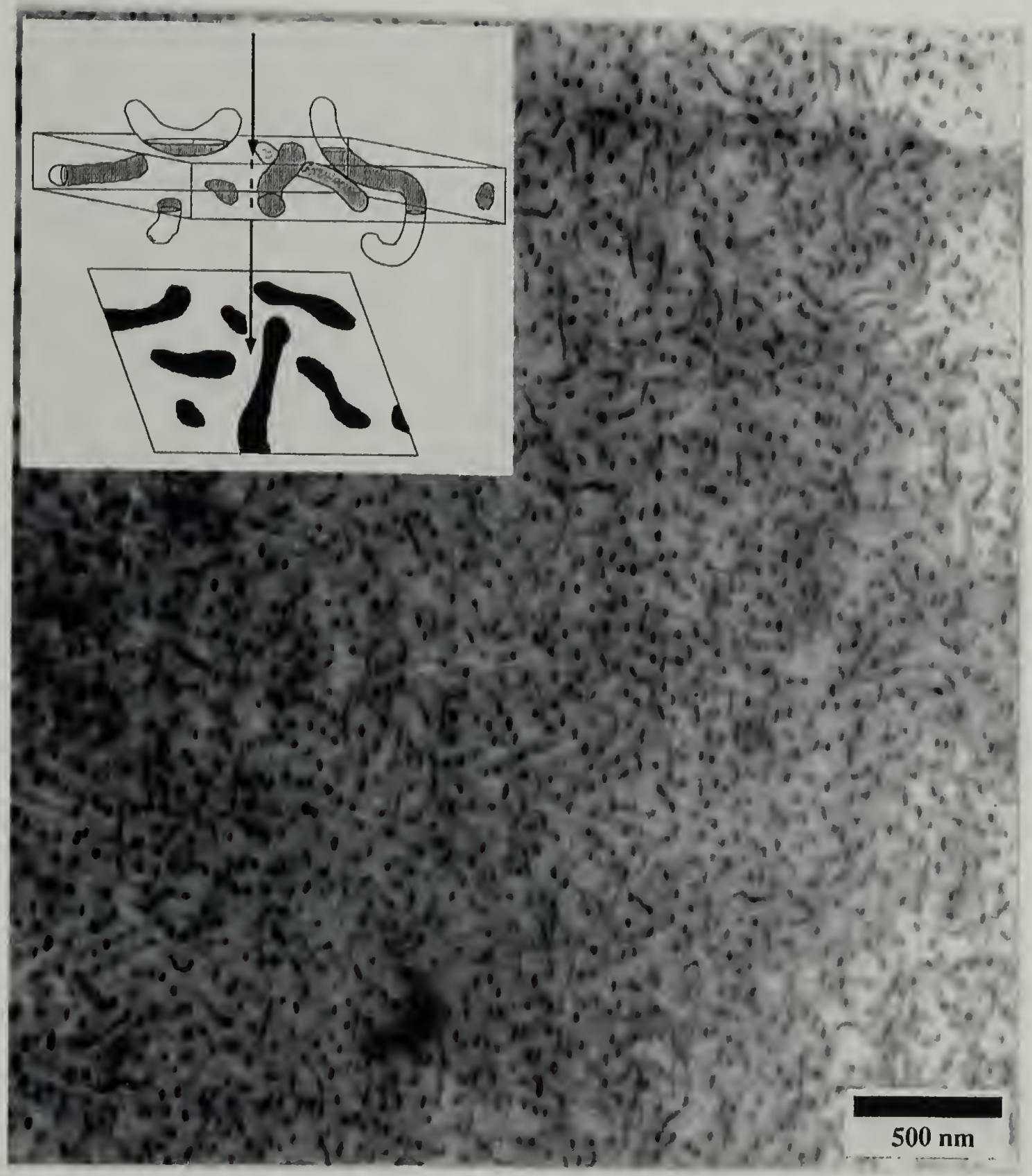


Figure 3.2: TEM micrograph of toluene-cast $I_2S$-81 annealed at 120°C for one week showing randomly oriented, dark PI worm-like micelles embedded in the PS graft matrix. Inset schematic showing the resultant 2-D TEM projection through a microtomed section of the randomly oriented, worm-like micelles.

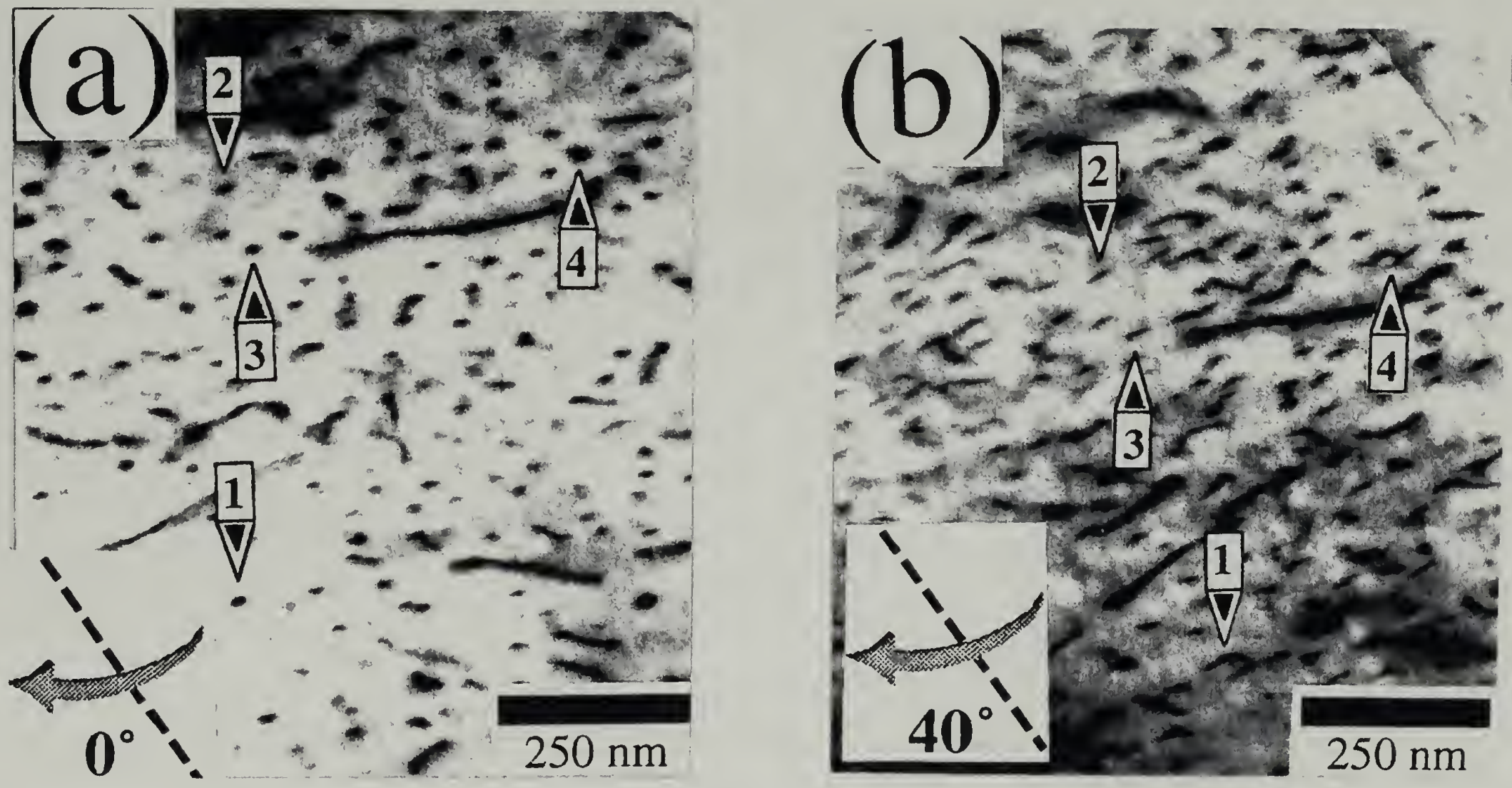


Figure 3.3: TEM tilt series of toluene-cast ROW phase. a) Ultrathin section at high magnification with 0° tilt. b) Same area tilted 40° about the tilt axis. Several transitions from spherical to worm-like projections are marked with numbered arrows in the micrographs.

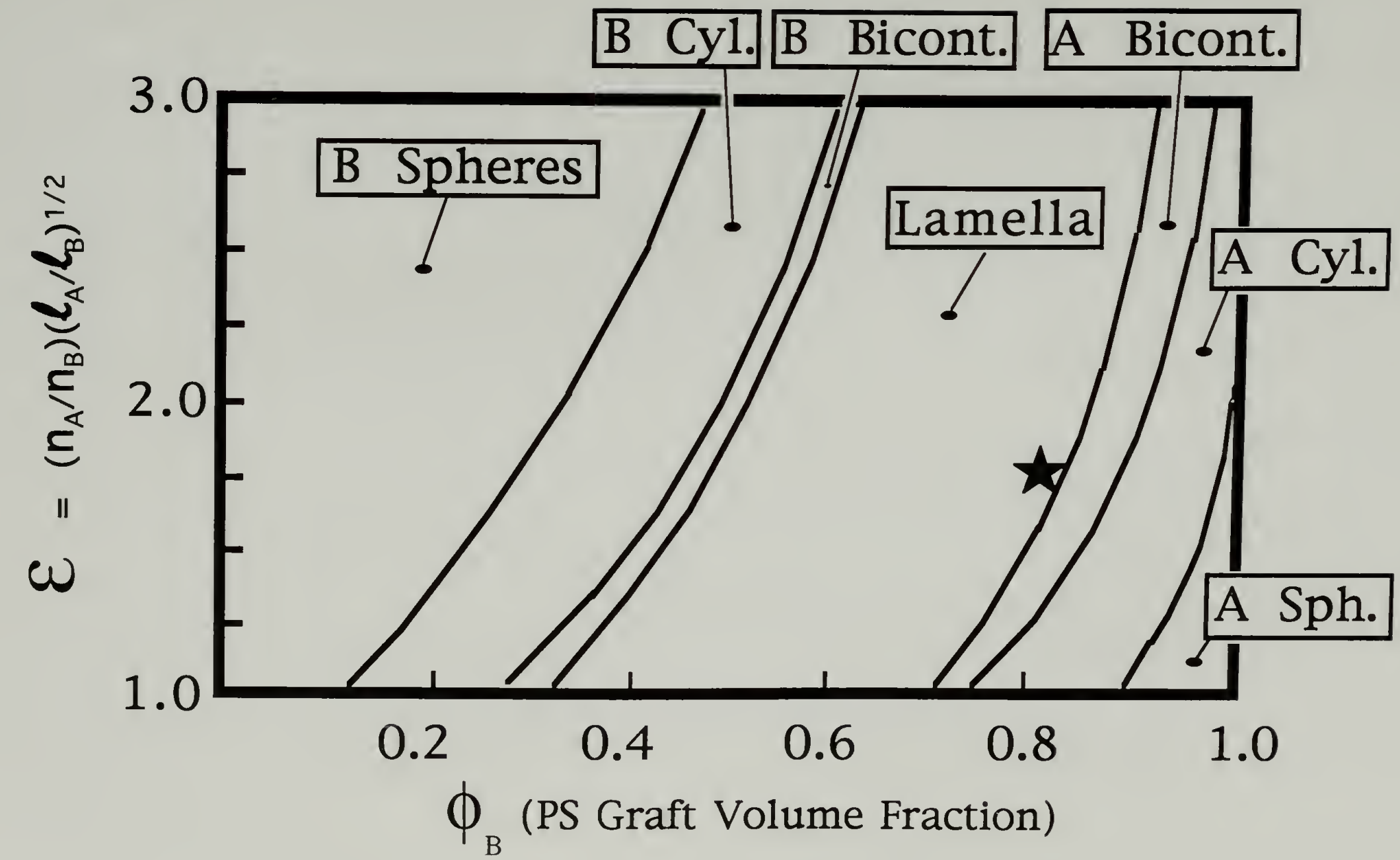


Figure 3.4: Theoretical phase diagram calculated by Milner. The ★ at $\varepsilon \sim 1.80$ represents sample $L_2S$-81 with $\phi_s = 0.81$.

represented in the square root ratios of $l_a$ and $l_b$ with $l_i = V_i / R_i^2 = v_i / b_i^2$ where $V_i$ and $R_i$ are the molecular volume and radius of gyration of the respective blocks and $v_i$ and $b_i$ are the segment volume and Kuhn length of the respective blocks. If the constituent blocks are conformationally symmetric then $\varepsilon$ is simply the ratio of the number of A and B arms in the molecule. For our PS-PI simple graft block copolymers, $\varepsilon \approx 1.8$ due to the statistical similarity of the PS and PI block materials.[3]

At $\varepsilon = 1$ the phase diagram models linear, AB diblock phase behavior with the phases being symmetric around $\phi_b = 0.5$. However, as one increases the arm number of one species relative to the other or varies the relative chain statistics of A and B the phase behavior becomes extremely asymmetric with volume fraction. Hadjichristidis *et al.*[6] recently characterized the bulk phase behavior of three $A_2B$ block copolymers or "miktoarm" blocks. The asymmetry of the graft architecture forced two samples , a 37 vol. % poly(styrene) "$I_2S$" graft (isoprene backbone and a single styrene graft emanating from the middle of that backbone) and a 40 vol. % (poly)styrene SIB miktoarm star (the rubbery phase consists of mixed isoprene and butadiene blocks), into cylindrical phases where the bulk morphology would be bicontinuous or lamellar respectively in diblock architecture analogs of the same molecular weight. All of the $I_2S$ samples in our previous study, with PS graft volume fractions ranging from 0.08 to 0.89, displayed the shifted morphology behavior predicted by theory *except* for $\phi_s = 0.81$ which forms the ROW phase.

According to Milner's theory, for $\varepsilon \approx 1.8$, at any $\phi_s$ above approximately 0.82 the two PI blocks of the $I_2S$ molecule should reside on the concave side of the PS/PI interface (see Figure 3.3). This is in contrast to diblock architecture where above approximately $\phi_s = 0.66$ a single PI block per diblock molecule is confined to the concave side of the interface.[7,8] Experimentally, our $I_2S$ sample at $\phi_s = 0.81$, hereafter referred to as $I_2S$-81, is very close to this calculated transition of the PI chains to the concave side. However, instead of forming the theoretically calculated bicontinuous

phase the system microphase separates into the ROW phase. The lateral crowding of the two PI chains per molecule causes increased chain stretching. The coupling of this crowding and subsequent stretching of the PI chains with the PI volume fraction being just low enough to force the PI chains to the concave side of the interface seems to frustrate the formation of a lattice in the system.

To test the equilibrium nature of the ROW phase in $I_2S$-81 a series of selective solvent casting and extended annealing experiments were performed. The results support the equilibrium nature of the observed worm-like phase as well as provide an unusual opportunity to visualize several stages in the phase transition from a selective solvent cast, non-equilibrium layered morphology into the final, equilibrium ROW phase.

## 3.3 Experimental

### 3.3.1 Sample Characteristics and Film Casting

The synthesis of $I_2S$ block copolymers and the subsequent characterization of their molecular weights, polydispersities, and molecular architectures, including the $\phi_s$ = 0.81 sample of interest in this paper, are described in another publication.[3] The sample studied in this work, $I_2S$-81, has a $M_n$=89,400 g/mol and $M_w$ of 90,800 g/mol as measured by membrane osmometry and LALLS respectively. $M_w/M_n$ = 1.04 while the wt. % of PS is 0.84 as measured by SEC and SEC-UV respectively. The PS graft is deuterated, so the $\phi_s$=0.81 was calculated at room temperature using $\rho$ = 1.14 g/ml$^3$ and $\rho$ = 0.91 g/ml$^3$ for d-PS and PI respectively.

Solid films approximately 1 mm thick of the $I_2S$ block copolymer were slowly cast from 5 wt. % polymer solutions in cyclohexane, a selective solvent for PI, and dioxane, a selective solvent for PS. The solubility, or Hildebrand, parameters, $\delta$, are 17 MPa$^{1/2}$ for the predominantly 1,4 addition PI and 16.8 MPa$^{1/2}$ for cyclohexane while PS and dioxane have values of 18 MPa$^{1/2}$ and 20 MPa$^{1/2}$ respectively indicating the

selectivity of cyclohexane for PI and dioxane for PS.[9,10] Casting was performed at room temperature, and the evaporation of solvent was controlled to form a solid film after 10-14 days. The films were given several more days at room temperature and atmospheric pressure and an additional several days under high vacuum at room temperature to allow residual solvent to evaporate.

### 3.3.2 Annealing Treatments and TEM Preparation

Several pieces of both the cyclohexane and the dioxane cast films were annealed for one week at 120 °C in a high vacuum oven. This annealing treatment is consistent with other experiments intended to drive sample cast from toluene, a non-preferential solvent, further toward equilibrium.[3] This type of annealing experiment has been found to allow morphologies formed by solvent casting to slightly enlarge their long spacing and their average grain size, hence, allowing the equilibrium lattice symmetry formed in the microphase separation process to simply reach an even more stable, minimum free energy state.[4,11-13]

Next, a set of prolonged annealing experiments at higher temperatures was performed on the cyclohexane prepared samples, both pre-annealed, as-cast samples and those which underwent the initial annealing treatment at 120°C mentioned above. In our other work[3] a series of seven $I_2S$ samples covering a wide range of volume fractions were found to resist oxidation after annealing in a high vacuum oven for a period of one week at 120°C. This was monitored via GPC experiments performed on the samples, including $I_2S$-81 studied in this work, both before they were solvent cast and after they were annealed. The pre-casting and post-annealing GPC traces were essentially identical revealing highly narrow molecular weight distributions (PDI < 1.04) with no detectable change in molecular weight. However, in an effort to eliminate any possible sample oxidation with prolonged annealing at higher temperatures the cyclohexane-cast $I_2S$-81 samples were first placed in glass ampules and evacuated on a

high vacuum line to approximately 0.1 μm ($10^{-4}$ Torr) pressure. Next, the entire system was purged with dehydrated, high purity Argon gas and subsequently evacuated. The evacuation and inert gas purge cycle was performed a total of three times per sample. The preparation was concluded by sealing the vials under high vacuum with a torch. The vacuum sealed ampules were then annealed for 20 days either at 125°C or 150°C. Sample purity after the long annealing process was tested by recasting two portions of the annealed $I_2S$-81 sample, one in toluene and the other in cyclohexane. The phase behavior obtained in both cases was the same as found by using virgin material. This indicates the limited degredative and oxidative effect of the extended annealing process on the $I_2S$-81 sample.

Estimated $\chi N$ values for the system at elevated annealing temperatures of 125° C to 150°C range from 62 to 83 while at room temperature $\chi N > 100$ [14-16] placing the system in the strong segregation limit (SSL) throughout the experiments. The large variability in $\chi N$ values is due to the various methods employed in the measurement and calculation of $\chi$: 1) homopolymer phase behavior studies, and 2) fitting of homogeneous diblock melt SAXS data to Leibler's calculated structure factor.[17] Compositional and molecular weight effects on $\chi$ are neglected, and while the $A_2B$ architecture has been calculated to have a small enlarging effect on $\chi N_s$ relative to linear diblocks of the same molecular weight[18] any effect at the much lower temperatures employed in these experiments would be small and not take the system out of the SSL.

All samples for transmission electron microscopy (TEM) were microtomed in a Reichert-Jung cryoultramicrotome. Sections approximately 300-600 Å thick were cut with a Diatome cryo diamond knife at a sample temperature of -110°C and a knife temperature of -90°C. The sections were stained in $OsO_4$ vapors for four hours. Bright-field TEM experiments were performed on a JEOL 100CX electron microscope operated at 100kV accelerating voltage.

## 3.4 Results and Discussion

### 3.4.1 Selective Solvent Cast/Unannealed

Figure 3.5 is indicative of the lamellar-like morphology formed when $I_2S$-81 is cast with cyclohexane, a selective solvent for PI. The samples producing this morphology were cast from solution but were not thermally annealed prior to microtoming and TEM imaging. As the microdomains of PS and PI form during the casting from cyclohexane the solvent is partitioned unequally between the microdomains. Therefore, the PI volume fraction is effectively larger at the point of PS microphase separation, pushing the morphology into the lamellar region of the $I_2S$ phase diagram. When the remaining solvent evaporates from the PI phase, the neat $I_2S$ block copolymer is kinetically trapped at room temperature in a non-equilibrium lamellar phase.

It is interesting to note that the lamellar microdomains in Figure 3.5 differ somewhat in morphology from lamellar structures produced in PS-PI block copolymers by cooling from the melt or casting from a non-preferential solvent such as toluene. The morphology of the cyclohexane cast samples resembles sheets of cloth that have been folded back and forth. We postulate that this folded sheet morphology arises because the block copolymer in selective solvent microphase separates by first forming sheet-like micelles with solvent poor PS layers separated by solvent rich PI layers. These sheet-like micelles initially may be separated by a fair amount of solvent. However, when the cyclohexane is removed to produce the kinetically trapped morphology shown in Figure 3.5 the previously formed sheet-like micelles compact to fill space and, in so doing, may fold back and forth.

### 3.4.2 Intermediate Folded Lace Structure

Annealing experiments allowed the kinetically trapped, folded-sheet lamellar structure to relax into its equilibrium structure which we postulate to be the ROW

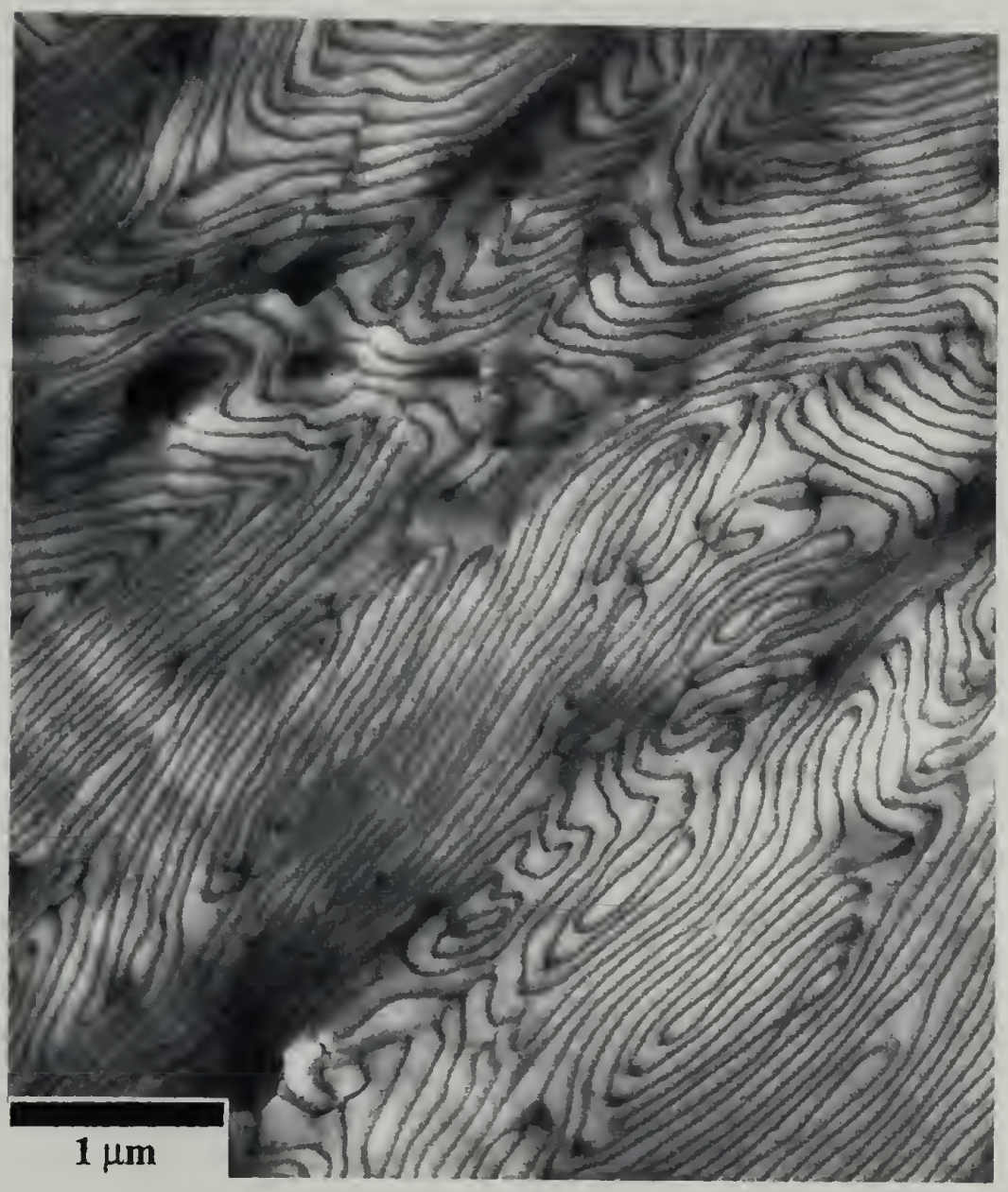


Figure 3.5: TEM micrograph of cyclohexane-cast $I_2S$-81. The kinetically trapped, non-equilibrium morphology consists of alternating dark layers of PI and light layers of PS.

phase. The folded lamella cyclohexane-cast samples which were annealed at 120°C for one week transformed into an intermediate structure between the folded-sheet lamellar structure and the (assumed to be) equilibrium worm phase. This quenched intermediate morphology, which we refer to as folded-lace, is shown in Figure 3.6 and Figure 3.7a and b. The PI layers of the folded lamella are observed to be perforated by numerous channels connecting the PS layers on either side. Figure 3.6 is a more global micrograph revealing the similarity of the folded-lace microstructure to the unannealed lamellar morphology in Figure 3.5. Figure 3.7a is an enlargement of a projection parallel with the layers of the folded lace structure. The dark spots within the dark PI layers are projections along the axes of the PI struts which constitute the lace structure. Figure 3.7b is a projection more normal to the lacy PI layers displaying the characteristic lace microstructure within a PI layer. The hole size of the lace seems to vary somewhat throughout the layers indicative of the intermediate, non-equilibrium nature of the structure. The observation of this intermediate morphology allows direct insight into the relaxation mechanism of the kinetically trapped, non-equilibrium structure into its final, equilibrium form. This transition can best be explained by employing the idea that the block copolymer molecular architecture and volume fractions prescribe a natural or preferred interfacial curvature. This concept has been widely used in modeling the structures of micelles and microemulsions involving small molecule amphiphiles.[19-21] In the strong segregation limit (SSL) the preferred interfacial curvature determines the shape of the Gaussian wedge that describes the conformation of the block copolymer chain in the microphase separated state.[22] This conformation, and thus the preferred interfacial curvature, is determined by the minimization of the sum in interfacial enthalpy and chain stretching entropy components of the free energy under the constraints that the chains must fill space to uniform density. The observation of the worm-like micelle structure in the $I_2S$ block copolymer at equilibrium indicates that the system prefers a curved interface with the two PI blocks on the concave side.


Figure 3.6: TEM micrograph of cyclohexane-cast $I_2S$-81 annealed at 120°C for one week. The sample displays the intermediate structure of dark PI layers of folded-lace embedded in a continuous light PS matrix.

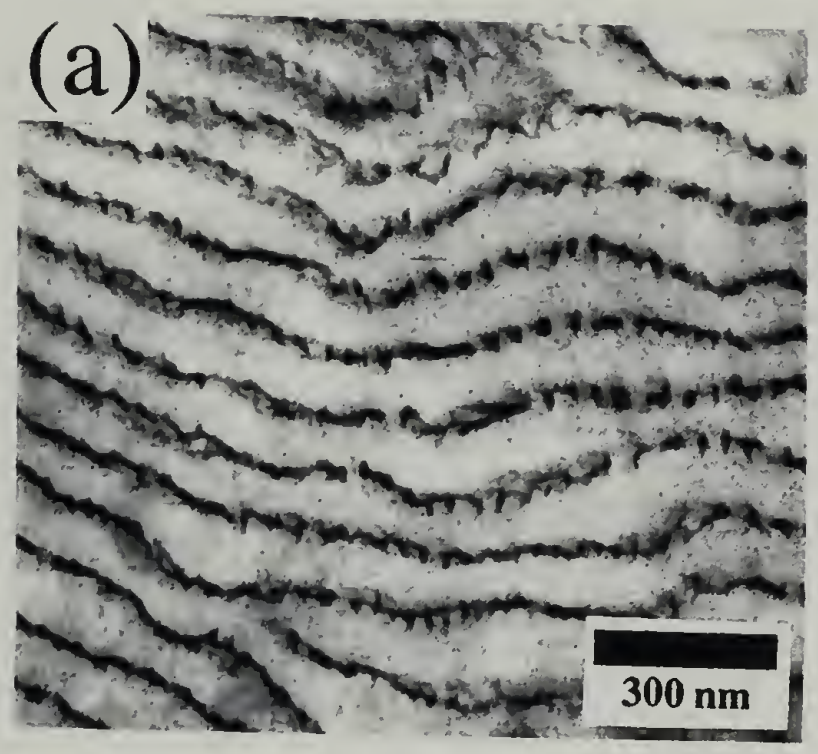


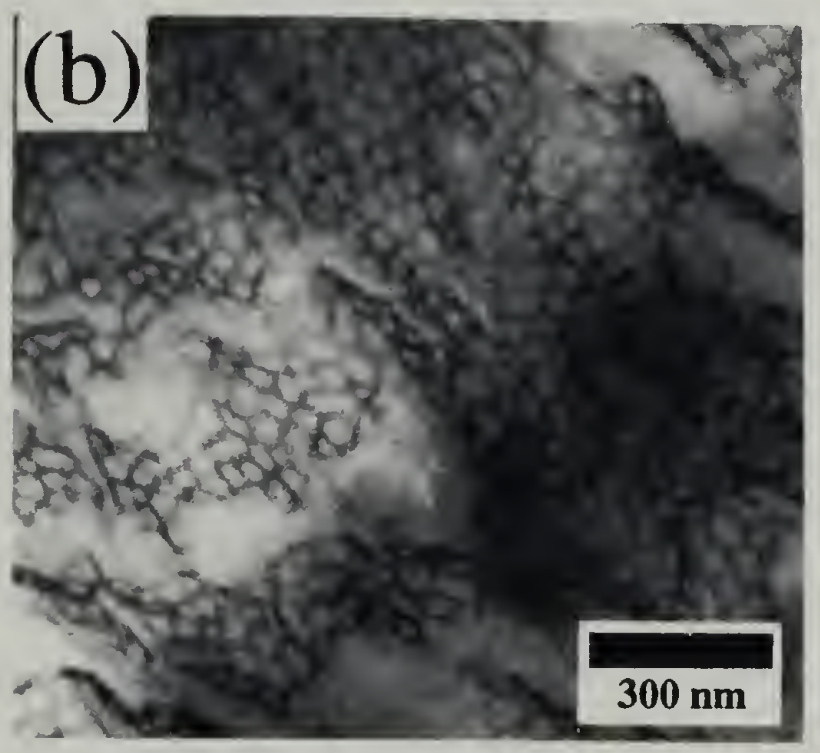


Figure 3.7: TEM micrographs of cyclohexane-cast $I_2S$-81 annealed at 120°C for one week at a high magnification displaying a projection parallel to the layers of folded-lace in (a) and displaying a projection predominantly perpendicular to the folded-lace in (b).

The kinetically trapped, folded sheet lamellar system, produced by casting in a selective solvent, forces the $I_2S$ molecules to accommodate a flat interface. Since this is not the preferred interfacial curvature for these molecules the sum of interfacial and chain stretching energies will not be minimized. These non-equilibrium chain conformations provide the stored energy that drives the transition back to worm-like micelles once the system is heated in the vacuum oven and thus given the mobility to rearrange.

The first annealing temperature employed, 120°C, is high enough to allow the system molecular mobility and still put the system in the strong segregation regime. Thus, the system does not have the option of disordering and reforming the equilibrium structure. Instead, the system must find a kinetic pathway for the transition from lamella to the ROW phase that keeps the strongly segregated interface intact except for localized, discontinuous breaks or jumps. The TEM micrographs in Figure 3.6 and Figure 3.7 indicate how this is accomplished. Upon annealing, the local driving force for each chain to experience a preferred interfacial curvature with the PI chains on the concave side results in a undulation of the lamellar layers. This undulation builds in amplitude until the PI layers actually become perforated by PS channels. The point at which interfacial undulations poke through the PI layers to form holes represents a localized discontinuous break in the otherwise continuously deforming and evolving interfacial structure. The PI branches which separate the holes in the PI layers relax and become like a mesh or lace of interconnected cylinders. In so doing they approach their preferred interfacial curvature.

Several groups have observed equilibrium morphologies in different systems similar to the folded-lace intermediate structure. In their study of order-order transitions in low molecular weight diblock copolymers, Khandpur, *et al.*[23] observed an equilibrium "hexagonally perforated lamellar" phase, or HPL, in the weakly to intermediately segregated (high temperature and low $\chi N$) regime. The HPL phase consists of alternating layers of PI and PS in which the PS layers are perforated by PI

channels in hexagonal symmetry. Disko, *et al.*[24] have observed a "catenoid lamellar" phase, identical in structure to the HPL phase, in a strongly segregated blend of PS/PI diblock and PS homopolymer with the PS forming the channels through the PI layers. Also in a blend system of PS/PI, specifically utilizing $(AB)_n$ four arm starblock copolymers and PS homopolymer, Hashimoto, *et al.*[1] observed a "mesh" phase. This mesh phase most resembles the folded-lace structure in that the PS channels through the alternating PI layers don't occur in a hexagonal symmetry and fluctuate slightly in shape and size. While all of these morphologies resemble the folded-lace structure observed in this work, the folded-lace is inherently thermodynamically unique. All of the above phases represent *equilibrium* states of the respective systems whether they are weakly segregated, neat diblocks at high temperatures or strongly segregated blends at room temperature. To our knowledge, a quenched, *intermediate* layered-lace microstructure has never been observed in a neat, strongly segregated block copolymer system.

### 3.4.3 Equilibrium ROW Morphology

The prolonged, high temperature annealing experiments conducted on the cyclohexane-cast samples allow the observation of the full transition; folded-sheets, through folded-lace, and eventually all the way back to the randomly-oriented worm phase, or ROW. The prolonged annealing at 125°C and 150°C for 20 days allowed sufficient time and thermal energy for the system to relax into its equilibrium worm-like structure and erase the kinetically trapped non-equilibrium chain conformations. Figure 3.8 is a TEM micrograph of the cyclohexane-cast material after the extended annealing treatment at 125°C. The results of the 150°C annealing treatment are identical to the behavior represented in Figure 3.8. The entire morphological transformation is schematically represented in Figure 3.9. Originally, the samples displayed the folded lamellar morphology as shown in Figure 3.5. Identical results were also obtained for

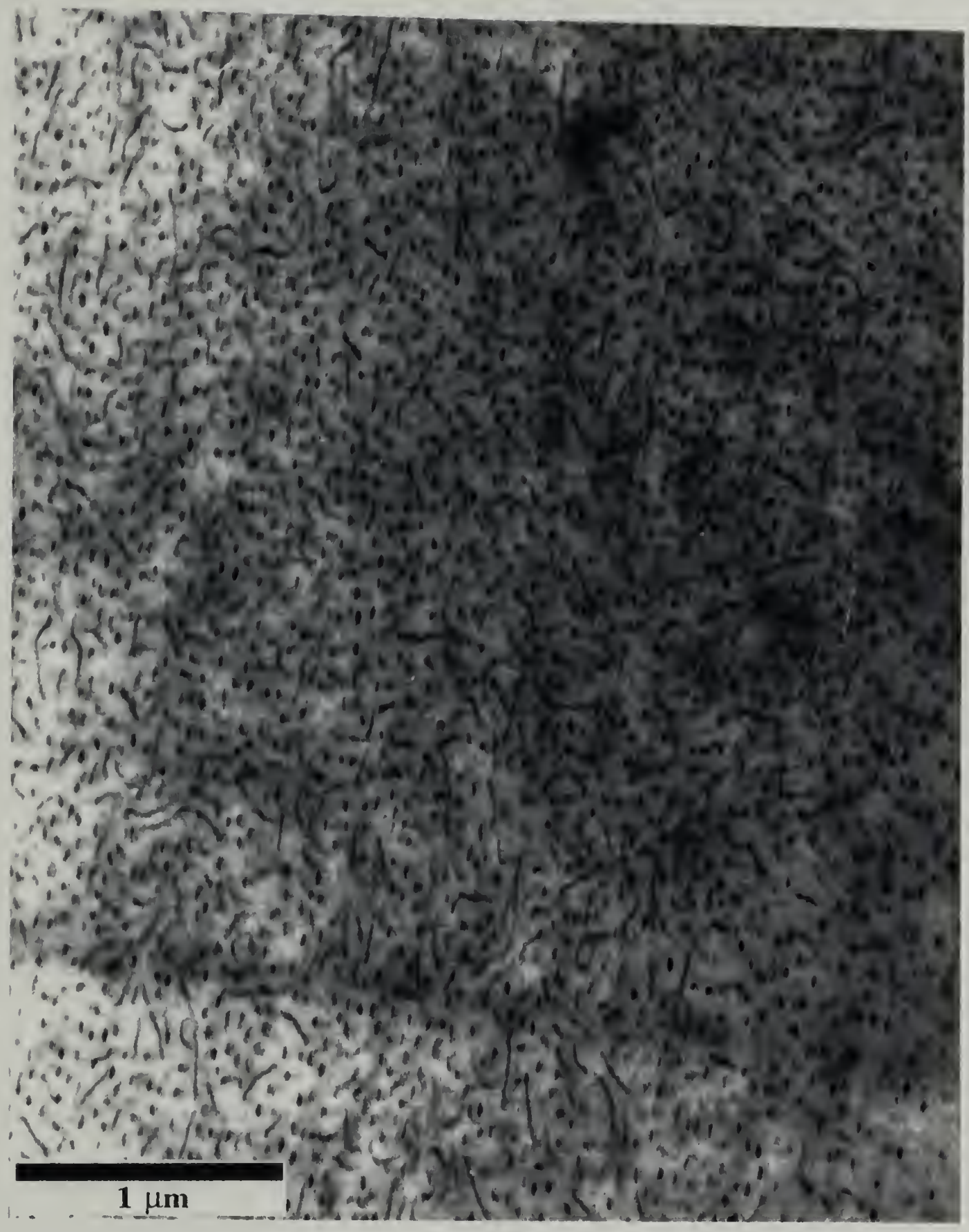


Figure 3.8: TEM micrograph of cyclohexane-cast $I_2S$-81 displaying the randomly oriented worm, or ROW, phase after annealing at 125°C for 20 days (also representative of the samples annealed at 150°C).

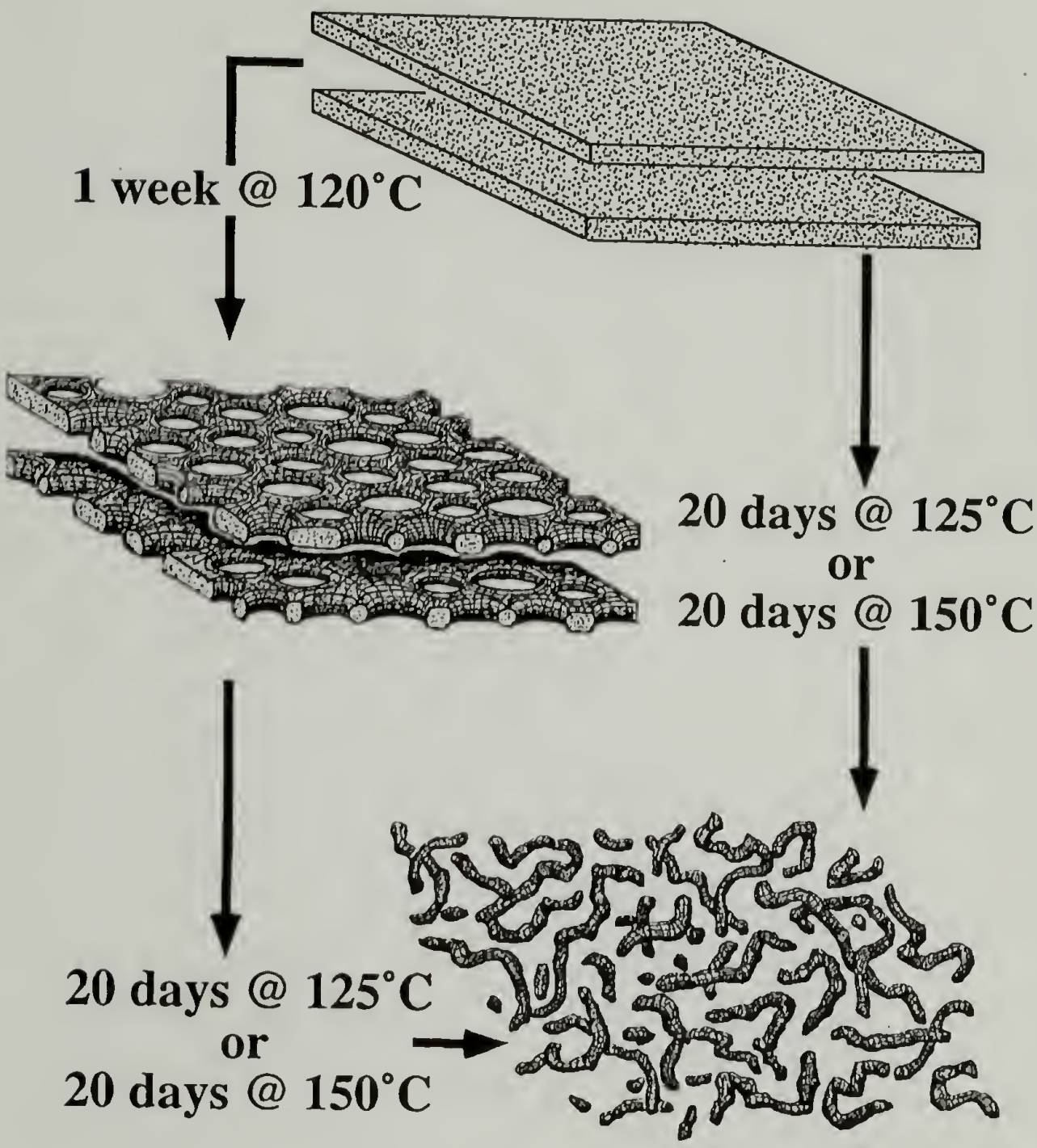


Figure 3.9: Schematic of the entire $I_2S$-81 morphological transition - selective solvent cast alternating layers of PI and PS through the folded-lace intermediate and finally reaching the ROW equilibrium phase.

folded-lace intermediate samples which were already previously annealed at 120°C for one week. Both the folded-lamellar structure and the intermediate folded-lace structure transformed into ROW phases almost identical to that formed when cast and annealed from the non-preferential solvent toluene. The PI worms produced by annealing the folded sheet structure appear more uniform in their shape and distribution in space since they originated from the well ordered, non-equilibrium layered structure as opposed to a non-preferentially solvated, homogeneous state. The transformation of both the original folded-lamellar structure and the folded-lace intermediate into essentially identical ROW phases supports the equilibrium nature of this novel, randomly oriented block copolymer phase.

Figure 3.10 is a TEM micrograph of dioxane-cast $I_2S$-81, both before and after the initial annealing treatment at 120°C for one week. The system microphase separated into a spherical micelle structure with dark PI spherical domains lying in a continuous matrix of PS. Just as in the cyclohexane-cast sample, as the system microphase separated the solvent was partitioned unequally between the PS domains and PI domains. Therefore, the PS microphase had an effectively larger volume fraction due to its swelling by the selective solvent forcing the PI blocks into the cores of the spherical micelles. When the remaining solvent evaporated the morphology was kinetically trapped somewhere within the spherical region of the phase diagram in Figure 3.4. However, this spherical non-equilibrium phase is unlike the non-equilibrium cyclohexane-cast samples. Because the selective solvent cast PI domains make up a dispersed structure it is essentially impossible for them to link together to form a less dispersed morphology such as cylinders, worms, or lamella even though such a transition might be energetically favorable. The PS coronas of these spherical micelles screen the PI cores from one another preventing them from joining together to produce more continuous PI domain structures. A thermoreversible order-order transition has been observed between cylinders and spheres in a weakly to intermediately segregated,

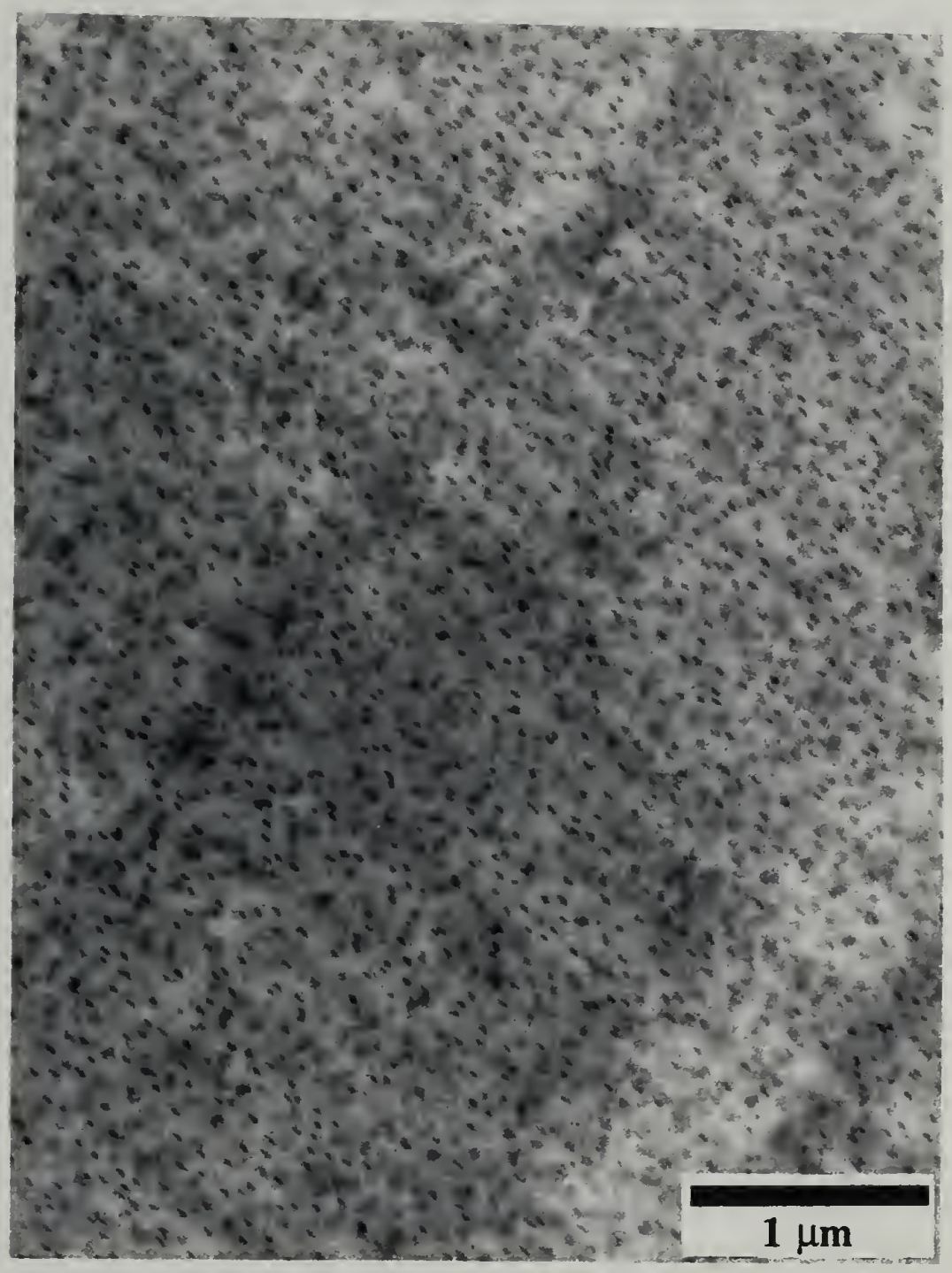


Figure 3.10: TEM micrograph of dioxane-cast $I_2S$-81 after annealing at 120°C for one week displaying kinetically trapped spherical PI micelles in a PS matrix.

low molecular weight PS/PI diblock.[25] While the transition from hexagonally packed cylinders to spheres only took between 30-60 minutes to occur the opposite transition required ~ 40 hours. Only at very high temperatures, placing the system in the intermediate or weak segregation limit where order-order transitions can occur, could large chain conformational changes take place and the unfavorable enthalpic interactions be significantly lowered so that the spherical micelles could link and form the equilibrium ROW phase.

## 3.5 Conclusions

A unique, randomly oriented worm micelle morphology, or ROW, is observed in an $I_2S$ simple graft block copolymer with $\phi_s = 0.81$. Via a set of selective solvent casting and prolonged, high temperature annealing experiments, combined with experimental results utilizing a non-selective solvent, this morphology was demonstrated to be the equilibrium state for the system. The worm structure occurs only at or near the particular volume fraction where the two PI backbone chains per molecule are first forced to the concave side of the PS/PI interface in the microphase separated state. In another paper, Pochan, *et al.*[3] find two other $I_2S$ samples, one with a slightly higher PS graft volume fraction ($\phi_s$=0.89) and one with a slightly lower PS volume fraction ($\phi_s$=0.66), which form a hexagonally packed PS cylindrical phase and alternating PS/PI lamellar phase respectively. While both of these phases were predicted theoretically the volume fraction window in which the ROW phase resides is predicted to be a bicontinuous, cubic phase.[2] The randomly oriented worm-like micelle phase does not necessarily preclude the existence of the theoretically predicted bicontinuous phase. However, the above experiments support the premise that the worm-like micelle morphology is an equilibrium structure which exists due to the novel graft architecture of the molecule and the unique relationship between the particular

volume fraction of $\phi_s = 0.81$ and the concavity of the PS/PI interface on which the two PI chains per molecule must reside.

## 3.6 References


(1) Hashimoto, T.; Koizumi, S.; Hasegawa, H.; Izumitani, T.; Hyde, S.T. "Observation of 'Mesh' and 'Strut' Structures in Block Copolymer/Homopolymer Mixtures." *Macromolecules*, **25**, 1433 (1992).

(2) Milner, S. T. "Chain Architecture and Asymmetry in Copolymer Microphases." *Macromolecules*, **27**, 2333 (1994).

(3) Pochan, D. J.; Gido, S. P.; Pispas, S.; Mays, J. W.; Ryan, A. J.; Fairclough, J. P. A.; Hamley, I. W.; Terrill, N. J. "Morphologies of Microphase-Separated $A_2B$ Simple Graft Copolymers." *Macromolecules*, **29**, 5091 (1996).

(4) Kinning, D.J.; Winey, K.I.; Thomas, E.L. "Structural Transitions from Spherical to Nonspherical Micelles in Blends of Poly(styrene-butadiene) Diblock Copolymer and Polystyrene Homopolymers." *Macromolecules*, **21**, 3502 (1988).

(5) Jung, K.; Abetz, V.; Stadler, R. "Thermodynamically Controlled Morphological Disorder in a Mircophase-Separated Cylindrical Block Copolymer." *Macromolecules*, **29,** 1076 (1996).

(6) Hadjichristidis, N.; Iatrou, H.; Behal, S. K.; Chludzinski, J. J.; Disko, M. M.; Garner, R. T.; Liang, K. S.; Lohse, D. J.; Milner, S. T. "Morphology and Miscibility of Miktoarm Styrene-Diene Copolymers and Terpolymers." *Macromolecules*, **26**, 5812 (1993).

(7) Helfand, E.; Wasserman, Z.R. "Strong-Segregation Theory of Microphase Separated Block Copolymers." *Macromolecules*, **9**, 879 (1976).

(8) Semenov, A. N. "Contribution to the Theory of Microphase Layering in Block Copolymer Melts." *Sov. Phys. JETP*, **61**, 7331 (1985).

(9) Brandrup, J., Immergut, E.H., Eds. *Polymer Handbook*, 3rd ed.; John Wiley & Sons: New York, 1989.

(10) Barton, A. F. M., Ed. *Handbook of Polymer-Liquid Interaction Parameters & Solubility Parameters*; CRC Press: Boston, 1990.

(11) Hashimoto, T.; Nagatoshi, K.; Todo, A.; Hasegawa, H.; Kawai, H. "Domain-Boundary Structure of Styrene-Isoprene Block Copolymer Films Cast from Toluene Solutions." *Macromolecules*, 7, 364 (1974).

(12) Thomas, E.L.; Kinning, D.J.; Alward, D.B.; Henkee, C.S. "Ordered Packing Arrangements of Spherical Micelles of Diblock Copolymers in Two and Three Dimensions." *Macromolecules*, **20**, 2934 (1987).

(13) Winey, K. I.; Thomas, E. L.; Fetters, L. J. "Swelling a Lamellar Diblock Copolymer with Homopolymer: Influences of Homopolymer Concentration and Molecular Weight." *Macromolecules*, **24**, 6182 (1991).

(14) Owens, J. N.; Gancarz, I. S.; Koberstein, J. T.; Russell, T. P. "Investigation of the Microphase Separation Transition in Low Molecular Weight Diblock Copolymers." *Macromolecules*, **22**, 3380 (1989).

(15) Mori, K.; Hasegawa, H.; Hashimoto, T. "Small-Angle X-Ray Scattering from Bulk Block Polymers in Disordered State. Estimation of $\chi$ Values from Accidental Thermal Fluctuations." *Polymer Journal*, **17**, 799 (1985).

(16) Rounds, N. A. University of Akron: Ph.D. Dissertation, 1970.

(17) Leibler, L. "Theory of Microphase Separation in Block Copolymers." *Macromolecules*, **13**, 1602 (1980).

(18) Olvera de la Cruz; Sanchez, I. C. "Theory of Microphase Separation in Graft and Star Copolymers." *Macromolecules*, **19**, 2501 (1986).

(19) Fogden, A.; Hyde, S. T.; Lundberg, G. "Bending Energy of Surfactant Films." *Journal of the Chemical Society. Faraday Transactions*, **87**, 949 (1991).

(20) Hyde, S. T. "Curvature and the Global Structure of Interfaces in Surfactant-Water Systems." *Colloque de Physique*, ***C7***, 209 (1990).

(21) Israelachvili, J. N. *Intermolecular and Surface Forces*, 2nd ed.; Academic Press: New York, 1992.

(22) Olmsted, P.D; Milner, S.T. "Strong-Segregation Theory of Bicontinuous Phases in Block Copolymers." *Physical Review Letters*, **72**, 936 (1994).

(23) Khandpur, A. K.; Foerster, S.; Bates, F. S.; Hamley, I. W.; Ryan, A. J.; Bras, W.; Almdal, K.; Mortensen, K. "Polyisoprene-Polystyrene Diblock Copolymer Phase Diagram near the Order-Disorder Transition." *Macromolecules*, **28**, 8796 (1995).

(24) Disko, M. M.; Liang, K. S.; Behal, S. K.; Roe, R. J.; Jeon, K. J. "Catenoid-Lamellar Phase in Blends of Styrene-Butadiene Diblock Copolymer and Homopolymer." *Macromolecules*, **26**, 2783 (1993).

(25) Sakurai, S.; Kawada, H.; Hashimoto, T.; Fetters, L.J. "Thermoreversible Morphology Transition between Spherical and Cylindrical Microdomains of Block Copolymers." *Macromolecules*, 26, 5796 (1993).

# CHAPTER 4

# MORPHOLOGIES OF MICROPHASE SEPARATED CONFORMATIONALLY ASYMMETRIC DIBLOCK COPOLYMERS

## 4.1 Abstract

The equilibrium morphological behavior of a series of conformationally asymmetric linear diblock copolymers is characterized via small-angle x-ray scattering (SAXS) and transmission electron microscopy (TEM). The linear diblock molecules of polyisoprene and poly(*t*-butylmethacrylate) (PtBMA) are prepared anionically over a range of PtBMA volume fractions 0.17 to 0.85. Solution light scattering experiments are performed on PtBMA homopolymer at theta conditions, and the results were compared with PI data in the literature in order to characterize the degree of conformational asymmetry between the respective blocks. This conformational asymmetry is quantified by an $\varepsilon$ of 0.75. The experimental results are compared with morphological behavior calculated utilizing self-consistent mean field theory for a diblock system with $\varepsilon = 0.75$. At middle to high PtBMA volume fractions, $\phi_{PtBMA} > 0.30$, the experimental morphological behavior agrees well with the calculated behavior; the microphase boundaries are slightly shifted to higher volume fractions of the PtBMA block due to its larger Kuhn length. At $\phi_{PtBMA} < 0.30$, however, discrepancies are found in the volume fraction dependence of experimentally determined morphological behavior and that calculated theoretically. Interestingly, extremely well ordered cylindrical microstructures were observed for PI cylinder domains embedded in PtBMA matrices; these samples were prepared by solvent casting with no treatment, such as shearing, to enhance long range order. These well ordered cylinder structures contrast with PtBMA cylinders in a PI matrix on the opposite side of the phase diagram which have very poor long range order.

## 4.2 Introduction

### 4.2.1 Conformational Asymmetry Effects

The strongly microphase segregated (large $\chi N$ regime) morphological behavior of conformationally symmetric diblock copolymers is determined by the relative volume fractions of the respective block species and is calculated to be symmetric about 0.50 relative volume fraction.[1,2] However, by introducing only a slight difference in either the statistical segment lengths and/or segmental volumes between the constituents of a diblock, such as in the often studied system of polystyrene and polyisoprene, the microphase boundaries become asymmetric about $\phi_{PS} = 0.50$.[3,4] It has been theoretically predicted that by introducing substantial asymmetry in the chain statistics between the two blocks the volume fraction dependence of the observed morphological behavior can be more drastically altered.[5] In particular, if the A block in an AB linear diblock has a larger Kuhn length and/or a smaller segmental volume than the corresponding B block, the volume fraction dependencies of the various strongly segregated morphologies are found to shift towards higher relative volume fraction of the A block. This volume fraction shift alleviates a disparity in the entropic chain stretching penalty between the A and B blocks; the more highly coiled B chain is able to relax at the expense of the more expanded A chain. In this work, the effects of conformational asymmetry on the equilibrium microphase separated behavior of linear diblocks are experimentally probed utilizing diblocks of polyisoprene and poly(*tert*-butylmethacrylate) (PI/PtBMA). The experimentally characterized morphological behavior of a series of nine samples is then compared to theoretical predictions for a system with similar conformational asymmetry.

### 4.2.2 Asymmetry Parameter

Helfand and Sapse[6] predicted the contribution of non-local, entropic effects, due to differing chain statistics, to the interfacial profile and interfacial tension of binary polymer blends. They introduced the parameter $\beta_i^2 = (1/6)\rho_i b_i^2$, where $\rho_i$ is the number

density of Kuhn steps and $b_i$ is the Kuhn length of species i, to quantify the conformational asymmetry of the two component system. More recently, work has been done to characterize the degree to which the free energy of mixing of blends is affected by differing chain statistics of components.[7,8] Calculations within the construct of the Flory-Huggins theory were performed on nearly athermal mixtures in which excess free energies of mixing arose specifically from conformational differences between blend components. In the absence of local specific interactions, systems which contained a high degree of conformational asymmetry, represented by a ratio $\varepsilon = (\beta_A/\beta_B)^2$ either much greater or much less than unity, exhibited a positive excess free energy of mixing resulting in immiscibility. In earlier experimental work Bates, *et al.*[9] found large discrepancies between calculated and measured Flory-Huggins $\chi$ parameters of isotopically labeled polyolefin mixtures and diblocks. They showed a strong correlation between the discrepancies in $\chi$ parameter (considering enthalpic interactions) with the degrees of asymmetry between Kuhn segment lengths of the different components.

### 4.2.3 Previous Experimental Research

The thermodynamic implications of conformational asymmetry between the two blocks of a block copolymer were considered to explain experimental results several years before the theoretical background was formulated to address the issue. Almdal *et al.* tentatively ascribed the complicated phase behavior in a polyolefinic block copolymer system around the order-disorder transition (ODT) to the disparity in the unperturbed radii of gyration of the two blocks.[10] More recently, Gehlsen and Bates directly probed the effect of differing chain statistics between constituents of a diblock copolymer on the ODT's of a set of polyolefins before and after hydrogenation.[11] Several of the systems studied became quite conformationally asymmetric after hydrogenation. Higher ODT's were observed after hydrogenation due to the entropic excess free energy of mixing even though the blocks of the copolymers became more enthalpically compatible. As stated

earlier, the slight asymmetry of the well studied PS/PI phase diagram relative to volume fraction has been ascribed to the slight asymmetry in chain statistics between PS and PI,[3,4] but the systematic introduction of constituent blocks with larger ε's and the observation of their corresponding asymmetric strongly segregated phase behavior has not been previously performed.

### 4.2.4 Previous Theoretical Research

Self-consistent field theories have been developed in an attempt to calculate the effects of conformational asymmetry within a unified treatment of copolymers from the vicinity of the ODT to strong segregation.[5,12,13] If an AB linear diblock is conformationally symmetric the center of the lamellar region resides at 50/50 relative volume fraction. However, if the A block has a larger Kuhn length and/or lower segmental volume then its unperturbed radius of gyration, $R_{g,o}$, will be larger than that of the B block. It becomes energetically easier to stretch the expanded A blocks while more difficult to stretch the more coil-like B blocks. To reduce this mismatch in the entropic chain stretching penalty the AB interface will curve towards the A phase so that the B blocks can relax. This shifting of the curvature at the A/B interface shifts the volume fraction dependence of the respective morphologies to larger volume fractions of the A block. In Figure 1 of reference 5, where $\varepsilon = 0.6$, the center of the phase diagram is approximately $\phi_A = 0.57$ in agreement with the qualitative reasoning above. All subsequent order-order transitions (OOT's) are shifted to higher volume fractions of the more expanded A chains.

In order to specifically look at strongly segregated systems with conformational asymmetry a series of PI and PtBMA linear diblocks were synthesized. In PtBMA the bulky tert-butyl ester side groups sterically hinder backbone rotations resulting in a larger Kuhn length than in PI. The conformational asymmetry is found to slightly shift the microphase boundaries to larger volume fractions of PtBMA.

## 4.3 Experimental

### 4.3.1 Synthesis and Characterization of PtBMA Homopolymers

All purifications and polymerizations were conducted under high vacuum conditions using classical breakseal and constriction techniques.[14] The polymerization solvent, tetrahydrofuran (THF), was purified by sequential exposure to and distillation from sodium dispersion and sodium/potassium alloy (weight ratio = 2:1). tert-Butylmethacrylate (Scientific Polymer Products) was dried over freshly ground $CaH_2$ followed by exposure to trioctylaluminum (Aldrich, 25 wt. % in hexanes) and distillation into evacuated ampules. The purified monomer was used immediately in polymerizations since, even at -78°C, it exhibited a strong tendency to polymerize on storage in this highly pure state. 1,1-Diphenylethylene (DPE) (Kodak) was purified sequentially over $CaH_2$, sodium metal, and n-butyllithium (Aldrich, 2.0 M in pentane); the DPE was then diluted with benzene in vacuo to appropriate concentrations. sec-Butyllithium (Aldrich, 1.3 M in cyclohexane) was used as initiator after purification by short-path high vacuum distillation followed by dilution with benzene to proper concentrations. Methanol, used to terminate polymerizations, was purified by exposure to several freeze-thaw cycles using liquid nitrogen and rigorous degassing followed by ampulization.

Polymerization involved charging a reactor with sec-butyllithium followed by addition of a 2-3 molar excess of DPE. A time period of 30 minutes at room temperature was employed for generation of the diphenylhexyllithium initiator (cherry red color). THF was then introduced into the reactor by distillation at -78° C. The tert-butylmethacrylate was charged by slow distillation into the rapidly stirred reactor with instant disappearance of the cherry red color. The polymerizations were run for 30-60 minutes at -78° C, depending on molecular weight, with efficient stirring. Immediately after termination with methanol the polymers were precipitated into water/methanol mixtures followed by isolation and vacuum drying.

Molecular weight distributions were analyzed using size exclusion chromatography (SEC); Waters Model 510 pump, Waters 410 differential refractometer, two ultrastyragel linear columns (American Polymer Standards Corp.), THF as eluent (flowrate 1mL/min), and data accumulation and analysis using Viscotek TriSEC software, version 2.70. Weight-average molecular weights ($M_w$), radii of gyration ($R_g$), and second virial coefficients ($A_2$) were measured using a Brookhaven BI2030AT light scattering unit with an $Ar^+$ ion laser operating at 488 nm. Cyclohexane (fractionally distilled from sodium) was used as solvent at a temperature of 10°C. This solvent/temperature combination constitutes a theta condition for anionically-produced PtBMA.[15] A custom-designed, temperature-controlled closed filtration loop was employed for sample clarification using 0.2 μm pore size Teflon membrane filters (Gelman Sciences). The refractive index increment, dn/dc, was measured as 0.058 mL/g using an Otsuka Electronics DRM-1020 double beam differential refractometer. Toluene and cyclohexane were used for instrument alignment and calibration. Measurements were conducted at 10 angles over the range of 30-135° and data were acquired and analyzed using the BI-ZP 4.0 Zimm Plot Software from Brookhaven.

Intrinsic viscosities [η] and Huggins coefficients were measured at 10°C in purified cyclohexane using Cannon Ubbeholde dilution viscometers. Conditions were chosen to eliminate the need for kinetic energy corrections (solvent flow times were about 150 sec). Relative viscosities ranged from 1.4 to 1.1, and data were fit using Huggins equation.

### 4.3.2 Synthesis and Characterization of PtBMA/PI Diblock Copolymer

Purifications are generally as described above. In addition, benzene was purified by exposure to concentrated sulfuric acid, calcium hydride, sodium dispersion, and oligostyryllithium. Isoprene (Aldrich) was exposed to calcium hydride, sodium

dispersion, and n-butyllithium (at least 20 minutes at O°C) followed by distillation into evacuated ampules.

Polymerizations were conducted in a manner chosen to assure high 1,4 content in the PI component. This involved polymerization of isoprene in benzene at 22°C using sec-butyllithium initiation. After waiting for sufficient time (> 24 hours) to insure complete conversion of isoprene to PI, THF was distilled into the reactor at -78°C. The frozen benzene, in THF, was completely dissolved by stirring, and then tert-butylmethacrylate was slowly introduced by distillation. No DPE capping step was employed.[16] Polymerizations were run for about 30 minutes followed by termination with methanol. Polymers were isolated by precipitation into methanol and were stabilized by addition of a small amount of butylated hydroxytoluene (BHT).

Characterization of polydispersities and compositions of the diblocks was achieved by SEC and 300 MHz proton NMR, respectively. As expected based upon polymerization conditions, the PI components exhibited high 1-4-microstructures (ca. 93% 1,4 and 7%3,4). $M_w$ values were determined in dry, distilled THF at room temperature using a Chromatix KMX-6 low-angle laser light scattering unit operating at a wavelength of 633 nm. The dn/dc value for each sample was measured under the same conditions using Otsuka Brice-Phoenix differential refractometers. Number-average molecular weights ($M_n$) were measured in toluene at 37°C using a Jupiter Model 231 membrane osmometer and regenerated cellulose membranes. Glass transition temperatures, $T_g$, were measured for the PtBMA phases of several diblocks and values in the range of about 60-70°C were found. These values are in the expected range due to the microphase separated state of the samples given the value of approximately 80°C which was measured for high molecular weight homopolymer. Molecular characteristics of the PI/PtBMA diblock copolymers are presented in Table 4.1.

Table 4.1

PI/PtBMA Diblock Copolymers-Molecular Characteristics: (a) Membrane osmometry, (b) Low-angle laser light scattering, (c) SEC, (d) $^1$H-NMR The compositions from $^1$H-NMR were converted to volume fractions using the gravimetrically measured densities of 1.02 g•cm$^{-3}$ for PtBMA at 25°C and 0.91 g•cm$^{-3}$ for PI at 25°C.

| Sample | $M_n \times 10^{-4}$ [a] | $M_w \times 10^{-4}$ [b] | $M_w/M_n$ [c] | Vol. Fraction PtBMA [d] |
|---|---|---|---|---|
| PtBMA-17 | 5.82 | 6.91 | 1.08 | 0.17 |
| PtBMA-22 | 5.35 | 5.91 | 1.18 | 0.22 |
| PtBMA-27 | 5.77 | 6.66 | 1.11 | 0.27 |
| PtBMA-32 | 6.43 | 6.95 | 1.07 | 0.32 |
| PtBMA-50 | 6.13 | 7.61 | 1.23 | 0.50 |
| PtBMA-60 | 6.18 | 6.62 | 1.11 | 0.60 |
| PtBMA-70 | 5.84 | 6.20 | 1.10 | 0.70 |
| PtBMA-75 | 5.54 | 5.61 | 1.13 | 0.75 |
| PtBMA-85 | 6.18 | 6.26 | 1.08 | 0.85 |

### 4.3.3 Sample Preparation for Morphological Characterization

Solid films approximately 1 mm thick were cast in 30 ml Pyrex beakers from 5 weight percent solutions of block copolymer in toluene. Toluene, which has a solubility parameter, $\delta$, of 17.8 $MPa^{1/2}$, was as close as we could come to a non-preferential solvent for PI ($\delta$ = 17 $MPa^{1/2}$) and PtBMA ($\delta \approx$ 18 $Mpa^{1/2}$), although it is slightly selective for PtBMA.[17] The evaporation of solvent was controlled to form a solid film after 14 days. An exact $\chi N$ determination for the PI/PtBMA system is difficult since phase behavior experiments on PtBMA are non-existent in the literature. Also, a rough estimation of $\chi$ based on solubility parameters does not account for the positive additions to the free energy of mixing due to entropic effects from conformational asymmetry.[11] The solubility parameter of polystyrene (PS) is 18 $MPa^{1/2}$, identical to that determined for PtBMA.[17] Therefore, we use experimentally determined[18-20] $\chi$ values of the more conformationally symmetric system of PS and PI to estimate $\chi N$ between PI and PtBMA. $\chi N$ estimated from PS and PI measurements should represent a lower bound for the PI and PtBMA block pair since the conformational asymmetry between PI and PtBMA will lead to positive additions to the free energy of mixing.[11] The block copolymer degree of polymerizations, N, were normalized relative to an average reference density, $\rho_o$, via the equation $N=\rho_o[(N_{PtBMA}/\rho_{PtBMA})+(N_{PI}/\rho_{PI})]$ where $\rho_o=[(\rho_{PtBMA})(\rho_{PI})]^{1/2}$ and $\rho_{PtBMA}$ and $\rho_{PI}$ values are 4.33 and 8.04 segments/unit volume respectively. Therefore, the lower bound of $\chi N$ for our samples is estimated to be 40-70 at the sample annealing temperature of 125°C, and 80-110 at 25°C. At this relatively high degree of segregation the phase boundaries are nearly independent of $\chi N$ (see reference 5, Figure 1 and Figure 4.6 of this paper). Thus our estimation of the $\chi$ parameter does not seriously compromise the conclusions of this study.

The cast PI-PtBMA films were placed under high vacuum for several days at 40°C to allow the evaporation of residual solvent. The vacuum oven temperature was ramped up to 125°C over a period of a day and held there for one week in order to promote the

development of well ordered, equilibrium morphologies. After annealing the temperature was slowly ramped down to 80°C over two days and then quickly lowered to room temperature. A second set of samples was quenched in liquid nitrogen after having annealed at 125°C for five days in order to observe any morphological differences arising in the intermediate segregation regime. Identical morphologies were observed in unannealed cast films, annealed films which were slowly cooled, and annealed films that were quenched in liquid nitrogen. Lattice order was found to be somewhat better developed in the annealed samples. These results further support the existence of large $\chi N$ values for the PI/PtBMA pair and place the sample series in the strongly segregated regime.

Sections approximately 300-800 Å thick were cut in a Reichert-Jung cryoultramicrotome equipped with a Diatome cryo diamond knife at a sample temperature of -110°C and a knife temperature of -90°C. The sections were subsequently stained in $OsO_4$ vapors for four hours and then observed in the transmission electron microscope (TEM).

### 4.3.4 Morphological Characterization

Transmission electron microscopy (TEM) was performed on a JEOL 100CX operating at 100kV. Small angle X-ray scattering (SAXS) experiments were performed with both a sealed tube source and at a synchrotron. The sealed tube experiments were performed on a Rigaku-Denki camera with CuK$\alpha$ X-ray radiation and pinhole collimation. Patterns were collected photographically with Kodak direct exposure film (DEF-5). Synchrotron SAXS experiments were performed on beamline 16.1 of the Synchrotron Radiation Source (SRS) at the Daresbury Laboratory, Warrington, U.K. Details of the electron storage ring, radiation, camera geometry, and data collection electronics have been given elsewhere.[21] White radiation from the electron ring was collimated using a cylindrically bent Ge(111) crystal to isolate an intense beam of

$\lambda = 1.50 \pm 0.01$ Å X-rays. The instrument is equipped with a 20 x 20 cm. area detector which has a spatial resolution of 500 μm and a count-rate limit of 500 kHz. The set-up employed an evacuated flight path and a 5 m. sample-to-detector distance. The bulk polymer films were sandwiched between two pieces of Kapton polyimide tape and then mounted in the beam path. An oriented specimen of wet collagen (rat tail tendon) was used to calibrate the SAXS detector. A parallel-plate ionization detector placed before the sample cell recorded the incident intensities. The experimental data were corrected for Kapton and camera background scattering, sample absorption, and the positional alinearity of the detector. Birefringence observations were performed on bulk films at room temperature with a Leitz optical microscope under cross polars.

## 4.4 Results and Discussion

### 4.4.1 Conformational Analysis of PtBMA

The molecular characteristics of the PtBMA homopolymers in cyclohexane at 10°C are summarized in Table 4.2. The very small $A_2$ values and large Huggins

Table 4.2

Molecular Characteristics of PtBMA in Cyclohexane Under Theta Conditions: (a) Z-average radius of gyration (b) Via SEC in THF

| $M_w \times 10^{-5}$ | $R_{g,z}$ (nm)[a] | $A^2 \times 10^5$ (ml•mol•g$^{-2}$) | $[\eta]$ dL•g$^{-1}$ | $k_H$ | $M_w/M_n$[b] |
|---|---|---|---|---|---|
| 1.76 | 16.2 | 3.2 | 0.326 | 0.65 | 1.20 |
| 2.91 | 18.4 | -0.9 | 0.394 | 1.01 | 1.16 |
| 4.15 | 23.0 | 3.3 | 0.481 | 0.78 | 1.27 |

coefficients suggest that measurements were conducted at, or very near to, the Flory theta state. This allows the characteristic ratio, $C_\infty$, to be evaluated directly for each sample using the equation[22] $C_\infty = 6R_g^2/n\,l^2 = (3R_g^2/M)/(l^2/M_o)$ where n is the number of main chain bonds of length l = 1.53 Å, M is molecular weight, and $M_o$ is the molecular weight of the repeating unit. In order to correct for polydispersity present in the samples the weight-average $R_g$ values were computed from the measured z-average values given in Table I assuming a Schulz-Flory distribution.[23,24] This approach yields an average $C_\infty$ value of 20.4 for PtBMA. This value compares reasonably well with the value of 23.8 estimated by Kozhokaryu and co-workers[25] using intrinsic viscosity data on high molecular weight fractions from radical polymerization in the good solvent butylacetate. On the other hand, our measured value of 20.4 is much larger than the value of 11.8 reported by Karandinos *et al.*[15] based on intrinsic viscosity measurements under theta conditions on anionically prepared specimens.

In the work of Kozhokaryu *et al.* samples covering the molecular weight range of $4.6 \times 10^5$ - $8.7 \times 10^6$ g/mol were employed. The hazards of estimating unperturbed dimensions from viscosity data on samples exhibiting very large excluded volumes are well-documented and are likely to lead to an overestimation of $C_\infty$.[26-28] The apparent disagreement between the theta condition viscosity data of Karandinos *et al.* and our light scattering data was more difficult to rationalize. We therefore conducted [η] measurements on the PtBMA samples prepared for the present study (Table II); these data give a $C_\infty$ value of 13.5 using the equations[22,29]

$$K_\theta = \frac{[\eta]_\theta}{M^{1/2}} = \frac{\phi_o(\langle r^2\rangle)_o}{M^{3/2}} \qquad (4.1)$$

$$C_\infty = \frac{\langle r^2\rangle_o}{n l^2} \qquad (4.2)$$

where $K_\theta$ is the unperturbed parameter, $\phi_o$ is the Flory hydrodynamic parameter (which we took as $2.5 \times 10^{23}$ mol$^{-1}$),[30] and $\langle r^2 \rangle_o$ is the unperturbed mean-square end-to-end distance. This difference between our result of the solution viscosity determined $C_\infty$ and that of Karandinos *et al* is not outside the experimental uncertainty and may reflect tacticity differences in the specimens.[15]

The intrinsic viscosity data analysis requires the assumption of a value of $\phi_o$ for a semi-flexible polymer chain, and thus caution should be exercised in estimating the chain stiffness for semi-flexible macromolecules such as PtBMA from intrinsic viscosity data. Light scattering represents a more reliable, direct method to measure the size of semi-flexible macromolecules since no *a priori* assumptions need to be made concerning the chain statistics of a polymer. Based on the light scattering measurements we calculated that the value of the Flory $\phi_o$ parameter is substantially smaller for PtBMA than it is for a typical flexible coil. The average value we compute using the equation

$$\phi_o = \frac{[\eta]M}{6^{3/2}R_g^3} \qquad (4.3)$$

and the data of Table II is 1.39 ($\pm$0.20) $\times 10^{23}$ mol$^{-1}$, a value much smaller than the theta condition random coil value.[31-33] This smaller value is consistent with a lower degree of flexibility of PtBMA as compared to "typical" random coils such as polyisoprene and polystyrene. In fact, $\phi_o$, has a limiting value of zero for an infinite rod.[32]

Even though the PtBMA backbone is very stiff relative to a freely rotating chain, as indicated by the large $C_\infty$, the steric mechanism chosen to make the backbone stiff actually tempers the conformational asymmetry. By utilizing large side groups in order to make the backbone stiff and the statistical segment length large one also makes the segment volume larger and the number density of segments correspondingly lower. If one assumes Gaussian chain behavior of PtBMA in the bulk and defines a segment as the

monomer ($M_o$ =142.2 g/mol where N =$M_{tot}/M_o$) then, utilizing the measured theta condition $R_g$ data in Table II, one calculates an average segment length of 1.06 nm for PtBMA from $R_g^2=(Nb^2)/6$. This segment length is larger than literature values of approximately 0.68 nm for 1,4 PI as determined by SANS from the melt.[11] However, the number density, $\rho_{PtBMA}$, is now equal to $(\xi_{PtBMA}/M_o)(N_A)$ where $\xi$ is the mass density of PtBMA or $[(1.02g/cm^3)/(142.2g/mol)](6.02x10^{23}) = 4.33x10^{21}$ segments/$cm^3$ or 4.33 segments/$nm^3$. If we do the same calculation for PI by defining a segment as a monomer unit with a mass density of 68.12 g/mol then $\rho_{PI}$ =8.04 segments/$nm^3$. Bearing in mind that the small number of 1,2 and 3,4 linkages in the PI lowers the PI segment length slightly from the value of 0.68 nm, the combination of these segment lengths and densities leads to an approximate conformational asymmetry parameter of $\varepsilon$ =0.75 for PI/PtBMA. The large differences in characteristic ratios seem to indicate a very large degree of conformational asymmetry in the block pair. However, the much larger segmental volume for PtBMA, and the subsequently much lower number density of segments, provides for a system with only moderate conformational asymmetry.

### 4.4.2 Morphological Characterization

The assigned morphologies for the entire series of PI/PtBMA diblocks are listed in Table 4.3 along with the d spacings for the lowest angle scattering maxima. In the discussion that follows the numerical designation in the name of each sample indicates the volume percent of the PtBMA block. Most of the samples produced powder patterns in the SAXS experiments due to the small grain size of the microstructure and are represented as one dimensional plots, in Figures 4.1 and 4.2, of integrated intensity vs. scattering vector q, where $q = \{4\pi/\lambda\}\sin\{\theta/2\}$ ($\lambda$ is the radiation wavelength and $\theta$ is the scattering angle). However, samples PtBMA-70 and PtBMA-75 display extremely high degrees of long range order in their hexagonally packed cylinder microstructures and produce the highly ordered hexagonal spot patterns displayed in Figure 4.3.

Table 4.3

PI/PTBMA Morphology Characteristics: (a) $d_1 = 2\pi/q_1$ where $q_1 = 4\pi/\lambda(\sin\theta_1)$ and $2\theta_1$ is the scattering angle for the lowest angle Bragg peak; corresponds to $d_{(10)}$ for hexagonal cylinders, $d_{(001)}$ for lamellae, and $d_{(110)}$ for body-centered cubic.

| Sample | $\phi_{PtBMA}$ | $d_1$(Å)[a] | Morphology | Optical Birefringence |
|---|---|---|---|---|
| PtBMA-17 | 0.17 | 331±5 | cubic array of PtBMA spheres in PI matrix | No |
| PtBMA-22 | 0.22 | 349±5 | cubic array of PtBMA spheres in PI matrix | No |
| PtBMA-27 | 0.27 | 359±5 | cubic array of PtBMA spheres in PI matrix | No |
| PtBMA-32 | 0.32 | 419±5 | hexagonally packed PtBMA cylinders in PI matrix | Yes |
| PtBMA-50 | 0.50 | 393±5 | alternating PtBMA and PI lamellae | Yes |
| PtBMA-60 | 0.60 | 398±5 | alternating PtBMA and PI lamellae | Yes |
| PtBMA-70 | 0.70 | 331±5 | hexagonally packed PI cylinders in a PtBMA matrix | Yes |
| PtBMA-75 | 0.75 | 308±5 | hexagonally packed PI cylinders in a PtBMA matrix | Yes |
| PtBMA-85 | 0.85 | 233±5 | cubic array of PI spheres in PtBMA matrix | No |

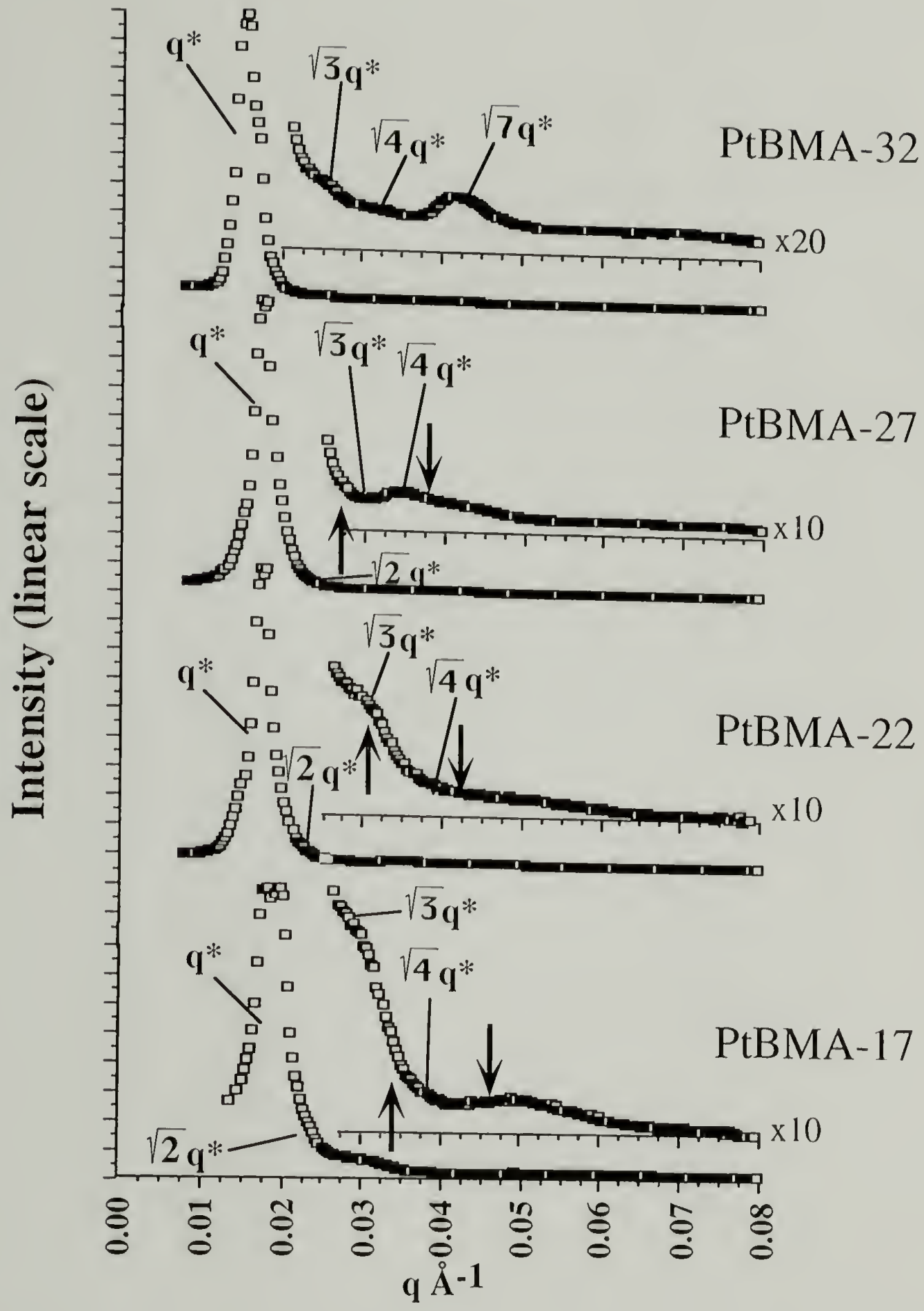


Figure 4.1: One dimensional synchrotron SAXS plots of total integrated intensity of the isotropic powder patterns vs. scattering vector, q, of the PI/PtBMA diblock samples with $\phi_{PtBMA} < 0.50$. The strong maxima in PtBMA-17, 22, and 27 correspond to q* of poorly ordered cubic lattices of PtBMA spheres with the expected positions of higher reflections marked at $q_n/q^*$ of $\sqrt{2}$, $\sqrt{3}$ , and $\sqrt{4}$. The expected positions of the first minima and maxima of the sphere SPFF are marked by up and down arrows, respectively. The $q_n/q^*$ ratios of 1, $\sqrt{3}$, $\sqrt{4}$, and $\sqrt{7}$ confirm a hexagonal array of cylinders in PtBMA-32.

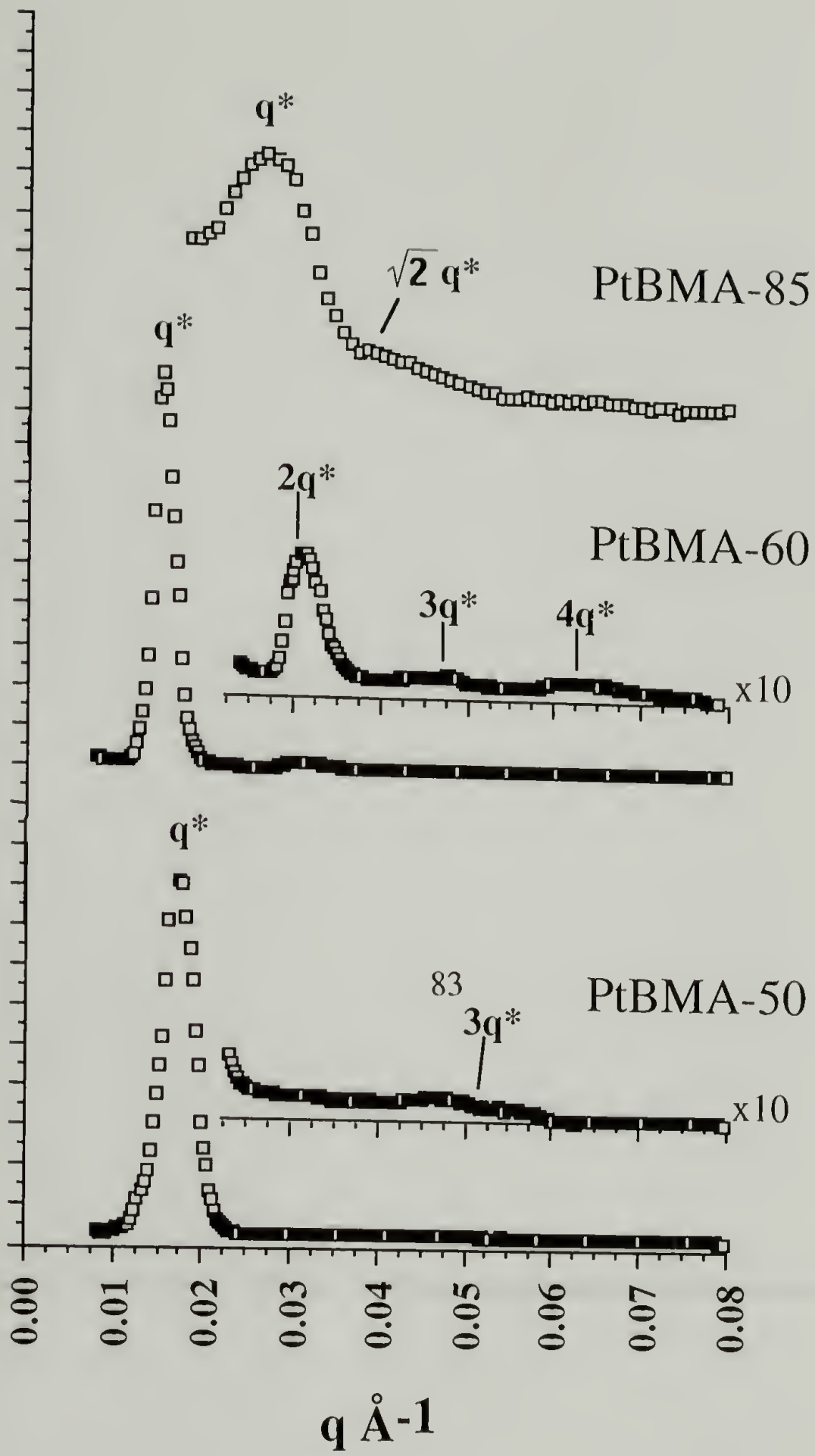


Figure 4.2: One dimensional SAXS plots of total integrated intensity of the isotropic powder patterns vs. scattering vector, q, of the PI/PtBMA diblock samples with $\phi_{PtBMA} \geq 0.50$. The SAXS patterns from PtBMA-50 and 60 are characteristic of alternating lamellar phases with higher order reflections of the long spacing. PtBMA-85 contains the first two Bragg maxima for a cubic array of spheres at $q_n/q^*$ ratios of 1 and $\sqrt{2}$.

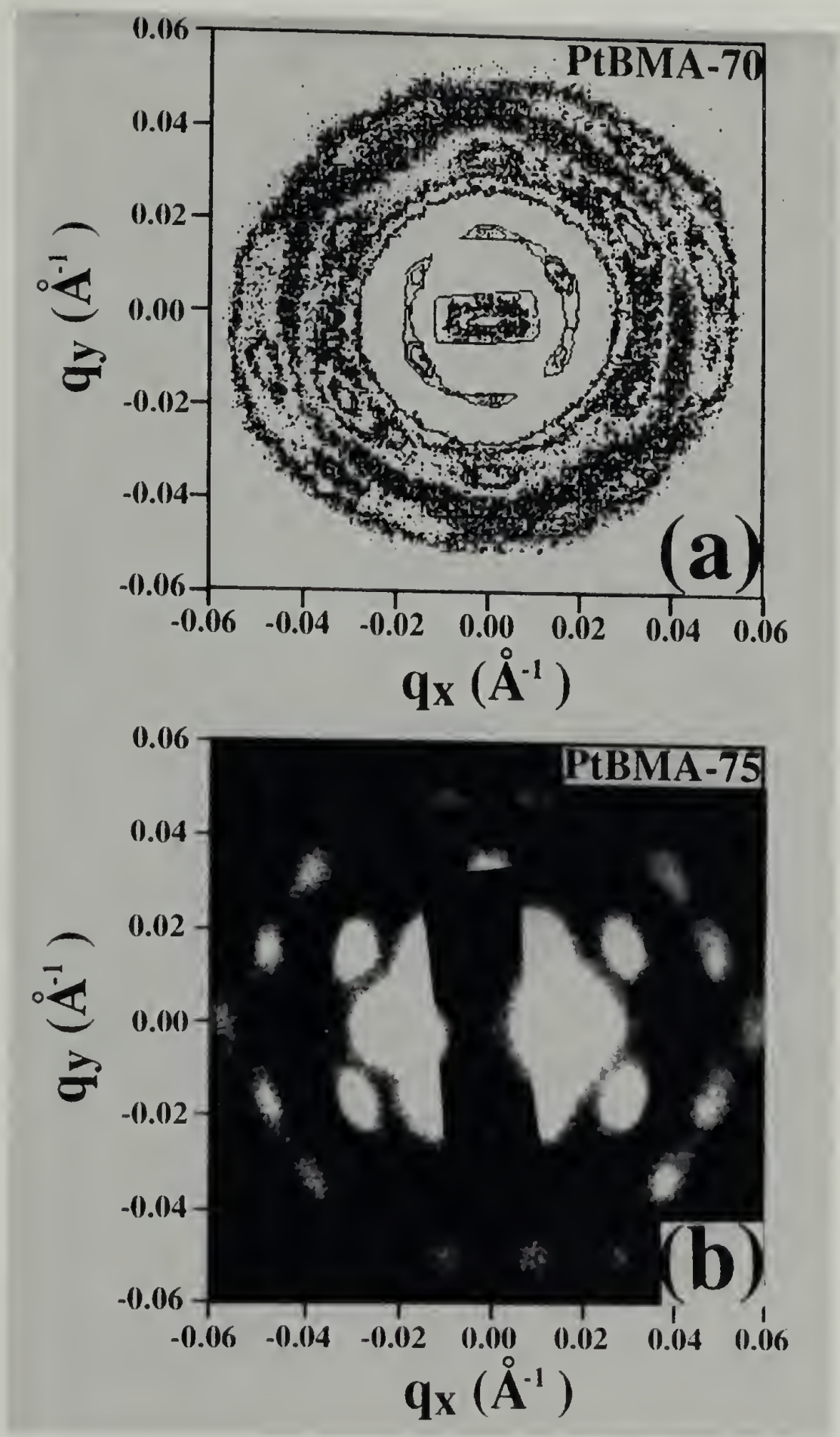


Figure 4.3: Two dimensional hexagonal SAXS patterns of samples PtBMA-70 and 75 taken parallel to the film surface indicative of scattering almost exclusively parallel with the hexagonally packed cylinder axes. (a) contour plot of the synchrotron SAXS pattern of PtBMA-70 with the (11) reflection absent. (b) SAXS pattern of PtBMA-75 as collected on direct exposure film in the Rigaku-Denki pinhole camera with the (20) reflection absent. The (10) reflection is partially hidden by the main beam.

As can be seen in the TEM micrograph in Figure 4.4a, PtBMA-27 displays a microphase separated spherical structure. However, a cubic lattice symmetry is limited to the length scale of several PtBMA domains. The three samples with the lowest relative volume fraction of PtBMA; PtBMA-17, PtBMA-22, and PtBMA-27; displayed the same morphological behavior so only one representative micrograph, of PtBMA-27, is displayed. The existence of a poorly ordered cubic lattice underlying the PtBMA domains is supported by the SAXS data. The azimuthally integrated, isotropic SAXS patterns displayed in Figure 4.1 for each these three spherical samples show a strong and discrete first scattering peak followed by much weaker higher scattering angle peaks. The expected positions of maxima associated with a body-centered lattice are marked on the patterns with their respective scattering vector ratios relative to q*. Also, the expected position of the first maximum and minimum of the spherical single particle form factor (SPFF) are marked on each pattern with a downward and upward arrow respectively. The i'th form factor maxima and minima of the spheres were calculated[34,35] via the relations $q_iR_{sMax}$ =5.76, 9.10,... and $q_iR_{sMin}$ =4.43, 7.73, ... $R_s$ is calculated assuming a body-centered cubic lattice with the equation $\phi = (8)^{1/2}\pi/3(R_s/d)^3$ where $\phi$ is the relative volume fraction of the minority, sphere forming component and $d_{110} = 2\pi/q^*$ is the longest spacing measured by SAXS. The broad maxima at higher q in PtBMA-27 and PtBMA-17 correspond well with the SPFF maxima. PtBMA-22 and PtBMA-27 also contain weak, broad shoulders at approximately $\sqrt{3}q^*$ indicative of a lattice. The peak expected at $\sqrt{2}q^*$ cannot be resolved from the strong q* maximum in any of the low PtBMA spherical samples, although it is obvious from the TEM micrograph in Figure 4a that the sample is indeed a spherical micelle phase and not a hexagonal cylindrical lattice. The GPC experiments for these spherical samples, as well as the entire PI-PtBMA series, reveal no sample degradation or oxidation during the annealing process. None of the

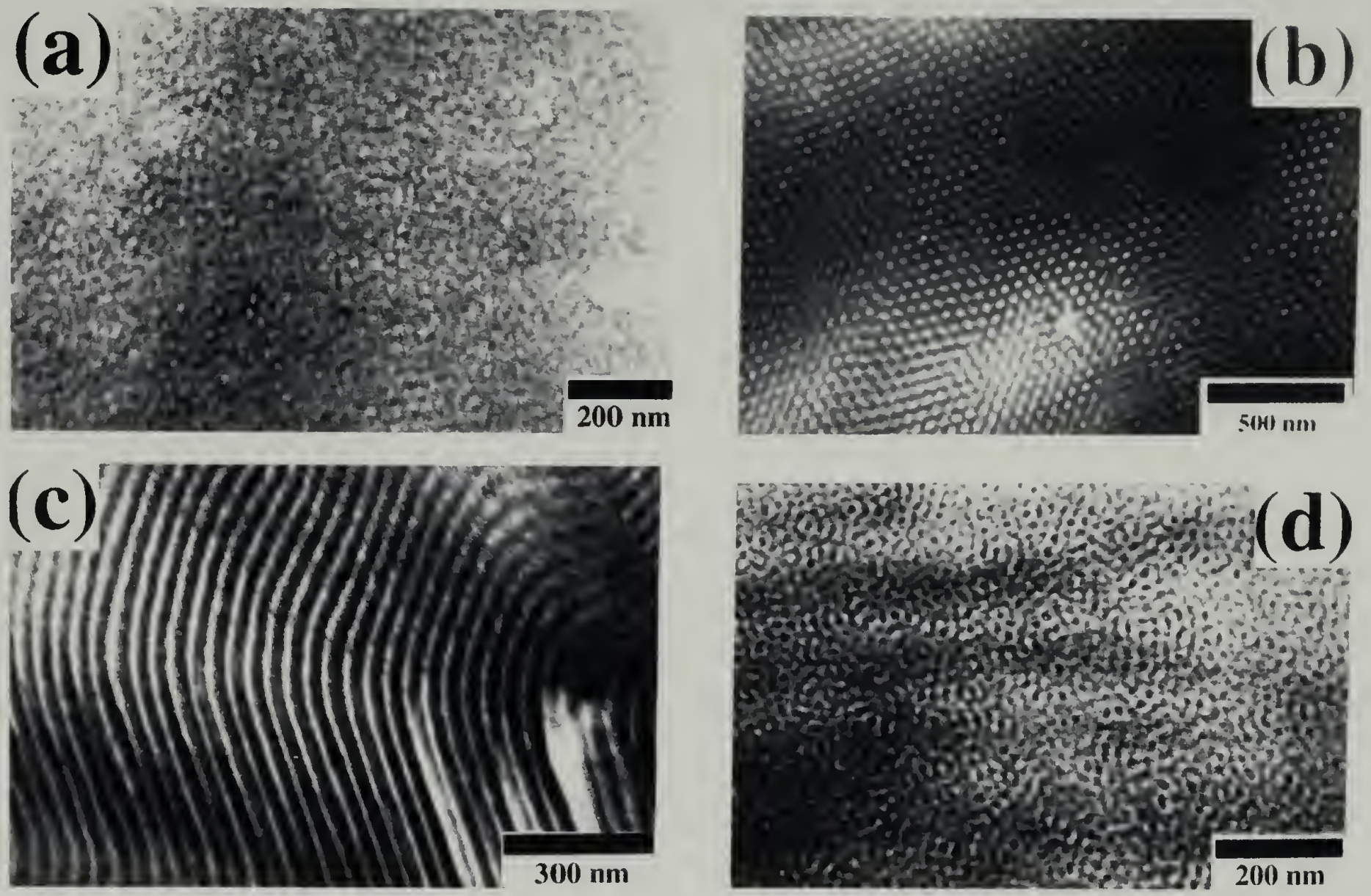


Figure 4.4: TEM data with PI appearing dark due to $OsO_4$ staining while PtBMA appears light. a) TEM micrograph of PtBMA-27 showing PtBMA spherical micelles with weak lattice ordering in a PI matrix. b) TEM micrograph of PtBMA-32 showing pockets of 6-fold symmetry of PtBMA cylinders in a PI matrix due to a projection along the cylinder axes. c) TEM micrograph of PtBMA-50 showing a projection parallel to the alternating PI/PtBMA lamellae. d) TEM micrograph of PtBMA-85 showing spheres of PI in a matrix of PtBMA with very small grains of cubic lattice.

samples with spherical morphology displayed any optical birefringence, an observation consistent with a cubic structure.

In order to verify the equilibrium nature of this poorly ordered cubic morphology the samples were cast two additional times from toluene and annealed at lower temperatures of 120°C and 100°C for one week. These two temperatures are still well above the observed $T_g$ of 80°C for the glassy PtBMA block[36] and thus should allow significant relaxation of any non-equilibrium effects. The spherical micelle morphologies formed in the recasting and reannealing experiments were identical to those formed at 125°C.

Moving to slightly higher PtBMA volume fractions, sample PtBMA-32 displays hexagonally packed PtBMA cylinders in a PI matrix. This is determined from the electron micrograph in Figure 4.4b and from the characteristic ratios of $q_n/q^* = 1, \sqrt{3}, \sqrt{4}$, and $\sqrt{7}$ in the azimuthally integrated isotropic SAXS data in Figure 4.1. The long range order of the hexagonal lattice is not well developed as indicated by the isotropic nature of the SAXS data; the average grain size (diameter) is limited to about 1 μm. PtBMA-50 and PtBMA-60 are both alternating lamellae morphologies as seen in the SAXS data in Figure 4.2 and the electron micrograph in Figure 4.4c. All three of these samples displayed optical birefringence consistent with the non-cubic lattice assignments of hexagonally-packed cylinders and alternating lamellae respectively.

Samples PtBMA-70 and PtBMA-75 display tremendous long range order which is evident in their two dimensional SAXS patterns shown in Figure 4.3. The PtBMA-70 and PtBMA-75 samples were quiescently cast from dilute solution and then annealed following exactly the same procedure as all the other samples in the series. Therefore, the striking long-range order observed in the hexagonally packed cylindrical microstructure of these two samples is noteworthy. Both patterns were taken with the x-ray beam parallel with the surface of the sample films placing the cylinder axes exclusively within the plane of the film. SAXS patterns taken with the x-ray beam perpendicular to the film surfaces

produced uniaxial arc patterns consistent with scattering perpendicular to the cylinder axes. Figure 4.5 is an electron micrograph taken from a section of PtBMA-70 microtomed perpendicular to the surface of the bulk film. This micrograph demonstrates that the PI cylinder axes lie in the plane of the bulk film, and it illustrates the high degree of perfection and long range order of the hexagonal lattice. PtBMA-75 was observed to contain identical lattice structure in electron microscopy experiments. A Bragg reflection is absent in both patterns, the (11) in PtBMA-70 and the (20) in PtBMA-75. These can be attributed to the convolution of the first minimum in the SPFF scattering from cylindrical micelles with the above mentioned Bragg reflections. Similar Bragg peak absences in hexagonally packed cylinders have been attributed to SPFF minima in both isotropic powder pattern SAXS data[34,37] and two dimensional anisotropic scattering from an extrusion-oriented cylindrical sample.[38] Utilizing the relationship $(qR_{cyl}) = 3.83, 7.02,$ etc. representing the systematic minima of the cylindrical SPFF[34] cylinder radii of 116Å and 95Å can be calculated for PtBMA-70 and PtBMA-75 respectively. These values are commensurate with radii estimated from the electron micrographs. $\phi_{PI}$ can then be calculated from these radii utilizing the relationship $\phi_{cyl} = (\sqrt{3}/2)(\pi)(R_{cyl}/d_{100})^2$ where $d_{100}$ is calculated from $2\pi/q^*$ ($q^*$ the is the lowest angle Bragg peak of the hexagonal lattice). This calculation yields $\phi_{PI}$ equal to 33.4% for PtBMA-70 and $\phi_{PI}$ equal to 25.6% for PtBMA-75, values consistent with those calculated after the syntheses of the samples. These results confirm that the SPFF minima are the cause of the Bragg peak absences in the SAXS patterns for PtBMA-70 and PtBMA-75.

There is a marked difference in degree of long range order between the samples with PI forming the cylindrical domains, samples PtBMA-70 and PtBMA-75, and that with PtBMA forming the cylindrical domains, sample PtBMA-32. We stress that all these samples were cast, annealed, and observed in exactly the same way, so differences in the observed long range order are not likely to be due to different sample histories. An almost identical long-range order effect was seen in a series of model $I_2S$ graft

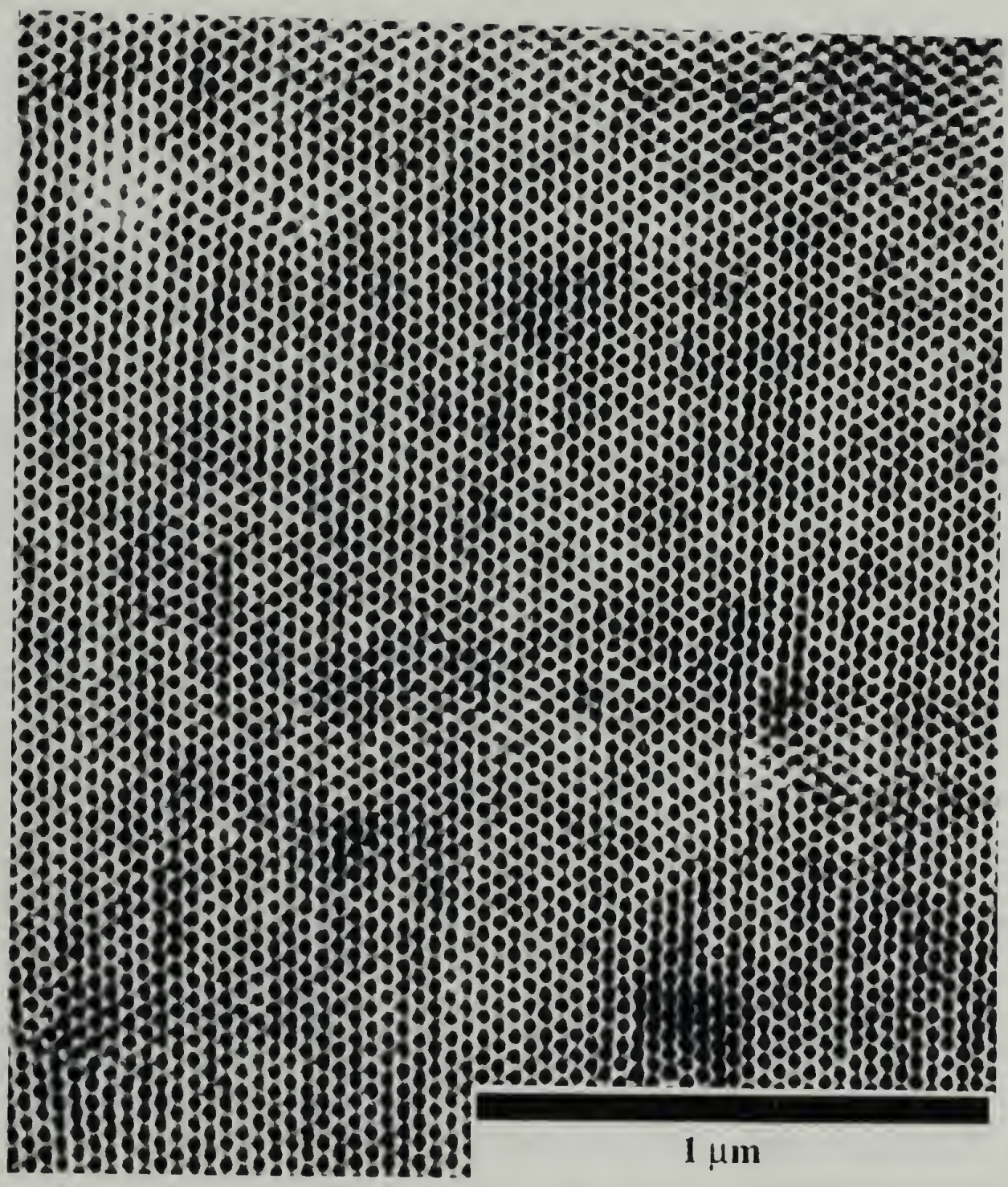


Figure 4.5: TEM micrograph of PtBMA-70. The sample section was microtomed perpendicular to the film surface and shows a projection along the cylinder axis of the extremely well ordered hexagonal microstructure.

copolymers.[39] This molecular architecture consisted of a polyisoprene backbone onto which was grafted a single block of polystyrene directly at the center. This novel "Y" architecture produced short, highly stretched corona blocks on one side of the phase diagram while on the other the corona blocks were longer and less stretched. The samples with the short, highly stretched corona chains contained a very high degree of long range order in the cylindrical microstructure while the samples with long relaxed corona blocks displayed a poor degree of long range order. This previous example showed that the degree of long range order and lattice precision to be controlled by the "stiffness" of the interaction between neighboring micelles through the contact of their corona blocks. We expect that the difference in the degree of long range order between PI-PtBMA diblocks with PtBMA corona blocks (PtBMA-70 and -75) and diblocks with PI corona blocks (PtBMA-32) arises from a similar effect. However, in these samples the PtBMA corona block in PtBMA-70 and -75 and the PI corona blocks in PtBMA-32 are all approximately similar in volume fraction. The difference has to be in the flexibility of the corona block forming chains. The less flexible PtBMA blocks, when forming the corona, lead to precise lattice formation and tremendous long range order. The more flexible PI blocks, when forming the corona, lead to less precise lattice formation and less long range order.

PtBMA-85, the sample with highest relative volume fraction of PtBMA, displays a similar spherical morphology to that seen in samples PtBMA-17, 22, and 27 although the phases are now inverted with PI domains in a PtBMA matrix. A discrete Bragg peak corresponding to q* with a weak shoulder at $\sqrt{2}q^*$ can be seen in Figure 4.2 indicative of a cubic lattice of spheres with poor long range order. This pattern was collected on X-ray film in a pin-hole camera with an X-ray tube source. Therefore, the q* peak appears much more broad than in the data taken with the more well collimated synchrotron X-ray source. The micrograph in Figure 4.4d contains dark spherical PI domains in a light PtBMA matrix with very small areas of lattice order. This sample was also recast and

annealed at the lower temperatures of 120°C and 100°C with identical morphological behavior found revealing the robust nature of this cubic spherical morphology.

### 4.4.3 Comparison with Theory

In order to make a direct comparison with the current experimental results, an additional set of SCFT calculations was performed with $\varepsilon = 0.75$ using the same approach as in reference 1. The free energies were calculated for the experimentally observed diblock morphologies (B spheres, B cylinders, AB lamella, A cylinders, and A spheres) across the full range of component volume fractions and for $\chi N$ values of 20, 30, 40, 60, and 80 (the A block represents the more coil-like block while B represents the more expanded chain, PI and PtBMA respectively in our experiments). The resulting phase boundaries, determined by the unit cell with the lowest free energy at each volume fraction, are plotted in Figure 4.6. The experimentally determined morphological behavior is represented by the series of vertical lines from $\chi N$ 20-50 where each line represents the sample with that particular PtBMA volume fraction on the ordinate. The solid vertical lines represent agreement between experimentally determined and calculated morphology. The alternating dot/dash vertical lines represent regions of disagreement between experimentally determined and calculated morphology.

An approximate $\chi N$ range of 40-70 was estimated for the PI/PtBMA sample series based on $\chi$ values determined for PS and PI. In this range seven of the samples basically agree with the theoretically predicted morphological behavior. Only samples PtBMA-22 and -27, which form PtBMA spheres, differ substantially from the theoretical predictions of cylinders in both cases. Samples PtBMA-70 and -85 do not agree with the theoretical prediction if the value of $\chi N$ is greater than the very bottom of the range we have estimated for this parameter. The SCFT calculations utilized the conventional unit cell approximation (UCA) which induces a small shift in the phase boundaries. However, not using the UCA results in a slightly worse, not better agreement for PtBMA-70 and -85.[40]

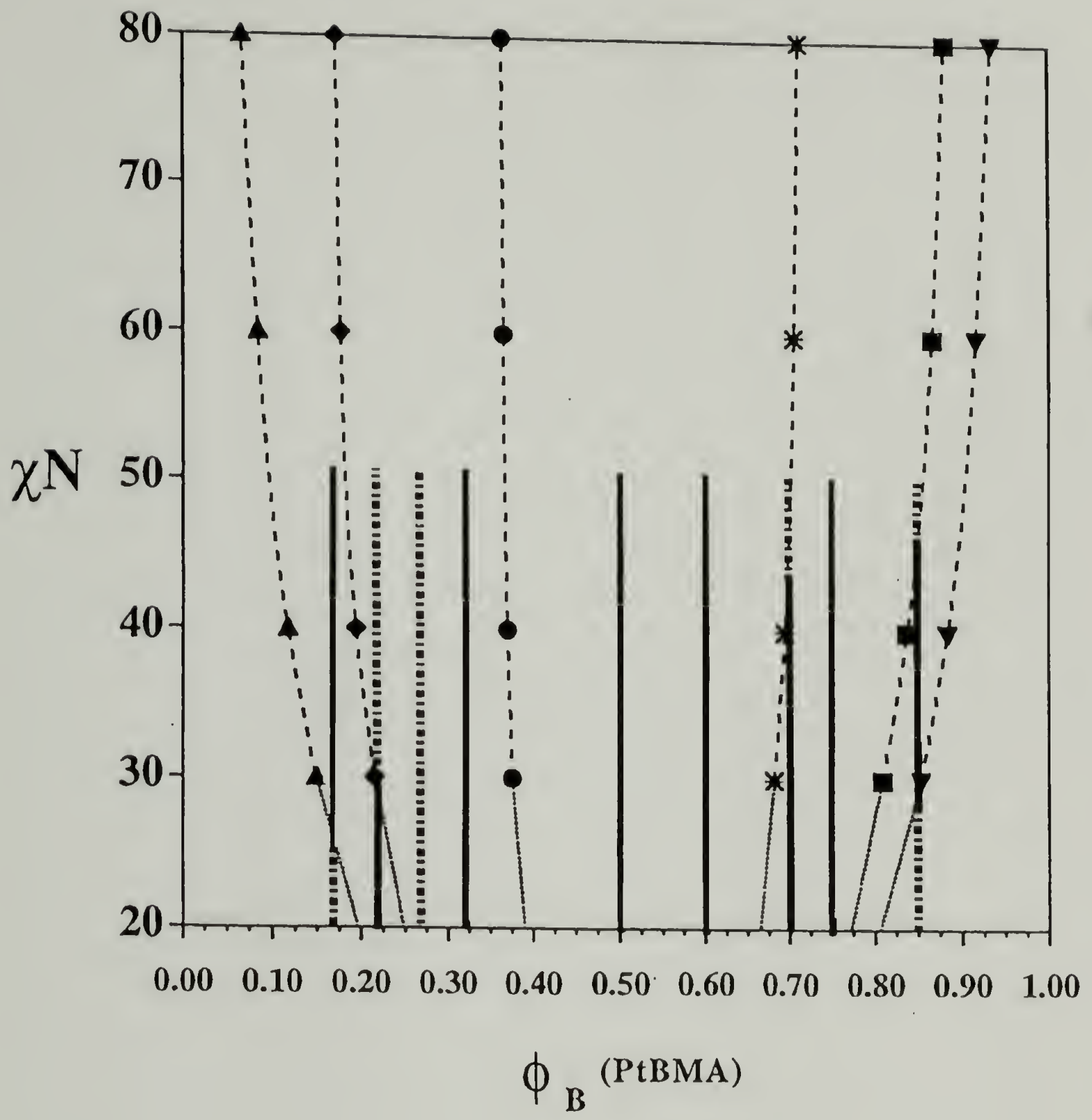


Figure 4.6: Calculated phase diagram for linear diblock copolymer series with $\varepsilon = 0.75$. The B block in the calculations has the larger product of $\rho_o b^2$ in the calculation of $\varepsilon$ which represents PtBMA in the experimental work. The phase boundaries are demarcated as follows: ▲ Homogeneous to B spheres, ◆ B spheres to B cylinders, ● B cylinders to alternating AB lamellae, ✳ lamellae to A cylinders, ■ A cylinders to A spheres, and ▼ A spheres to homogeneous. The PI/PtBMA sample series is represented by the set of vertical lines at the respective volume fractions of the samples. Experimental and theoretical agreement is indicated via a solid line while discrepancies are shown with alternating dotted and dashed lines.

The very slight discrepancies in PtBMA-70 and -85 around $\chi N = 50$ can be attributed to uncertainty in calculating $\varepsilon$ due to the range of literature values for PI density and statistical segment length and the standard deviation of our own $R_g$ values determined for PtBMA in Table II. However, the significant discrepancies for PtBMA-22 and PtBMA-27 can not be accounted for by uncertainty in $\varepsilon$.

An initial concern was the possibility of nonequilibrium effects from the solvent casting process due to diffusional transport limitations. During evaporation of the solvent and the traversing of the ODT a spherical microphase is predicted to occur at all compositions over a finite window of low $\chi N$.[41] As more solvent evaporates the barrier to diffusion of the minority chains through the incompatible matrix may quickly become large and the morphology at that particular polymer/solvent concentration will become kinetically frozen and trap, for example, PtBMA-27 in a spherical morphology instead of the expected cylinder morphology. Simple annealing treatments above $T_g$ of both constituent blocks may not be a strong enough perturbation to drive the system to equilibrium in the dry state. It is impossible at large $\chi N$, in the strongly segregated state, to transform a dispersed spherical phase into a more connected cylindrical phase.[42] Much weaker segregation must be attained before order-order transition from spheres to cylinders can occur.[35]

If the solvent casting kinetically trapped a weakly segregated equilibrium phase of spheres due to diffusion limitations one would expect this effect at asymmetric volume fractions on both sides of the phase diagram. But, we find that samples PtBMA-70 and -75 form extremely well developed cylindrical phases at similar or higher asymmetries in composition than in PtBMA-27. In addition, recent experimental results in the region of the diblock copolymer ODT reveal that a cubic spherical phase is rarely detected between the homogeneous and hexagonal cylinder phase on cooling from the block copolymer melt[43] contrary to theory.[41] Another piece of evidence against kinetic limitations of the solvent casting process is the fact that toluene is slightly selective for PtBMA. This

would have the effect of driving the phase behavior artificially towards that expected at larger relative volume fractions of PtBMA, favoring the formation of hexagonally packed cylinders for PtBMA-22 and -27.

The above reasoning suggests that the spherical phases in PtBMA-22 and -27 are equilibrium, strongly segregated phases. The confinement of the experimental/theoretical disagreement around the PtBMA sphere to cylinder transition suggests other, more intriguing causes for the discrepancies. Firstly, there may be a large compositional dependence to $\chi$ between PI and PtBMA. This would have the effect of lowering $\chi N$ for the samples with large asymmetry in relative volume fraction and perhaps bring PtBMA-27 into agreement with the calculated behavior. But this would also have the effect of simultaneously greatly lowering the $\chi N$ for all other samples with asymmetric volume fractions and would drive PtBMA-17, 22, 75, and 85 all into disagreement with the calculations. Also, sample PtBMA-75, which is even more highly asymmetric in volume fraction than PtMBA-27, formed an extremely well ordered hexagonally packed cylindrical microstructure indicative of a strongly segregated, equilibrium state for the system. A compositional dependence of $\chi$ for the PI/PtBMA system would only fine tune the values of $\chi N$ but does not account for the discrepancies at low relative volume fractions of PtBMA.

Another possibility to explain the discrepancies between calculated and experimentally determined phase behavior is the possibility of a compositional dependence of the $\varepsilon$ parameter and the conformational asymmetry effect which it represents. One can split the sample series into two parts. The first part, all samples with $\phi_{PtBMA} > 0.30$, agrees with the calculated morphology behavior. The other part of the sample series, the PtBMA sphere forming samples with $\phi_{PtBMA} < 0.30$, disagree with the calculations to varying extents depending on the value of $\chi N$ one chooses. This suggests that the entropy gained by the relaxation of the more flexible block, at the expense of forcing an increase in the AB interfacial curvature towards the more rigid block, may have

greater importance at high relative volume fractions of the more flexible block, i.e. where spherical micelles of PtBMA exist in a matrix of PI. As the relative volume fraction of the PI coil block decreases the morphological consequences of the energy penalty of increased stretching for the PI block relative to the PtBMA block decreases. For $\phi_{PtBMA} > 0.32$ it seems that the entropic chain stretching penalty disparity between PI and PtBMA is not able to effect the morphological behavior in a significant way; the system behavior is not noticeably different from even the conformationally symmetric case where all OOT's are symmetric around $\phi$=0.50.[44] To rigorously test the concept of a compositional dependence of $\varepsilon$ the phase behavior of several series of samples must be characterized. Each series with a different value of $\varepsilon$ should encompass a wide range of relative volume fractions of stiff block to coil block. Initial work towards this goal is underway in our laboratory.

## 4.5 Conclusions

The strongly segregated morphological behavior of a series of conformationally asymmetric linear diblock copolymers of polyisoprene and poly(tert-butylmethacrylate) was characterized across a wide range of relative volume fractions. The experimentally determined phase behavior was compared to that calculated utilizing a self consistent mean-field theory developed for linear, conformationally asymmetric block copolymers at finite segregations (finite values of $\chi$N). The mismatch of unperturbed chain dimensions between PI and PtBMA due to a difference in statistical segment lengths is theoretically predicted to produce a significant difference in entropic chain stretching penalties between the more coiled block (PI) and the more expanded block (PtBMA) in the microphase separated state. This, in turn, should push the volume fraction windows in which the strongly segregated morphologies are found to higher volume fraction of the more expanded PtBMA block. Experimental results are consistent with small phase boundary shifts calculated for middle to high relative volume fraction of the expanded PtBMA block

($\phi_{PtBMA} > 0.30$). However, disagreement was found between experiment and the calculated morphological behavior at $\phi_{PtBMA} < 0.30$ with spheres persisting to relatively large volume fractions of PtBMA. The discrepancy may be due to a compositional dependence of the entropic chain stretching penalty disparity between the more expanded PtBMA block and the more coiled PI block or possibly to non-equilibrium effects. More work is needed in order to fully understand the discrepancies between the experimentally determined and calculated phase behavior and to probe the possibility of any compositional dependence of conformational asymmetry in the strongly segregated state of diblock copolymers.

## 4.6 References


(1) Helfand, E.; Wasserman, Z. R. "Block Copolymer Theory. 6. Cylindrical Domains." *Macromolecules*, **13**, 994 (1980 ).

(2) Semenov, A. N. "Contribution to the Theory of Microphase Layering in Block Copolymer Melts." *Sov. Phys. JETP*, **61**, 7331 (1985).

(3) Bates, F. S. "Block Copolymers." *Science*, **251**, 845 (1991).

(4) Helfand, E.; Wasserman, Z. R. "Block Copolymers." In: *Developments in Block Copolymers*; I. Goodman, Ed.; Elsevier: New York, 1982; Vol. 1.

(5) Vavasour, J. D.; Whitmore, M. D. "Self-Consistent Field Theory of Block Copolymers with Conformational Asymmetry." *Macromolecules*, **26**, 7070 (1993).

(6) Helfand, E.; Sapse, A. M. "Theory of Unsymmetric Polymer-Polymer Interfaces." *The Journal of Chemical Physics*, **62**, 1327 (1975).

(7) Bates, F. S.; Fredrickson, G. H. "Conformational Asymmetry and Polymer-Polymer Thermodynamics." *Macromolecules*, **27**, 1065 (1994).

(8) Fredrickson, G. H.; Liu, A. J.; Bates, F. S. "Entropic Corrections to the Flory-Huggins Theory of Polymer Blends: Architectural and Conformational Effects." *Macromolecules*, **27**, 2503 (1994).

(9) Bates, F. S.; Schulz, M. F.; Rosedale, J. H.; Almdal, K "Correlation of Binary Polyolefin Phase Behavior with Statistical Segment Length Asymmetry. *Macromolecules*, **25**, 5547 (1992).

(10) Almdal, K.; Koppi, K. A.; Bates, F. S.; Mortensen, K. "Multiple Ordered Phases in a Block Copolymer Melt." *Macromolecules*, **25**, 1743 (1992).

(11) Gehlsen, M. D.; Bates, F. S. "Conformational Asymmetry in Poly(vinylcyclohexane) Containing Diblock Copolymers." *Macromolecules*, **27**, 3611 (1994).

(12) Matsen, M. W.; Schick, M. "Stable and Unstable Phases of a Diblock Copolymer Melt." *Phys. Rev. Lett.*, 72, 2660 (1994).

(13) Matsen, M. W.; Bates, F. S. "Conformationally Asymmetric Block Copolymers." *J. Polym, Sci., Polym. Phys.* **35**, 945 (1997).

(14) Morton, M.; Fetters, L. J. "Anionic Polymerization of Vinyl Monomers." *Rubber Chemistry and Technology*, **48**, 359 (1975).

(15) Karandinos, A.; Nan, S.; Mays, J. W.; Hadjichristidis, N. "Solution Properties and Unperturbed Dimensions of Stereoregular Poly(*t*-butylmethacrylates)." *Macromolecules*, **24**, 2007 (1991).

(16) Long, T. E.; Broske, A. D.; Bradley, D. J.; McGrath, J. E. "Synthesis and Characterization of Poly(*t*-butylmethacrylate-*b*-isoprene-*b*-*t*-butylmethacrylate) Block Copolymers by Anionic Techniques." *J. Polym. Sci., Polym. Chem. Ed.*, **27**, 4001 (1989).

(17) Barton, A. F. M., Ed. *Handbook of Polymer-Liquid Interaction Parameters & Solubility Parameters*; CRC Press: Boston, 1990.

(18) Rounds, N. A. University of Akron: Ph.D. Dissertation, 1970.

(19) Mori, K.; Hasegawa, H.; Hashimoto, T. "Small-Angle X-Ray Scattering from Bulk Block Polymers in Disordered State. Estimation of $\chi$ Values from Accidental Thermal Fluctuations." *Polymer Journal*, 17, 799 (1985).

(20) Owens, J. N.; Gancarz, I. S.; Koberstein, J. T.; Russell, T. P. "Investigation of the Microphase Separation Transition in Low Molecular Weight Diblock Copolymers." *Macromolecules*, 22, 3380 (1989).

(21) Bras, W.; Derbyshire, G. E.; Ryan, A. J.; Mant, G. R.; Felton, R. A.; Lewis, R. A; Hall, C. J.; Greaves, G. N. "Synchrotron X-Ray Camera for Simultaneous Wide-Angle and Small-Angle Scattering." *Nucl. Instrum. Methods Phys. Res.*, **A326**, 587 (1993).

(22) Flory, P. J. *Statistical Mechanics of Chain Molecules*; Wiley-Interscience: New York, 1969.

(23) Brandrup, J., Immergut, E.H., Eds. *Polymer Handbook*, 3rd ed.; John Wiley & Sons: New York, 1989; p. IV-310.

(24) Bareiss, R. E. "Polymolecularity Correction Formulae for the Claculation of Weight and Number Average Mean Squared Radii of Gyration from Experimentally Determined Z-Average Mean Squared Radius of Gyration. *Eur. Polym. J.*, **19**, 847 (1983).

(25) Kozhokaryu, M.; Skazka, V. S.; Berdnikova, K. G. "The Chain Statistics of Poly(*t*-butylmethacrylate)." *Vysokomol. Soedin.*, **8**, 1063 (1967).

(26) Stockmayer, W. H. "Some Remarks on Excluded Volume and on Intrinsic Viscosity Plots" *Br. Polym. J.*, 9, 89 (1977).

(27) Yamakawa, H. *Modern Theory of Polymer Solutions*; Harper and Row: New York, 1971; Ch. 7.

(28) Stickler, M.; Panke, D.; Wunderlich, W. "Solution Properties of Poly(methylmethacrylate) in Methyl Methacrylate. 1. Viscosities from the Dilute to the Concentrated Regimes." *Makromol.* Chem., **188**, 2651 (1987).

(29) Fox Jr., T. G.; Flory, P. J. "Unperturbed Coil Dimensions from Dilute Solution Viscometry." *J. Phys. Colloid Chem.*, **53**, 197 (1949).

(30) Zimm, B. H. "Chain Molecule Hydrodynamics by the Monte-Carlo Method and the Validity of the Kirkwood-Riseman Approximation." *Macromolecules*, **13**, 592 (1980).

(31) Fujii, Y.; Tamai, Y.; Konishi, T.; Yamakawa, H. "Intrinsic Viscosities of Oligo and Poly(methylmethacrylates." *Macromolecules*, **24**, 1608 (1991).

(32) Konishi, T.; Yoshizaki, T.; Yamakawa, H. "On the 'Universal Constants' $\rho$ and $\phi$ of Flexible Polymers." *Macromolecules*, **24**, 5614 (1991).

(33) Li, J.; Wan, Y.; Xu, Z.; Mays, J. W. "Third Virial Coefficients of Polystyrene in Different Theta Solvents." *Macromolecules*, **28**, 5347 (1995).

(34) Lewis, P. R.; Price, C. "The Morphology of $(Styrene)_x$ $Isoprene)_y$ $(Styrene)_x$ Block Copolymers." *Polymer*, **12**, 258 (1972).

(35) Sakurai, S.; Kawada, H.; Hashimoto, T.; Fetters, L.J. "Thermoreversible Morphology Transition between Spherical and Cylindrical Microdomains of Block Copolymers." *Macromolecules*, 26, 5796 (1993).

(36) Pispas, S.; Mays, J. W.; Pochan, D. J.; Gido, S. P. unpublished data, 1996.

(37) Hajduk, D. A.; Gruner, S. M.; Rangarajan, P.; Register, R. A.; Fetters, L. J.; Honeker, C.; Albalak, R. J.; Thomas, E. L. "Observation of a Thermotropic Order-Order Transition in a Diblock Copolymer." *Macromolecules*, **27**, 490 (1994).

(38) Folkes, M. J.; Keller, A. "The Birefringence and Mechanical Properties of a 'Single Crystal' from a Three Block Copolymer." *Polymer*, **12**, 222 (1971).

(39) Pochan, D. J.; Gido, S. P.; Pispas, S.; Mays, J. W.; Ryan, A. J.; Fairclough, J. P. A.; Hamley, I. W.; Terrill, N. J. "Morphologies of Microphase-Separated $A_2B$ Simple Graft Copolymers." *Macromolecules*, **29**, 5091 (1996).

(40) Matsen, M. W.; Whitmore, M. D. "Accurate Diblock Copolymer Phase Boundaries At Strong Segregations Using SCFT." *J. Chem. Phys.*, **105**, 9698 (1996).

(41) Matsen, M. W.; Schick, M. "Self-Assembly of Block Copolymers." *Current Opinion in Colloid and Interface Science*, **1**, 329 (1996).

(42) Pochan, D. J.; Gido, S. P.; Pispas, S.; Mays, J. W. "Morphological Transitions in an $I_2S$ Simple Graft Block Copolymer: From Folded Sheets to Folded Lace to Randomly Oriented Worms at Equilibrium." *Macromolecules*, **29**, 5099 (1996).

(43) Khandpur, A. K.; Foerster, S.; Bates, F. S.; Hamley, I. W.; Ryan, A. J.; Bras, W.; Almdal, K.; Mortensen, K. "Polyisoprene-Polystyrene Diblock Copolymer Phase Diagram near the Order-Disorder Transition." *Macromolecules*, **28**, 8796 (1995).

(44) Vavasour, J. D.; Whitmore, M. D. "Self-Consistent Mean Field Theory of the Microphases of Diblock Copolymers." *Macromolecules*, **25**, 5477 (1992).

# CHAPTER 5

# STUDIES INITIATED TO FURTHER PROBE THE EFFECTS OF MOLECULAR ARCHITECTURE AND CONFORMATIONAL ASYMMETRY ON BLOCK COPOLYMER PHASE BEHAVIOR

## 5.1 Introduction

The focus of this final experimental chapter is the initial morphological characterization of three new sample series further addressing the effects of molecular architecture and conformational asymmetry on block copolymer morphological behavior. Firstly, trifunctional chlorosilane coupling chemistry, the same method utilized in the synthesis of $A_2B$ symmetric graft copolymers studied in chapter 2, has recently been extended to the synthesis of three new graft block copolymers with novel molecular architectures. The first of these new architectures is identical to the $A_2B$ symmetric graft with the slight modification that the two A blocks are of different lengths. This new architecture is thereby named an asymmetric simple graft, or ASG. The other new graft architectures, the "π" and "H", contain two trifunctional coupling sights per molecule instead of one as found in $A_2B$ and ASG.Secondly, a comprehensive set of blending

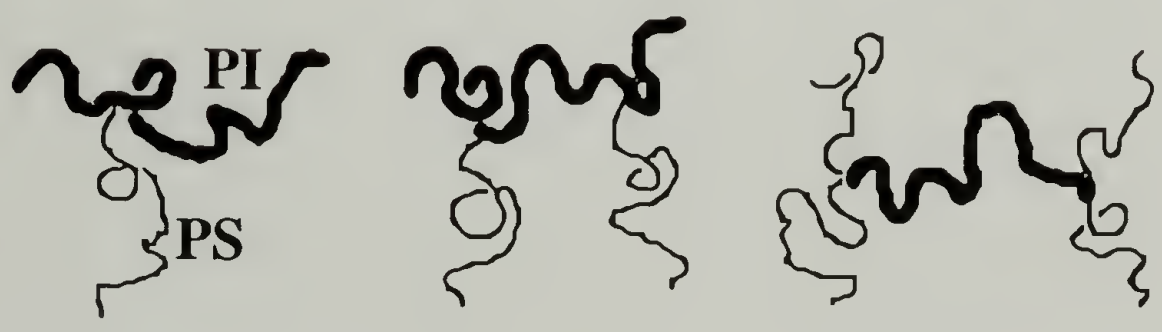


Figure 5.1: Schematic of ASG (off-center, asymmetric graft), (SI)I(SI) (π), and $S_2IS_2$ (H) graft architectures

experiments with the $A_2B$ simple grafts was initiated in order to more rigorously test the accuracy of the order-order phase boundaries calculated by Milner[1] (chapter 2) and to elucidate the volume fraction window of stability of the ROW phase (chapter 3). Thirdly, the concept of conformational asymmetry is being further pursued via the initial study of block copolymers with tunable degrees of conformational asymmetry.

The remainder of the chapter represents only the initial experiments that have been performed with these new samples. Rigorous investigations of the complete complicated graft architecture series, blends, and tunable conformationally asymmetric linear diblocks are currently in progress.[2-7]

## 5.2 ASG, "π", and "H" Molecular Architecture

### 5.2.1 Introduction

With the morphological behavior of the $A_2B$ architecture well characterized[8] (see chapters 2 and 3), as well as a series of $A_2B$ and $A_3B$ samples independently investigated,[9] research is now extending to more complex architectures. We have recently characterized the morphological behavior of several more complicated graft architectures based on trifunctional silane coupling agents as used in the synthesis of the $A_2B$ samples.[10] A total of three new architectures were produced with PI backbones and PS grafts. They are the asymmetric simple graft copolymer, or ASG, the (SI)I(SI), or π, multigrafted copolymer and the $S_2IS_2$, or H, multigrafted copolymer. For clarity, the ASG architecture, the simplest of these new architectures, is described first, although no experimental results concerning this type of architecture are presented. This molecule is similar in architecture to the $A_2B$ simple grafts with the exception that the two A (PI) backbone blocks are of different length. A 2:1 arm number asymmetry between A and B blocks is created in the microphase separated state just as found in symmetric $A_2B$ blocks. However, in the ASG system the A phase consists of a bimodal brush due to the two different lengths of backbone blocks. The asymmetry in lengths of the two A arms

introduces the parameter τ, first used in the calculations of Olvera de la Cruz and Sanchez,[11] which is the fractional length across the A backbone from which the single B (PS) graft emanates. For example, $\tau = 0.50$ in the limiting case of the $A_2B$ simple graft where the B graft is linked to two A arms of equal length while $\tau = 1.0, 0.0$ in a linear diblock. A complete study of the effects of this new architecture was recently completed.[2]

### 5.2.2 "π" and "H" Morphology Experimental

The other two new architectures which were experimentally investigated both involve two silane coupling sights per molecule allowing for more complicated architectures. In one new architecture the PI backbone has a trifunctional branch point on each of its ends to each of which are grafted two PS arms. This forms an $S_2IS_2$ molecule with the conceptual shape of the letter "H". Similarly, the other new architecture contains two trifunctional branch points approximately 20 vol. % from each end of a PI backbone from each of which are grafted only one PS graft. This strategy forms an overall (SI)I(SI) molecule with the shape of the Greek letter "π". Both molecules are schematically represented in Figure 5.1. The molecular characteristics of the two samples used in the morphological experiments are listed in Table 5.1. The π system formed a cubic array of PS spheres in a PI matrix after casting from the nonselective solvent

Table 5.1

$S_2IS_2$, or π, and (SI)I(SI), or H, Molecular Characteristics: (a) Membrane osmometry in toluene at 37°C, (b) LALLS in THF at 25°C, (c) $^1$H-NMR

| Sample | $M_n \times 10^{-4}$ (a) | $M_w$ (b) | Wt. Fraction PS(c) |
|---|---|---|---|
| $S_2IS_2$ | 17.1 | 17.4 | 0.42 |
| (SI)I(SI) | 13.3 | 14.7 | 0.24 |

toluene and subsequent annealing at 120°C for one week. This can clearly be seen in the electron micrograph of a cryomicrotomed, $OsO_4$ stained section in Figure 5.2. Due to the well developed long range order and large grain size of the microstructure it was possible to tilt between the [100] 4-fold projection and the [111] body diagonal projection of the cubic lattice as can be seen in Figure 5.2a and b respectively. Also, the first four reflections characteristic of a cubic lattice can be seen in the azimuthally integrated, one dimensional SAXS plot of log intensity vs. q in Figure 5.3a where $q = 4\pi/\lambda(\sin\theta/2)$ and $\theta$ is the scattering angle. The H system formed an alternating lamellar microstructure after casting from toluene and annealing at 120°C for one week. A characteristic micrograph revealing the layered microstructure is shown in Figure 5.4 while two orders of the lamellar long spacing can be seen Figure 5.3b.

### 5.2.3 "π" and "H" Morphology Discussion

The morphological behavior of these complex architectures can be rationalized by decomposing the molecules into simpler graft building blocks. This can be accomplished by conceptually cutting the PI backbones in half and forming two $A_2B$ species in the case of the H architecture and two ASG from the π architecture. The morphologies can then be directly compared to that predicted theoretically in Milner's calculated phase behavior as seen in Figure 5.5. Since the H molecule can be decomposed into two $A_2B$ symmetric grafts the experimental results can be directly compared to those theoretically predicted for $A_2B$ systems. The asymmetry parameter, ε, for H is approximately 2.2 on the phase diagram since A = PS and B = PI in the two $A_2B$ building blocks per molecule. The asymmetry parameter for π is more difficult to rationalize. Since the π molecule is split into two ASG building blocks the comparison with the calculated phase behavior for $A_nB_m$ architectures may not be theoretically justified; the calculation assumes that the multiple A or B arms are of the same length. While it is experimentally obvious that the system forms a spherical morphology, an exact ε cannot be assigned due to the differing

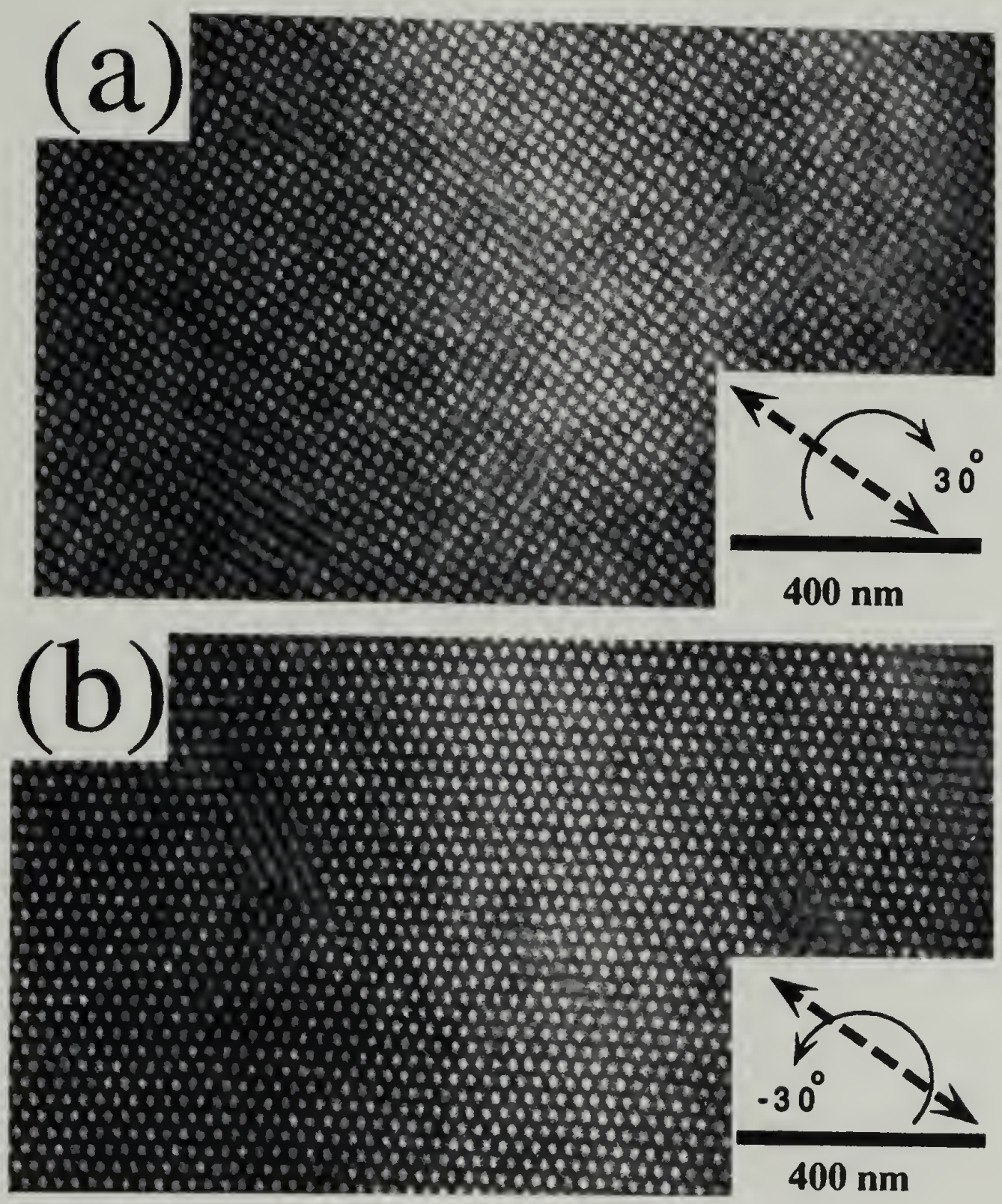


Figure 5.2 Tilt series of TEM images of the π material: (a) square pattern produced by projection along the [100] direction (edge) of the bcc unit cell; (b) hexagonal pattern produced by projection along the [111] direction ( body diagonal) of the bcc unit cell.

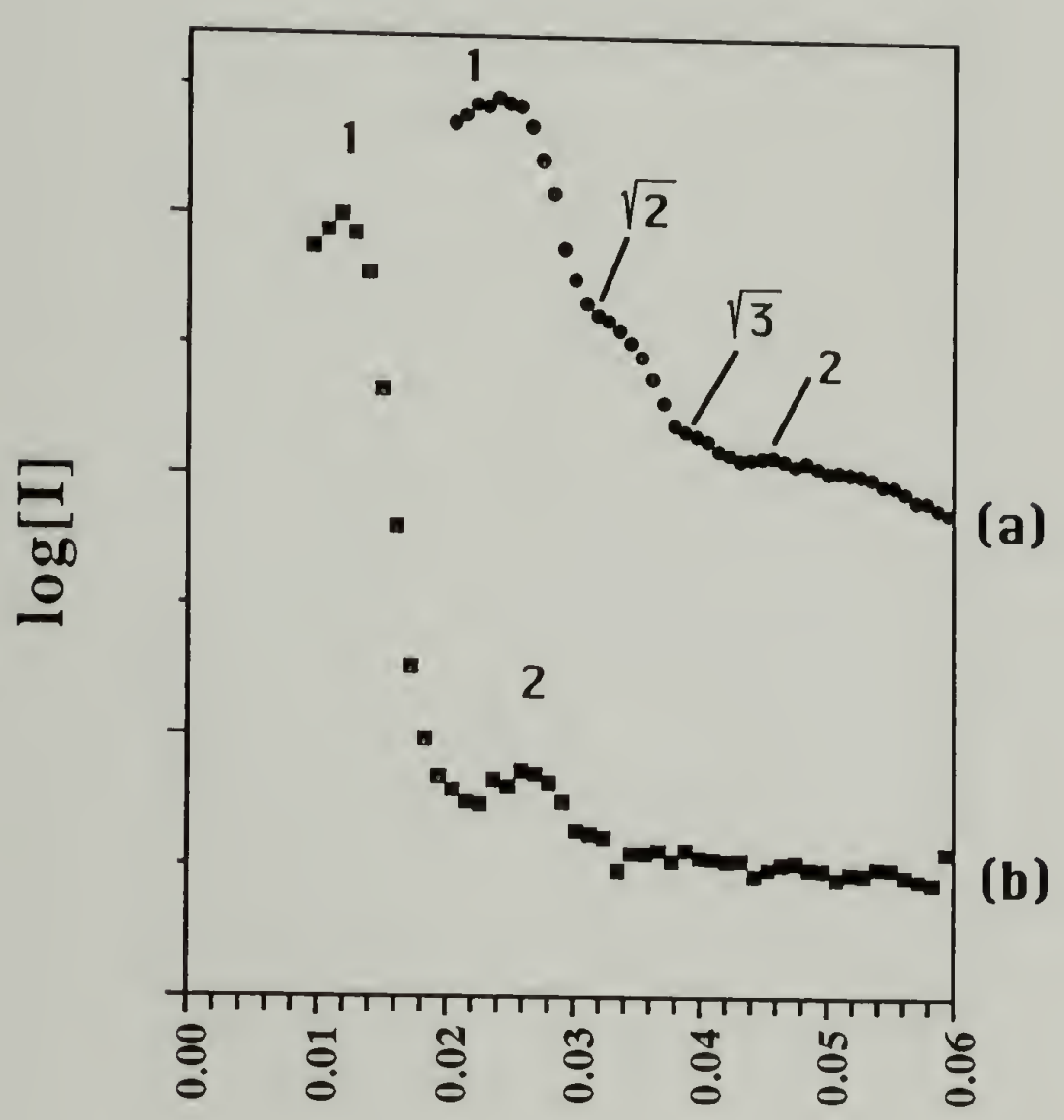


Figure 5.3: Azimuthally integrated, 1-dimensional SAXS patterns of log(I) vs scattering vector, q, of the complex graft architectures with scattering vector ratios indicated for (a) the π material and (b) the H material.

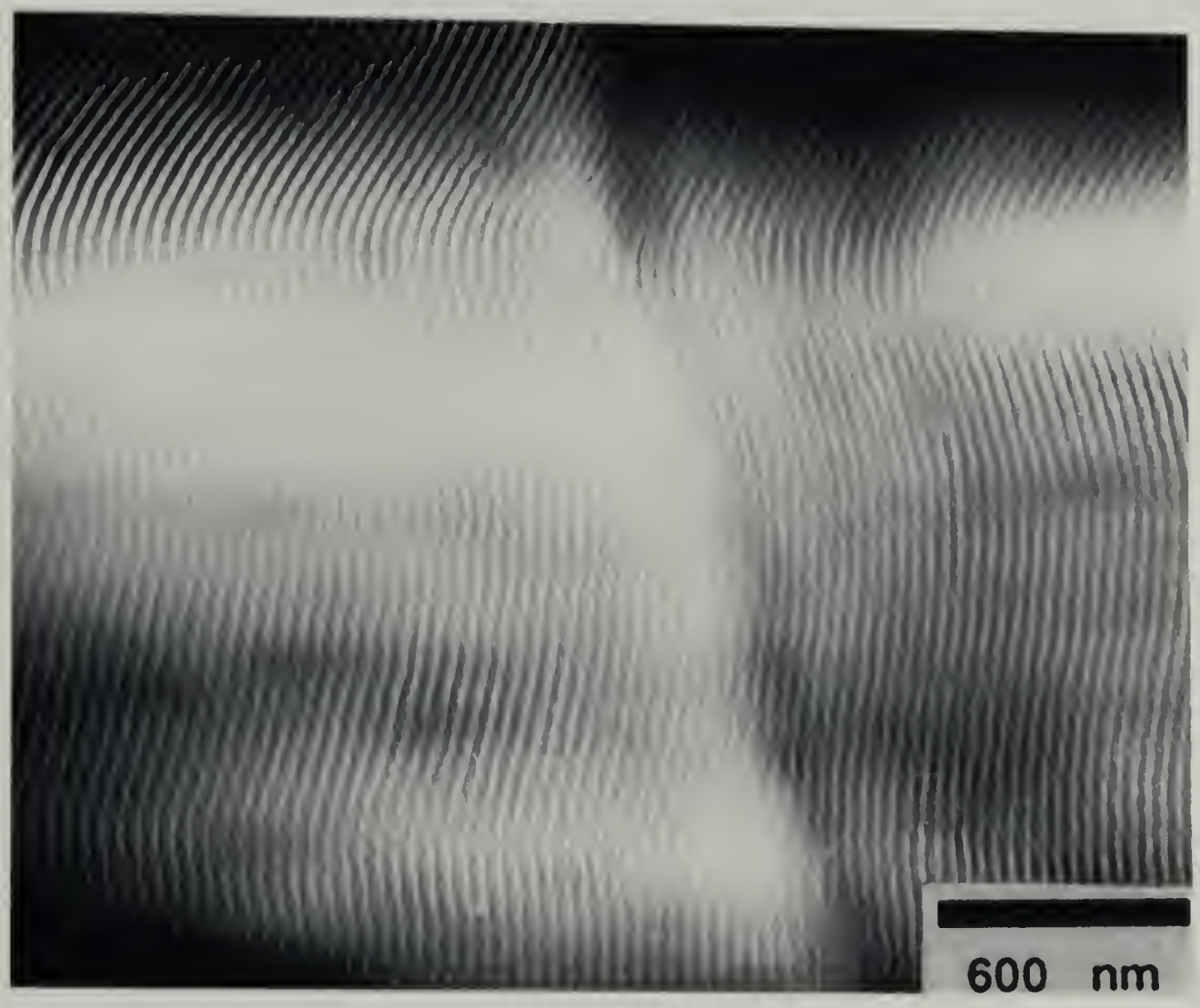


Figure 5.4: TEM micrograph of the lamellar morphology produced by the H material.

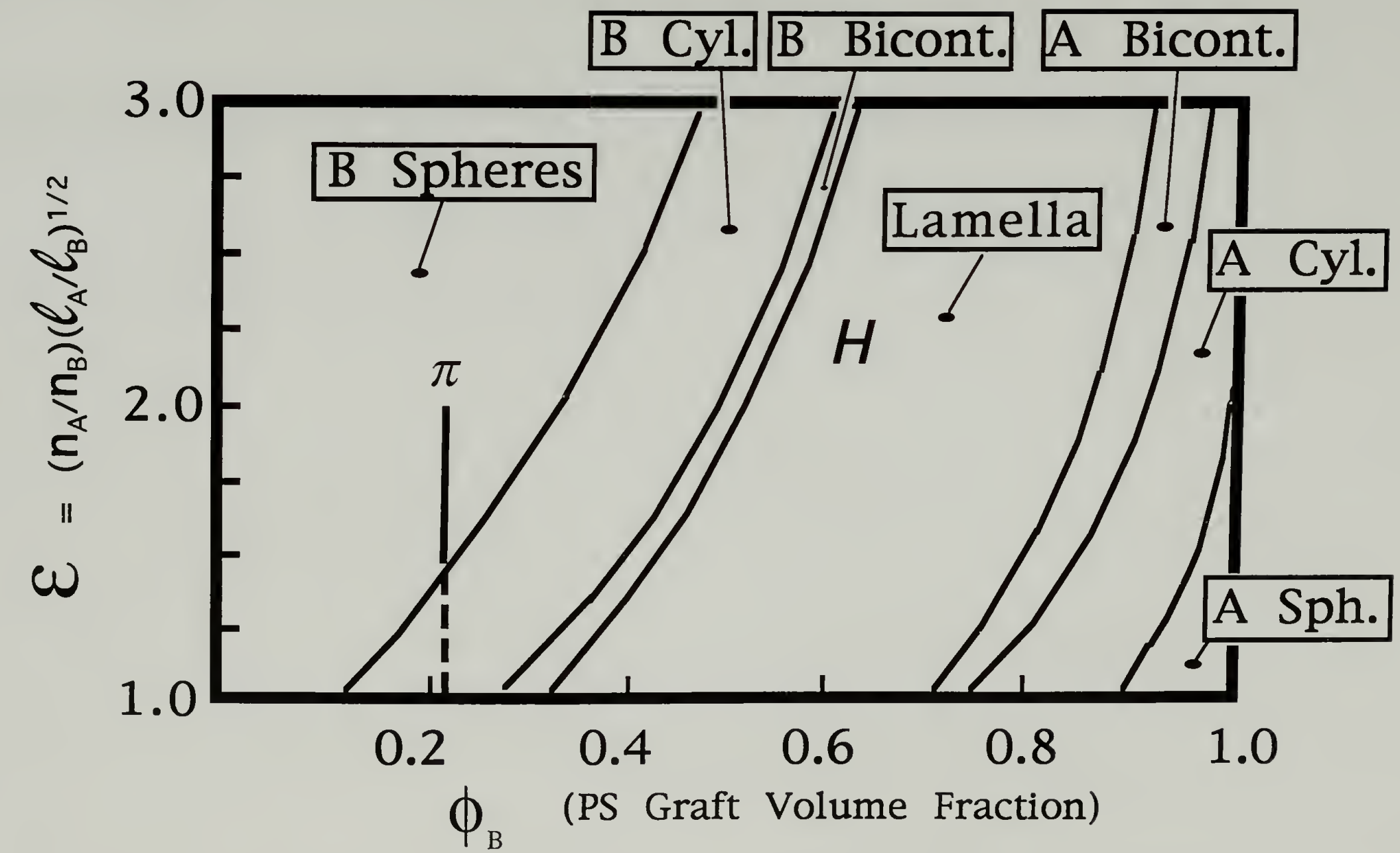


Figure 5.5: Theoretical morphology digram calculated by Milner for simple graft block copolymers. The symbol *H* indicates the mapping of the H architecture onto the diagram by formally dividing it into component simple grafts. The bold segment of the vertical line at a graft volume fraction of 0.21 represents the allowable range of ε for the partitioning of the π architecture.

lengths of the A arms in the ASG building blocks. However, as a first approximation, one can plot the π morphology on Milner's diagram at the relative volume fraction of its ASG building blocks over an allowable range of ε as defined by the sphere morphology region in Figure 5.5. With this caveat in mind, the morphological behavior of the two complex architectures is predicted well based on the theoretically predicted behavior of their constituent $A_2B$ or ASG building blocks.

The fact that one is able to rationalize the morphological behavior of graft copolymers with complex architectures based on its constituent simple building blocks is an important realization. It is hoped that a solid understanding of the morphological behavior of the simple architectures can be used to predict the phase behavior of even more complex molecular architectures. This construct is being thoroughly tested with the current synthesis and subsequent morphology studies of a full series of ASG, π, and H molecules across wide ranges of relative volume fractions.[2-4] These series will also help reveal the morphological implications of the grafting sight along the backbone via different values of τ. In addition to these studies, the molecular complexity is being pushed a step further with the recent synthesis and current morphological characterization of several comb block copolymers with PI backbones and multiple PS grafts.[12] If these comb block copolymers exhibit microphase separation it remains to be seen if the morphologies formed can also be rationalized via the known phase behavior of their constituent $A_2B$ and ASG building blocks as in the case of π and H.

## 5.3 $A_2B$ Binary Copolymer Blends

### 5.3.1 Introduction

In Chapter 2 the morphological characterization of a series of $A_2B$ (A=PI and B=PS) simple graft block copolymers was described in the context of theoretically predicted behavior. The experimental results agreed with the theoretical predictions across the entire sample series except when the relative volume fraction of the single PS

graft first became large enough to force the two PI backbone arms to the concave side of the PS/PI interface in the microphase separated state. Any lattice symmetry was frustrated in this region causing the formation of a randomly oriented, worm-like micelle, or ROW, morphology. In order to map the volume fraction window of stability of this new morphology a study of $A_2B$ copolymer blends with the ROW forming sample has been initiated.

One would ideally wish to study the equilibrium nature of a block copolymer phase with neat copolymer systems. However, the synthesis of block copolymers at every possible relative volume fraction is financially prohibitive, time consuming, and too imprecise to resolve fine features relative to molecular weight and composition. This problem is exacerbated when dealing with unique graft architectures formed via careful and time consuming silane coupling chemistry as in the synthesis of $A_2B$ symmetric graft block copolymers. These problems can be circumvented by performing blending experiments. In particular, by blending two well-defined graft copolymers which are very similar in relative volume fraction one can target precise volume fractions which fall between the two component copolymers. If the copolymers are miscible then the phase behavior displayed in the blend should closely approximate the expected phase behavior for a neat graft copolymer at the same overall composition as present in the blend. However, with the added degree of freedom in the two component system it is also possible to span biphasic regions which replace the order-order transitions between morphologies in a neat system.[13]

### 5.3.2 Experimental

The morphology of six blends focusing on the relative volume fraction region of the ROW phase have been characterized. Specifically, samples $I_2S$-1 and $I_2S$-2 were blended together to form blends PS-83, PS-85, and PS-87 at compositions intermediate between the two copolymers as indicated by the PS volume fraction in the blend title.

Also, blends PS-79, PS-77, and PS-75 were made with copolymers $I_2S$-2 and $I_2S$-3. The compositions of these six blends are schematically represented on the phase diagram Figure 5.6. The molecular characteristics of $I_2S$-1, $I_2S$-2, and $I_2S$-3 can be found in Chapter 2, Table 2.1. The blends were produced via non-selective solvent casting and subsequent annealing treatment identical to that performed on the neat graft copolymers in Chapter 2. Cryomicrotomey and TEM experiments were also carried out in identical fashion to that performed in Chapter 2. However, instead of SAXS experiments, the bulk samples were further characterized via small-angle neutron scattering (SANS). Significant neutron contrast was present in the samples due to the exclusive deuteration of the PS grafts. The SANS experiments were performed at the Cold Neutron Research Facility at the National Institutes of Standards and Technology in Gaithersburg, MD. Beam line NG3-SANS was used with a 5Å wavelength incident radiation parallel to the plane of the bulk films.

The electron micrographs and SANS for blends PS-83, -85, and -87 are shown in Figures 5.7, 5.8, and 5.9. The micrographs display a single morphological behavior in all three blends indicative of miscibility between the blend components. If one mixes block copolymers of significantly different molecular weight macrophase separation of the two block copolymers will occur giving rise to two distinct domain spacings and morphologies.[14] Blends PS-83 and PS-85 contain dispersed PI spherical micelles not arranged on a lattice. However, the PI domains in blend PS-87 seem to be hinting at ordering on a hexagonal lattice although the symmetry is barely observable. Also, the PI domains in PS-87 seem to be more elongated with a higher aspect ratio than the spherical domains in PS-83 and PS-85. Therefore, it seems that the phase behavior is moving towards that found in neat $I_2S$-1, hexagonally packed cylinders, as the volume fraction of PS increases. However, it is counterintuitive that the PI domains become spherical in blend PS-83 even though the constituent graft copolymers, $I_2S$-1 and $I_2S$-2, form more connected worm-like and cylindrical PI domains in the neat state, respectively.

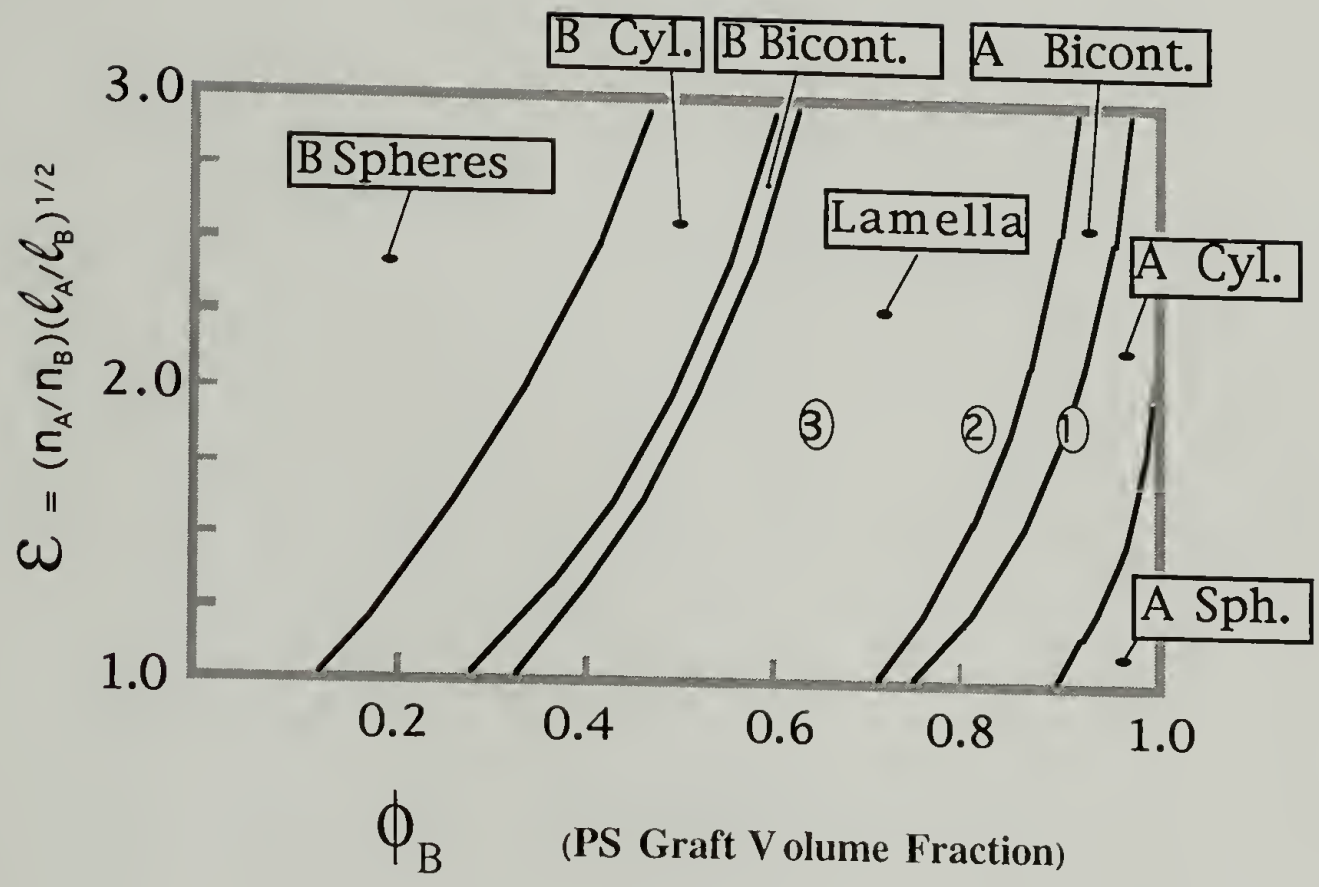


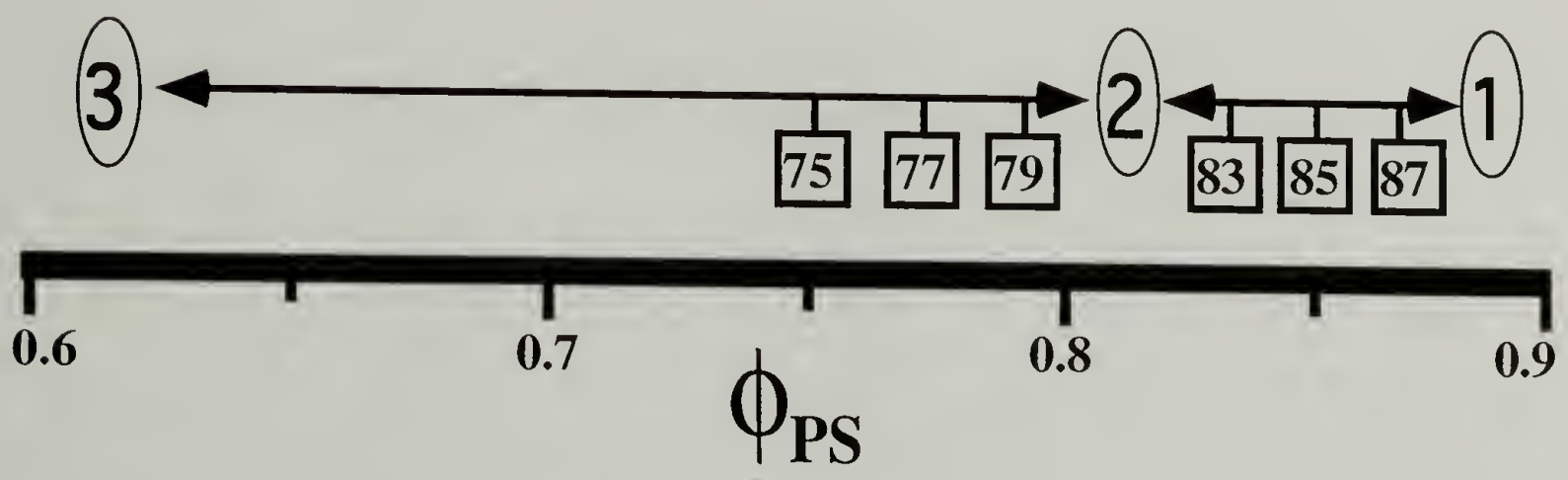


Figure 5.6: Theoretical morphology diagram calculated by Milner for simple graft block copolymers. The x-axis is enlarged to highlight the blend compositions targeted in the mixing of I2S-2 with I2S-3 and I2S-1.

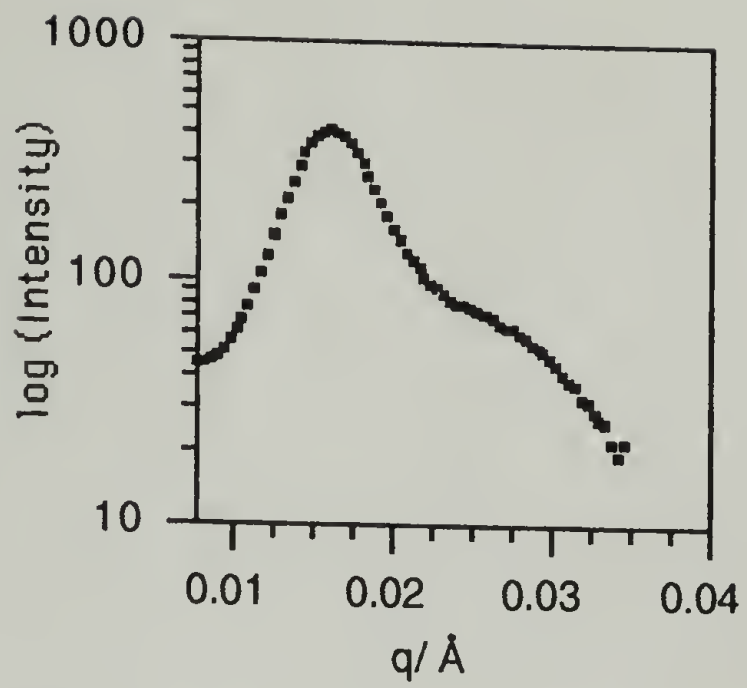


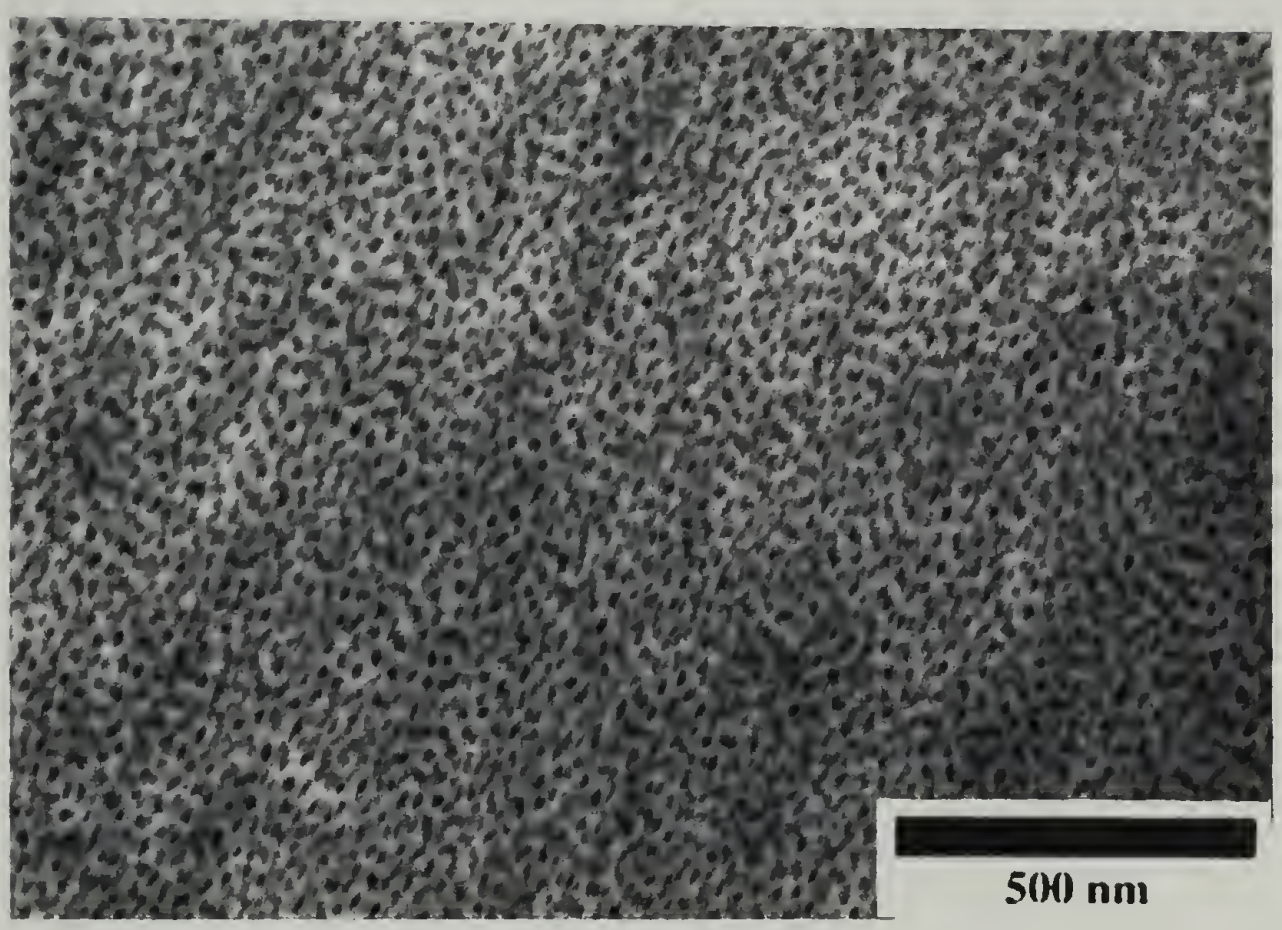


Figure 5.7: TEM micrograph and azimuthally integrated SANS data of intensity vs. scattering vector, q, for Blend PS-83.

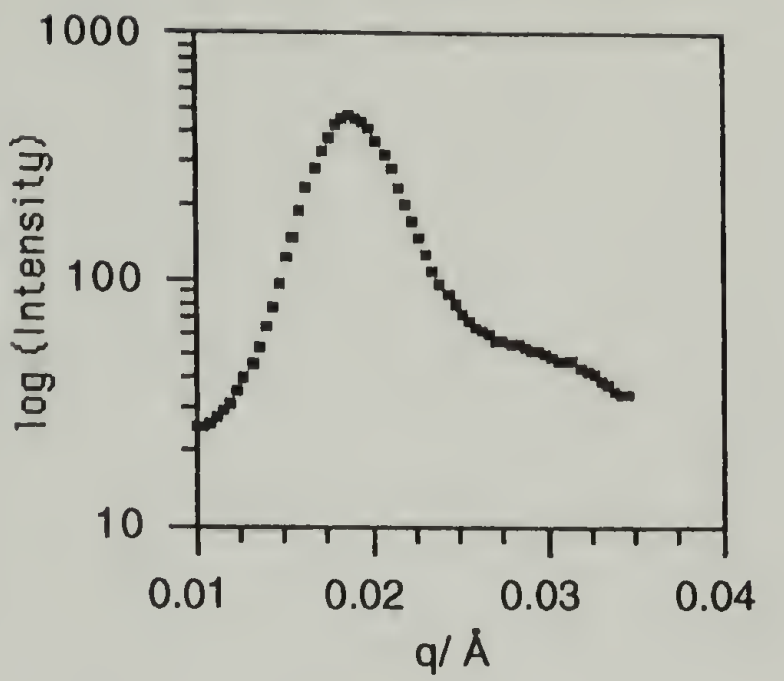


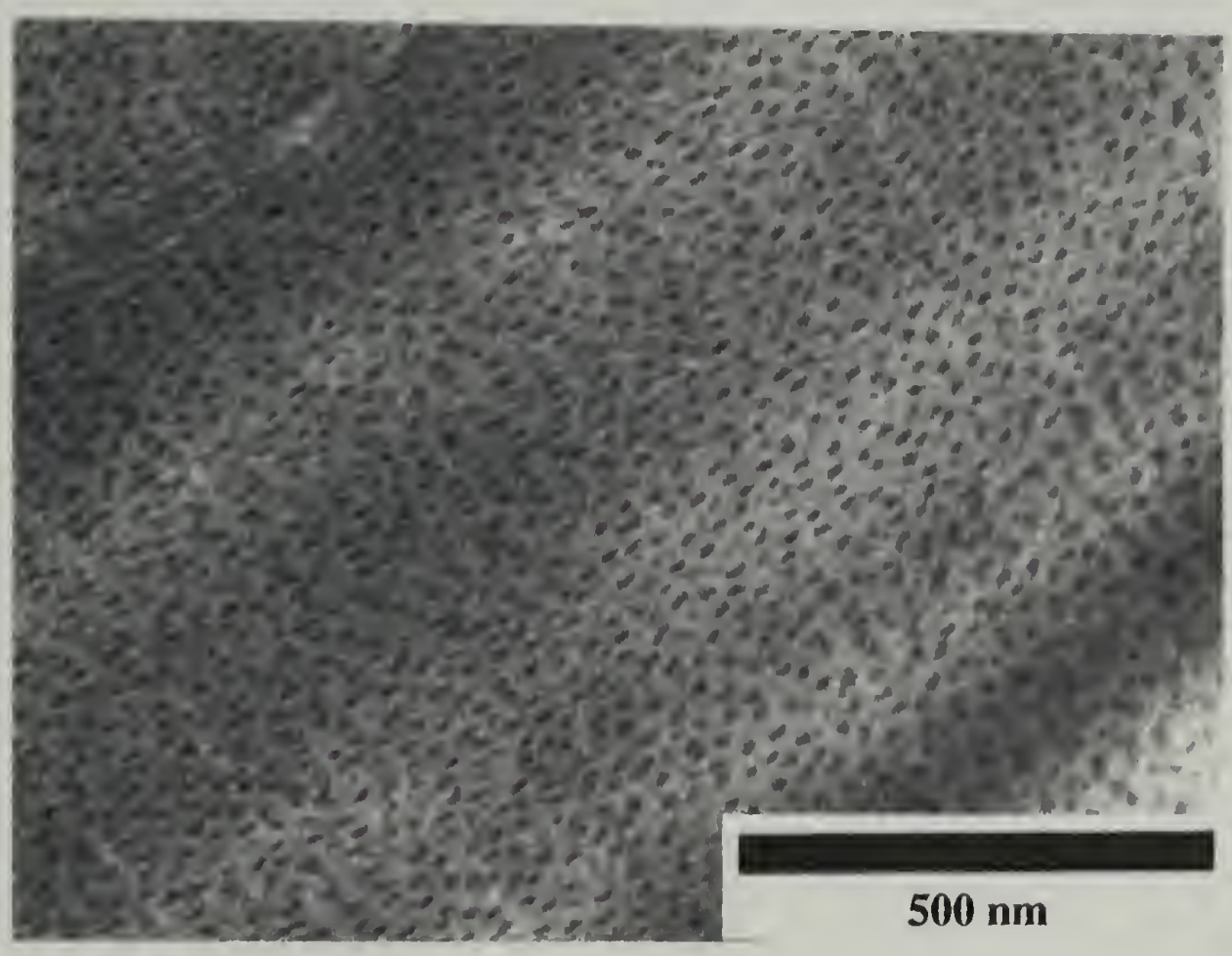


Figure 5.8: TEM micrograph and azimuthally integrated SANS data of intensity vs. scattering vector, q, for Blend PS-85.

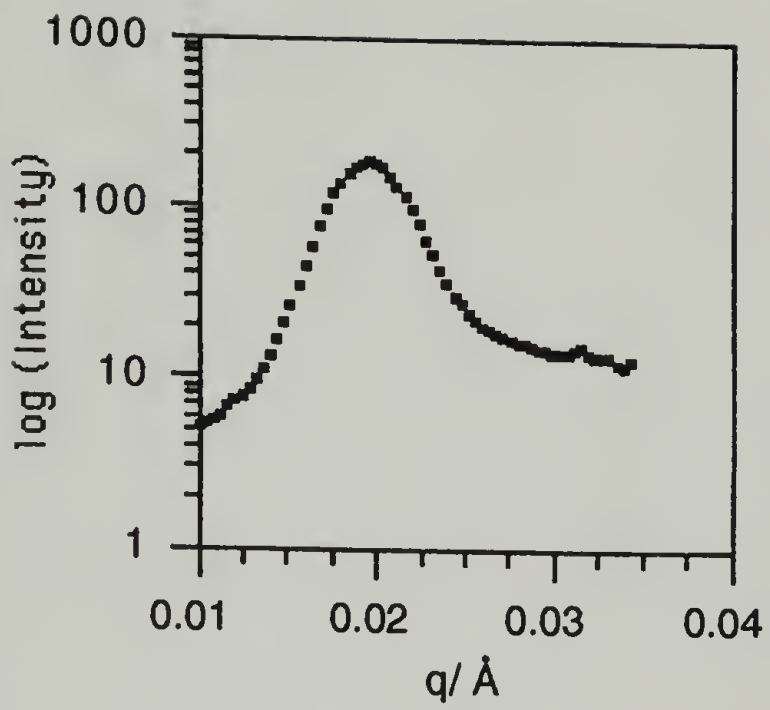


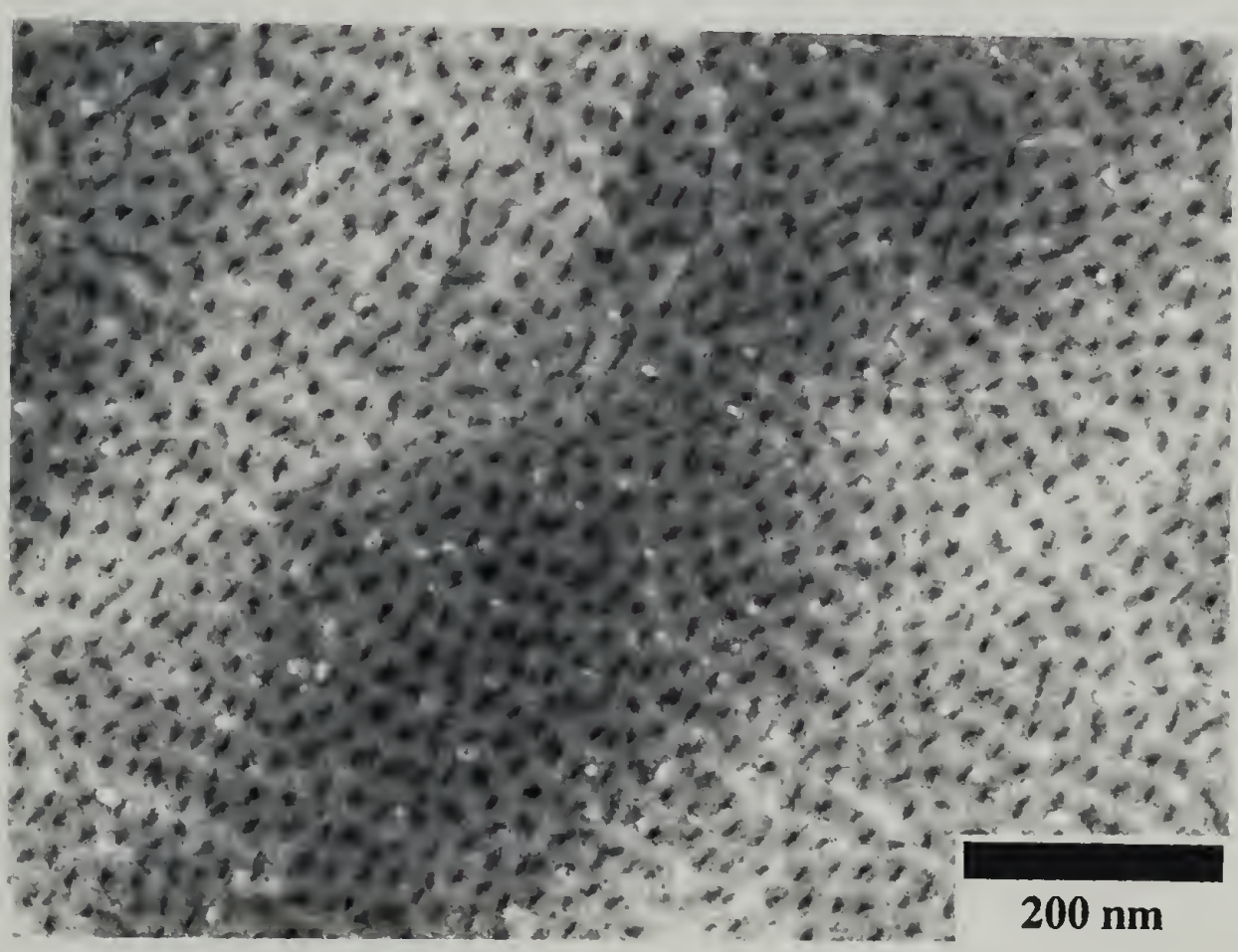


Figure 5.9: TEM micrograph and azimuthally integrated SANS data of intensity vs. scattering vector, q, for Blend PS-87.

The single peak in all three of the SANS patterns arises from the interparticle scattering maximum due to the lack of a strong underlying lattice in all three blends.

The electron micrographs and SANS for PS-79, PS-77, and PS-75 are shown in Figure 5.10, 5.11, 5.12. The morphological behavior of blend PS-79, which contains mostly $I_2S$-2 with only 9 wt. % of $I_2S$-3 added, is strikingly different from the neat $I_2S$-2 ROW phase even though the volume fraction of PS has only decreased by 2 volume percent from $\phi_s = 0.81$ to $\phi_s = 0.79$. Regions of PI layers in a PS matrix can clearly be seen coexisting with regions of a bicontinuous, web-like structure. Due to the apparent miscibility of $I_2S$-1 and $I_2S$-2 in PS-83, PS-85, and PS-87 and since the constituent block copolymers all have similar volume fractions and almost identical molecular weights, PS-79 may represent a biphasic region between the bicontinuous and lamellar regions seen in Figure 5.6. Also, even though 90 wt. % of PS-79 consists of $I_2S$-2, no discrete grains of ROW phase are present also indicative of miscibility between components. No scattering maxima is detected in the SANS data of PS-79 due to the random orientation of both the PI layers and the PI web structures in the coexisting morphologies. Moving to slightly lower PS relative volume fraction in blend PS-77 a much more obvious layered structure can be seen in the electron micrograph. The bicontinuous web-like structure, as seen in PS-79, is no longer present and the regularity of the layered structure is significant enough to produce a weak scattering maximum in the SANS data at $q = 0.071$ nm$^{-1}$. Finally, in PS-75 a much more traditional lamellar morphology is found with a stronger SANS maxima at $q = 0.075$ nm$^{-1}$. With a $\phi_s = 0.75$ the predicted morphology behavior is solidly within the lamellar region of the phase diagram in Figure 5.6.

### 5.3.3 Discussion

A couple of conclusions can be drawn from these initial copolymer blending experiments. Firstly, and most significantly, is that the lattice frustration caused by packing the two PI arms on the concave interface in $I_2S$-2 ($\phi_s = 0.81$) seems to persist in

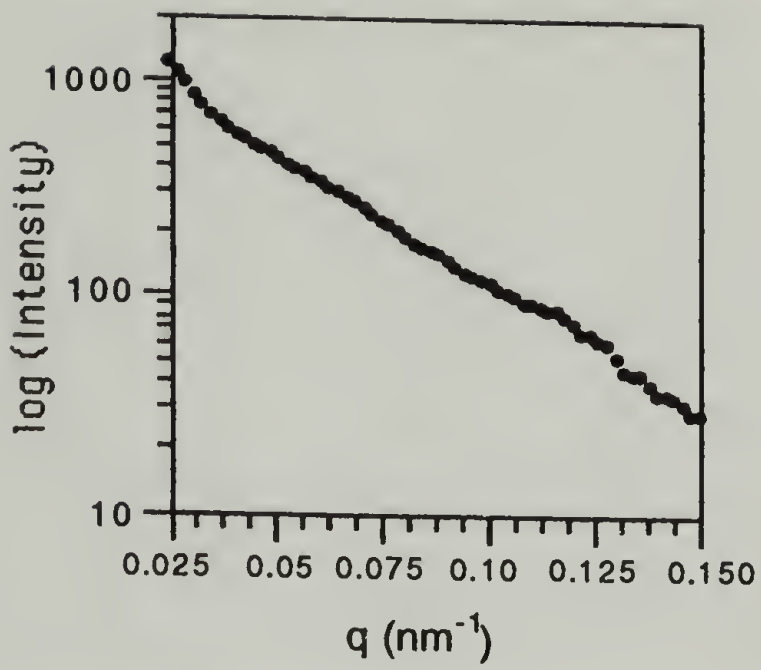


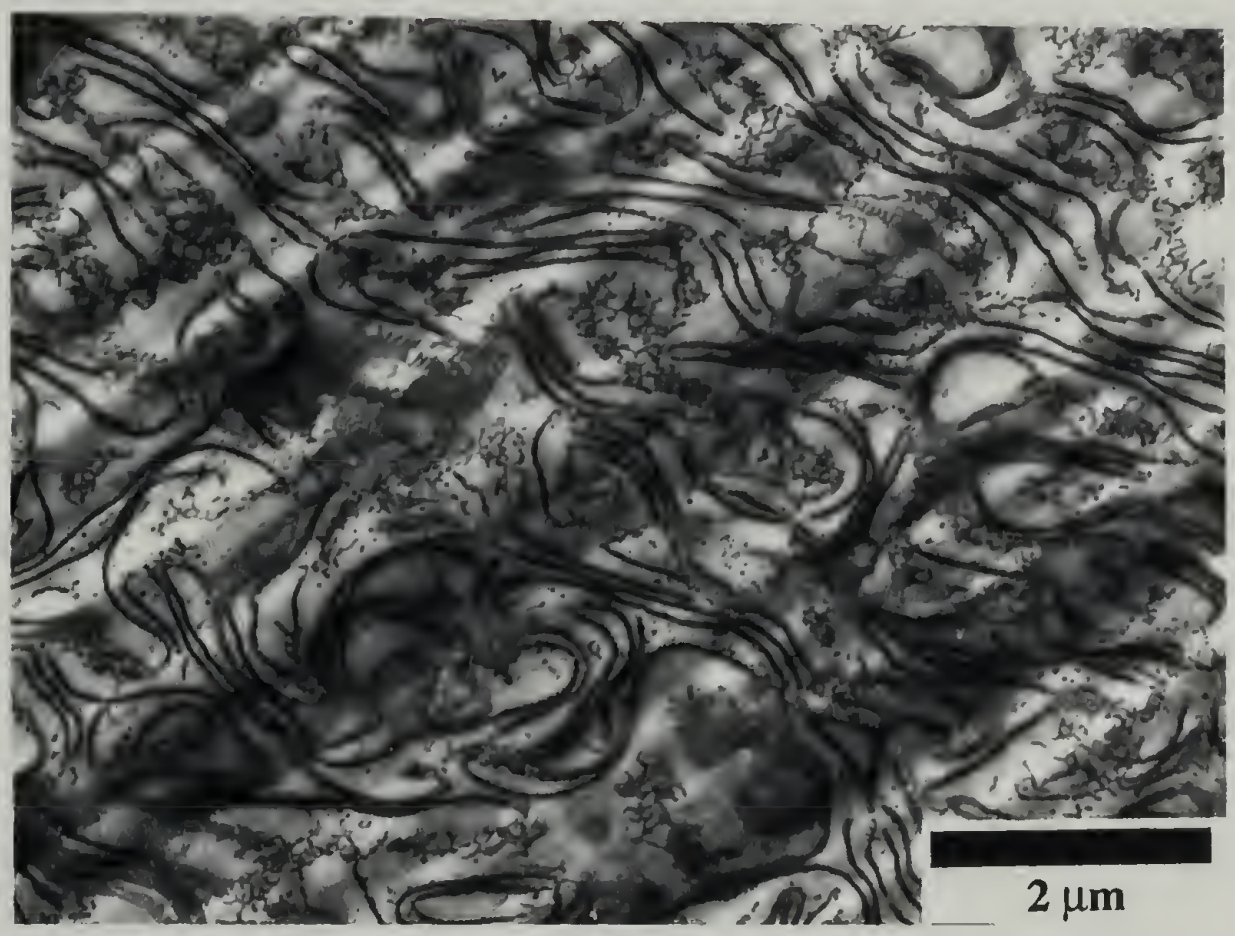


Figure 5.10: TEM micrograph and azimuthally integrated SANS data of intensity vs. scattering vector, q, for Blend PS-79.

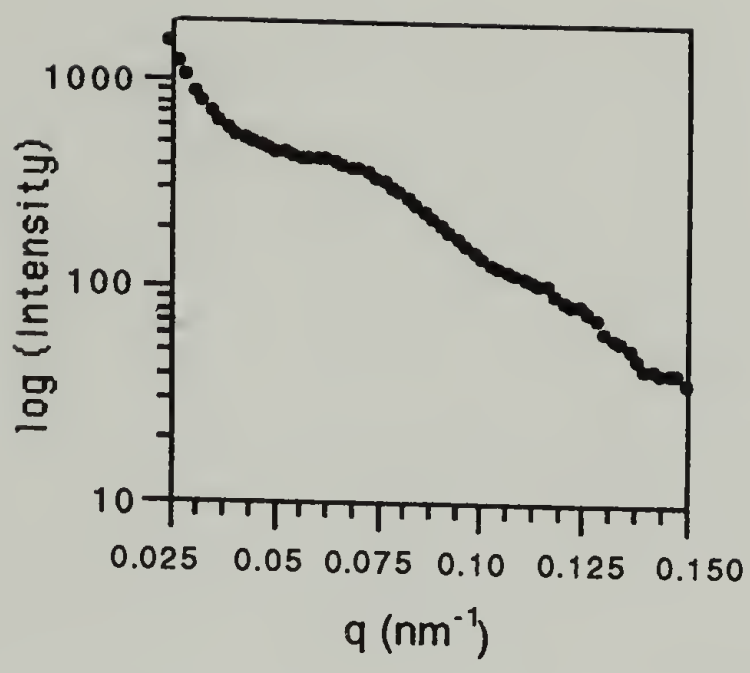



Figure 5.11: TEM micrograph and azimuthally integrated SANS data of intensity vs. scattering vector, q, for Blend PS-77.

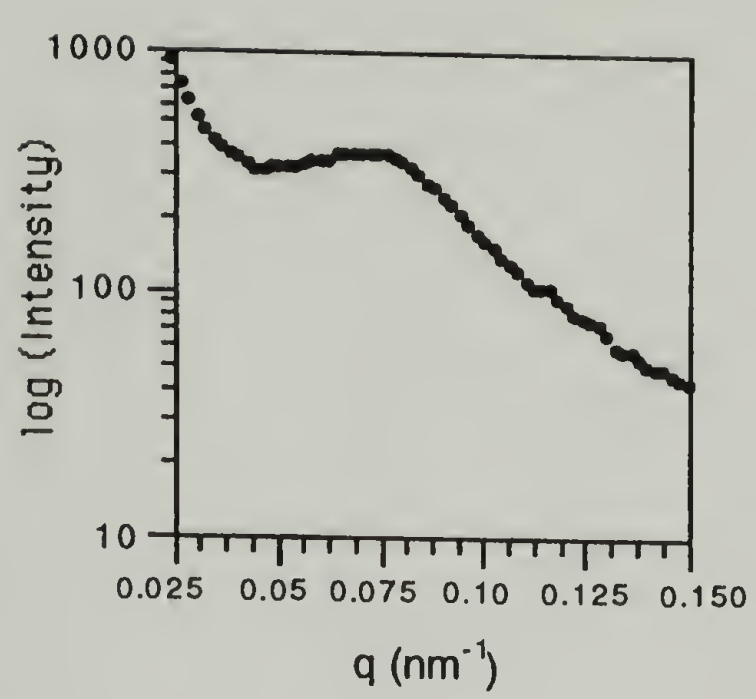


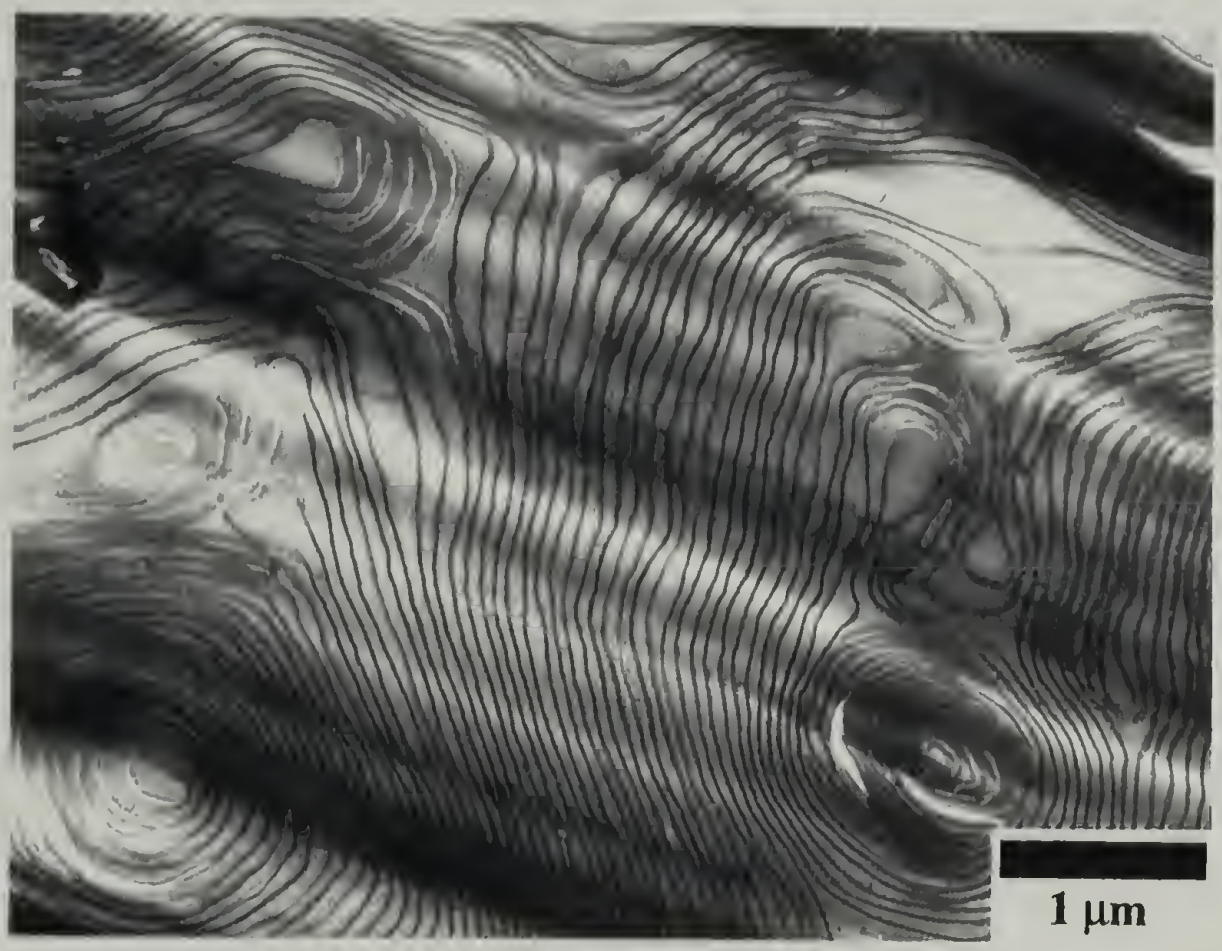


Figure 5.12: TEM micrograph and azimuthally integrated SANS data of intensity vs. scattering vector, q, for Blend PS-75.

blends up to $\phi_s = 0.87$. Secondly, the window of stability for the ROW phase must begin right around $\phi_s = 0.81$ since PS-79 at $\phi_s = 0.79$ is biphasic with only a bicontinuous PI web structure and an alternating PI/PS layered structure present. A hexagonal lattice seems to be forming in PS-87. However, it is curious that spherical PI domains are formed in PS-83, PS-85, and PS-87 even though both components form cylinder-type domains in the neat state. It is also not absolutely known at this time whether the bicontinuous web-like structure seen in PS-79 is an equilibrium structure in a biphasic region or if it is due to composition gradients of the minority blend component. The above initial conclusions and questions are currently being addressed with the study of an extensive set of homopolymer blends and additional copolymer blends with $I_2S$-3, $I_2S$-2, and $I_2S$-1 across a wide range of overall relative volume fractions and even more intermediate relative volume fractions between the neat graft copolymers.

## 5.4 PS/Poly(cyclohexadiene) Linear Diblocks with Tunable Conformational Asymmetry

### 5.4.1 Introduction

While the morphology work on this unique linear diblock is in its early stages, there are some intriguing initial morphology results which are worth mentioning. The two constituent blocks of this series of linear diblock copolymers consist of PS and poly(cyclohexadiene), or PCHD. The unsaturated monomer unit of PCHD is cyclic in nature and provides for a unique opportunity in block copolymer physics. In the study of block copolymers one must normally rely on many different block pairs in order to probe universal effects such as conformational asymmetry. A good example are the PI/PtBMA molecules in Chapter 4. PI/PtBMA is characterized by an $\varepsilon = 0.75$ which is slightly more conformationally asymmetric than the often studied model system of PS/PI with $\varepsilon \sim 0.90$. In order to increase $\varepsilon$ even further one would need to synthesize a completely new block copolymer pair for each new $\varepsilon$ desired. Entirely new synthetic strategies for each new sample, along with unknown thermodynamic interactions between the novel block pairs,

makes a comprehensive study of conformational asymmetry practically impossible. However, these obstacles are circumvented in the study of PS/PCHD linear diblocks. One can controllably dehydrogenate the unsaturated backbone rings of PCHD and form poly(p-phenylene) segments thereby increasing the stiffness of the chain depending on how much aromaticity is formed in the backbone.[15] Therefore, the conformational asymmetry can be precisely controlled and adjusted with the same beginning block pair, so only one new synthetic strategy needs to be performed.

### 5.4.2 Experimental

A set of PS/PCHD linear block copolymers has been synthesized by Dr. Jim Zhou in the lab of Prof. Jimmy Mays at the University of Alabama at Birmingham. The molecular characteristics of the polymers are listed in Table 5.2. The diblocks are named

Table 5.2

PS/PCHD Diblock Copolymers-Molecular Characteristics: (a) Membrane osmometry, (b) SEC, (c) $^1$H-NMR

| Sample | $M_n \times 10^{-4}$ [(a)] | $M_w/M_n$ [(b)] | Wt. Fraction PCHD[(c)] |
|---|---|---|---|
| PCHD-36 | 5.82 | 1.07 | 0.36 |
| PCHD-38 | 5.35 | 1.27 | 0.38 |
| PCHD-29 | 5.77 | 1.07 | 0.29 |
| PCHD-24 | 6.43 | 1.08 | 0.24 |
| PCHD-6 | 6.13 | 1.07 | 0.06 |

after their respective weight fraction of PCHD. Since the only initial experiments have been performed on the sample series, only the morphological behavior of the completely unsaturated PS/PCHD block copolymers was observed as cast from toluene, a relatively

non-selective solvent for the block pair assuming that PCHD has a solubility parameter similar to that of PI and other non-cyclic, unsaturated polymers. The sample preparation technique was identical to that used in the preparation of the PI/PtBMA samples in Chapter 4. Staining was performed with $OsO_4$ due to the unsaturation of PCHD in order to provide contrast in electron microscopy experiments.

After solvent casting and annealing only the samples most symmetric in relative weight fraction, PCHD-36 and PCHD-38, displayed any clear microphase separated morphology. All other samples, PCHD-29, -24, and -6, displayed a disordered morphology with only local fluctuations in composition. Representative micrographs of the ordered and disordered morphologies can be seen in Figure 5.13a and b, respectively. The microstructure in PCHD-36 and PCHD-38 seems to be cylindrical in nature due to the presence of projections both parallel and perpendicular to the axes of the tube-like PCHD domains in Figure 5.13a. The projections along the cylinder axes seem to contain 4-fold symmetry instead of the more traditional six-fold symmetry of a hexagonal lattice although it is premature to assign a particular lattice with only limited electron microscopy data and no supporting small angle x-ray scattering data.

### 5.4.3 Discussion

Based on this very preliminary characterization, it seems that the PS/PCHD pair may have a rather low $\chi$ interaction parameter between them, placing the systems studied in the weakly segregated state. It appears that grains of an ordered morphology are nucleating, and subsequently growing, from the disordered phase since annealed specimens of PCHD-36 and PCHD-38 appear to have larger average grain sizes of the cylinder-like morphology than their unannealed counterparts. Small angle x-ray scattering is definitely needed to determine any difference in microstructure grain size and long-range order. The growth of grains of a cylindrical morphology out of a homogeneous phase is qualitatively consistent with the nucleation and growth of lamellar morphologies

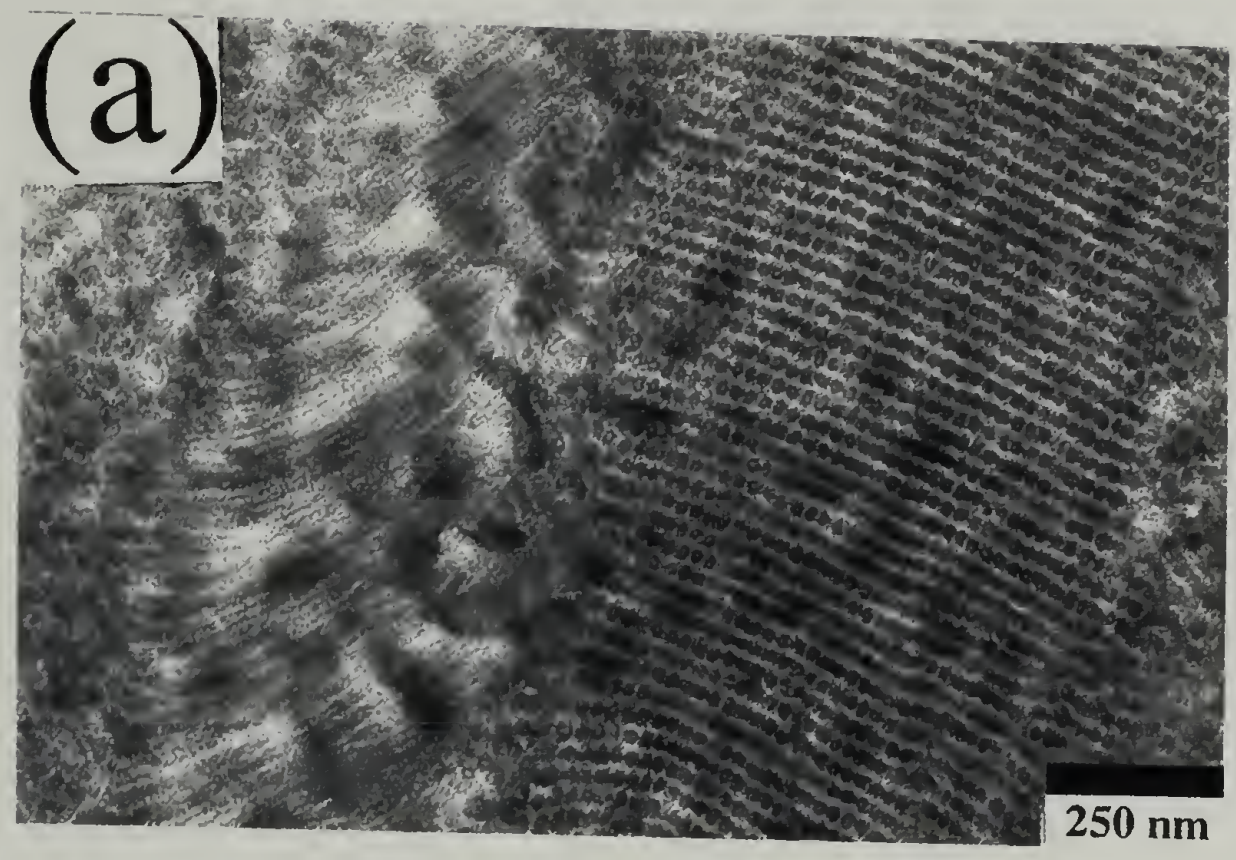


Figure 5.13: TEM micrographs of PS/PCHD block copolymers. (a) morphology of PCHD35 containing both end-on projections and projections perpendicular to the tube-like micelles of the minority PCHD component with disordered regions on both the far left and right of the micrograph. (b) morphology of PCHD-29 containing a disordered morphology with only local compositional fluctuations.

as seen in quenched melts of low molecular weight PI/PS linear diblocks.[16] Non-selective solvent casting at room temperature seems to place the PS/PCHD diblocks in the vicinity of the ODT where annealing of the more compositionally symmetric samples, PCHD-36 and PCHD-38, above the $T_g$'s of the constituent blocks allows significantmobility of the chains to form an A/B interface with a specific curvature from which grains of ordered microstructure may grow. Contrastingly, the remaining samples with relative wt. % of PCHD < 0.30 seem to never traverse the ODT and remain in the disordered state. The formation of an ordered lattice in the more compositionally symmetric samples, while those more asymmetric in composition remain disordered, is qualitatively consistent with the shape of the predicted ODT for linear diblocks; lower values of $\chi N$ are required for microphase separation in compositionally symmetric diblocks than in asymmetric systems.[17] However, much more work is needed to support the proposition that the system is weakly segregated. Additional experiments should include longer annealing times at different temperatures with extensive small angle x-ray analysis to quantify the appearance, growth, and identification of the microstructure. Also, small angle x-ray or neutron scattering experiments need to be performed on PS/PCHD copolymers in the homogeneous state in order to quantify the $\chi$ parameter between PS and PCHD. Only then can the systematic dehydrogenation of the PCHD be performed and the effects of controllably increased conformational asymmetry be observed. In fact, by forming poly(p-phenylene) segments and increasing the conformational asymmetry $\chi$ should become larger[18,19] (see 4.3.3 for a discussion of the effects of conformational asymmetry on $\chi$ ) placing the systems in stronger degrees of segregation which may induce the formation of more regular microstructures.

## 5.5 References


(1) Milner, S. T. "Chain Architecture and Asymmetry in Copolymer Microphases." *Macromolecules*, **27**, 2333 (1994).

(2) Lee, C.; Gido, S. P.; Pitsikalis, M.; Mays, J. W.; Tan, N. B.; Trevino, S.; Hadjichristidis, N. "Synthesis, Characterization, and Morphology of Asymmetric Simple Graft Block Copolymers." *Macromolecules*, in press (1997).

(3) Lee, C.; Gido, S. P.; Poulos, Y.; Mays, J. W.; Tan, N. B.; Trevino, S.; Hadjichristidis, N. "H ($S_2IS_2$) Double Graft Copolymers: Effect of Molecular Architecture on Morphology." *J. Chem. Phys.*, in press (1997).

(4) Lee, C.; Gido, S. P.; Poulos, Y.; Mays, J. W.; Tan, N. B.; Trevino, S.; Hadjichristidis, N. "p (SI)I(SI) Double Graft Copolymers: Effect of Molecular Architecture on Morphology." in preparation.

(5) Lee, C.; Pochan, D. J.; Gido, S. P.; Mays, J. W.; Hadjichristidis, N. "Morphologies of Simple Graft/Homopolymer Blends." in preparation.

(6) Pochan, D. J.; Lee, C.; Gido, S. P.; Mays, J. W.; Hadjichristidis, N. "Morphologies of Simple Graft Binary Blends." submitted to *Macromolecules*, Aug. (1997).

(7) David, J.; Pochan, D. J.; Gido, S. P.; Zhou, J.; Mays, J. W. "Morphological Behavior of a Poly(styrene-*b*-cyclohexadiene) Block Copolymer with Tunable Conformational Asymmetry." in preparation.

(8) Pochan, D. J.; Gido, S. P.; Pispas, S.; Mays, J. W.; Ryan, A. J.; Fairclough, J. P. A.; Hamley, I. W.; Terrill, N. J. "Morphologies of Microphase-Separated $A_2B$ Simple Graft Copolymers." *Macromolecules*, **29**, 5091 (1996).

(9) Tselikas, Y.; Iatrou, H.; Hadjichristidis, N.; Liang, K. S.; Mohanty, K.; Lohse, D. J. "Morphology of Miktoarm Star Block Copolymers of Styrene and Isoprene." *J. Chem. Phys.*, **105**, 2456 (1996).

(10) Gido, S. P.; Lee, C.; Pochan, D. J.; Pispas, S.; Mays, J. W.; Hadjichristidis, N. "Synthesis, Characterization, and Morphology of Model Graft Copolymers with Trifunctional Branch Points." *Macromolecules*, **29**, 7022 (1996).

(11) Olvera de la Cruz; Sanchez, I. C. "Theory of Microphase Separation in Graft and Star Copolymers."*Macromolecules*, **19**, 2501 (1986).

(12) Beyer, F. L.; Gido, S. P.; Poulos, Y.; Hadjichristidis, N. "Morphology of Vergina Star 16-Arm Block Copolymers and Scaling Behavior of Interfacial Area with Graft Point Functionality." *Macromolecules*, **30**, 2373 (1997).

(13) Zhao, J.; Majumdar, B.; Schulz, M. F.; Bates, F. S.; Almdal, K.; Mortensen, K.; Hajduk, D. A.; Gruner, S. M. "Phase Behavior of Pure Diblocks and Binary Diblock Blends of Poly(ethylene)-poly(ethylethylene)." *Macromolecules*, **29**, 1204 (1996).

(14) Hashimoto, T.; Koizumi, S.; Hasegawa, H. "Ordered Structure in Blends of Block Copolymers. 2. Self-Assembly for Immiscible Lamella-Forming Copolymers." *Macromolecules*, **27**, 1562 (1994).

(15) Zhong, X. F.; François, B. "Soluble Polystyrene-*b*-Poly(*p*-Phenylene) Block Copolymers Prepared from Polystyrene-*b*-Poly(1,3-Cyclohexadiene) Precursors. Study of the Aromatization Process. *Makromol. Chem.*, **192**, 2277 (1991).

(16) Hashimoto, T.; Sakamoto, N.; Koga, T. "Nucleation and Growth of Anisotropic Grain in Block Copolymers Near the Order-Disorder Transition." *Phys. Rev. E*, **54**, 5832 (1996).

(17) Leibler, L. "Theory of Microphase Separation in Block Copolymers." *Macromolecules*, **13**, 1602 (1980).

(18) Gehlsen, M. D.; Bates, F. S. "Conformational Asymmetry in Poly(vinylcyclohexane) Containing Diblock Copolymers." *Macromolecules*, **27**, 3611 (1994).

(19) Pochan, D. J.; Gido, S. P.; Zhou, J.; Mays, J. W.; Whitmore, M. D.; Ryan, A. J. "Morphologies of Microphase Separated Conformationally Asymmetric Diblock Copolymers." *J. Polym. Sci. Polym. Phys.*, in press (1997).

# CHAPTER 6

# CONCLUSIONS AND PROPOSED SUBSEQUENT RESEARCH

The experimental work described in this thesis conclusively demonstrates the strong effects of the simple graft molecular architecture and conformational asymmetry on the morphology of microphase separated block copolymers. The remaining paragraphs contain the specific conclusions drawn from each of the earlier experimental chapters as well as some new questions and possible research avenues discovered during the course of the thesis research.

## 6.1 $A_2B$ Simple Graft Architecture

### 6.1.1 $A_2B$ Simple Graft Conclusions

The experimental results of chapter 2 and chapter 3 confirm that the architectural asymmetry of the $I_2S$ block copolymers results in a large asymmetry of the strongly segregated morphology behavior relative to volume fraction. Therefore, molecular architecture is an additional controllable parameter with which one can manipulate the morphological behavior of block copolymers. $I_2S$-3 and $I_2S$-7 are the only samples from the studied series displaying the morphological behavior of their linear diblock analogues exhibiting lamellar and spherical microstructures, respectively. However, all other samples are shifted into new morphologies, which are unobtainable for that volume fraction in a diblock architecture, due to the crowding of the two PI blocks on the same side of the PI/PS interface in the microphase separated state. More interestingly, while $I_2S$-2 is calculated to shift from the center of the diblock cylindrical phase very close to the bicontinuous/lamellar phase boundary, it is seen experimentally that the microstructure consists of worm-like micelles which are not arranged on a lattice.

This unique, randomly oriented worm-like micelle morphology, or ROW, is only observed in $I_2S$-2 with $\phi_s$=0.81. Via a set of selective solvent casting and prolonged,

high temperature annealing experiments, combined with the non-selective solvent data, this morphology was demonstrated to be the equilibrium state for the system. The worm structure occurs only near the particular volume fraction where the two PI backbone chains per molecule are first forced to the concave side of the PS/PI interface in the microphase separated state. This crowding of the PI arms, combined with the concavity of the interface, frustrates an underlying lattice symmetry. Two other $I_2S$ samples, one with a slightly higher PS graft volume fraction ($I_2S$-1 at $\phi_s$=0.89) and one with a slightly lower PS volume fraction ($I_2S$-3 at $\phi_s$=0.66), were found to form a hexagonally packed PS cylinder phase and alternating PS/PI lamellar phase, respectively. While both of these phases were predicted theoretically, the volume fraction window in which the ROW phase resides is predicted to be a bicontinuous phase.[1] The ROW phase does not necessarily preclude the existence of the theoretically predicted bicontinuous phase. However, the above experiments support the premise that the worm-like micelle morphology is an equilibrium structure that exists due to the novel graft architecture of the molecule and the unique relationship between the particular volume fraction of $\phi_s = 0.81$ and the concavity of the PS/PI interface on which the two PI chains per molecule must reside. Also, while only in the initial stages, morphology experiments on copolymer/copolymer blends between the ROW forming $I_2S$-2 and the neighboring copolymers of $I_2S$-1 and $I_2S$-3 seem to place a definite OOT between lamellae and the ROW phase at $\phi_s \sim 0.81$.

### 6.1.2 $A_2B$ Simple Graft Proposed Research

There are several sets of experiments which are proposed to further map the volume fraction window of stability of the ROW phase and to probe the possible effect of molecular weight in $A_2B$ simple graft systems. More blending work is needed to conclusively map the volume fraction window of stability of the ROW phase. Specifically, PI and PS homopolymers of a very low molecular weight could be utilized in blends with $I_2S$-2 to traverse small, precise steps in volume fraction in order to

compare with the copolymer blend results as described in chapter 5. Also, if the ROW phase is truly an equilibrium state for $A_2B$ molecules with relative volume fractions in the neighborhood of $\phi_s = 0.81$ then one may be able to blend PS homopolymer with $I_2S$-3 and PI homopolymer with $I_2S$-1 in order to form the ROW phase. In addition, the OOT's of all of the theoretically predicted morphologies could be experimentally determined via homopolymer/copolymer blends with the remainder of the $I_2S$ sample series, and a more rigorous comparison with theory could then be made. As alluded to in chapter 5, there are already some homopolymer/copolymer blend studies underway in our research group to address the accuracy of the OOT's and to more precisely map the stability of the ROW phase.

Another interesting research topic in the area of graft copolymer morphology would be to study the effect of molecular weight on the morphology behavior in $A_2B$ systems. The overall molecular weight of the $A_2B$ series studied in chapters 2 and 3 is approximately 90 K g/mole. While this overall molecular weight is rather large, seemingly placing the system in the strongly segregated regime, it is important to note that the weight fraction of species A is split between two arms. In the samples with large relative volume fractions of PS graft, specifically $I_2S$-2 and $I_2S$-1, the molecular weight of the PI arms are approximately 9,000 and 5,000 g/mole. At these low molecular weights the PI arms may be much more highly stretched since they are in close proximity to the PI/PS interface and the common junction point with the PS graft. The much more stretched PI chain conformations may have a profound effect on the interfacial curvature and, consequently, the morphological behavior. Junction point effects could be the cause of the ROW morphology formation, the only sample found to disagree with the calculations of Milner. In the theoretical calculations of Milner any effects of the junction point were ignored since only very large molecular weights were assumed placing the system well into the strongly segregated state. The synthesis and characterization of several new $I_2S$ samples at the same relative volume fractions as in $I_2S$-2 and $I_2S$-1 but

with much larger molecular weights could be performed to check if junction point effects are actually negligible in the 90,000 g/mole results. Any differences between these high molecular weight systems and the morphological behavior characterized in the 90,000 g/mole systems in chapters 2 and 3 could be directly attributed to the above mentioned junction point effect. In fact, if the junction point effect is the cause of the ROW phase in the $I_2S$-81 sample, a much larger molecular weight system at the same relative volume fraction may form the theoretically predicted bicontinuous structure.

## 6.2 Conformational Asymmetry

### 6.2.1 PI/PtBMA Conclusions

The strongly segregated morphological behavior of a series of conformationally asymmetric linear diblock copolymers of polyisoprene and poly(tert-butylmethacrylate) was characterized across a wide range of relative volume fractions. The experimentally determined phase behavior was compared to that calculated utilizing a self consistent mean-field theory developed for linear, conformationally asymmetric block copolymers at finite segregations (finite values of $\chi N$). The mismatch of unperturbed chain dimensions between PI and PtBMA due to a difference in statistical segment lengths is theoretically predicted to produce a significant difference in entropic chain stretching penalties between the more coiled block (PI) and the more expanded block (PtBMA) in the microphase separated state. This, in turn, should push the volume fraction windows in which the strongly segregated morphologies are found to higher volume fraction of the more expanded PtBMA block. Experimental results are consistent with small phase boundary shifts calculated for middle to high relative volume fraction of the expanded PtBMA block ($\phi_{PtBMA} > 0.30$). However, disagreement was found between experiment and the calculated morphological behavior at $\phi_{PtBMA} < 0.30$. The discrepancy may be due to a compositional dependence of the entropic chain stretching penalty disparity between the more expanded PtBMA block and the more coiled PI block. More work is needed in

order to fully understand the discrepancies between the experimentally determined and calculated phase behavior and to probe the possibility of any compositional dependence of conformational asymmetry in the strongly segregated state of diblock copolymers.

### 6.2.2 PI/PtBMA and PS/PCHD Proposed Research

The concept of conformationally asymmetric linear diblocks with tunable asymmetry, as in the case of PS/PCHD linear diblocks, provides the intriguing opportunity to directly probe the effects of relative chain stiffness between blocks at a constant composition. A series of linear diblocks at a constant composition and molecular weight could be synthesized, and each sample could be subsequently made more conformationally asymmetric to a controllable extent via the catalyzed dehydrogenation of PCHD. Therefore, the direct effect of increasing conformational asymmetry at constant composition on the bulk morphological behavior could be observed. In addition, at some level of dehydrogenation the PCHD-co-*p*-phenylene block would become stiff enough along its contour to become liquid crystalline providing for a whole new realm of phase behavior. Also, at low temperatures these stiff blocks may begin to crystallize before microphase separation occurs providing for morphologies dominated by the formation of crystalline lamellae in the bulk state.

With the apparent nucleation and growth of microstructure in the most compositionally symmetric PS/PCHD samples, PCHD-36 and PCHD-38, the exact thermodynamic interactions between the block pair needs to be quantified. SAXS or SANS experiments need to be performed on the PS/PCHD diblocks in the homogeneous melt and fit to the structure factor calculated by Leibler.[2] This could quantify the potentially very low value of $\chi$ for the PS/PCHD block pair. If in fact $\chi$ is low, placing the system in the weakly segregated state, the PS/PCHD block copolymers would then provide ideal systems with which to monitor the kinetics of microphase separation. Since the grain size of ordered microstructure seems to be larger in PCHD-36 and PCHD-38

after annealing for a week, the growth kinetics of the microstructure seem to be very slow at the annealing temperatures utilized. Therefore, annealing temperatures around 120°C-180°C would provide ideal windows of accessible real-time microstructure growth kinetics while not being too high as to degrade or oxidize the blocks. Real-time SAXS experiments utilizing high flux x-ray sources, such as a rotating anode or a synchrotron source, and x-ray detectors could be performed in order to monitor the growth of microstructure in the melt. Also, samples could periodically be quenched in liquid nitrogen so that TEM experiments could be performed and a real space confirmation of the SAXS data could be obtained.

## 6.3 References


(1) Milner, S. T. "Chain Architecture and Asymmetry in Copolymer Microphases." *Macromolecules*, **27**, 2333 (1994).

(2) Leibler, L. "Theory of Microphase Separation in Block Copolymers." *Macromolecules*, **13**, 1602 (1980).

# BIBLIOGRAPHY


Aggarwal, S. L., Ed. *Block Copolymers*; Plenum Press: New York, 1970.

Almdal, K.; Koppi, K. A.; Bates, F. S.; Mortensen, K. "Multiple Ordered Phases in a Block Copolymer Melt." *Macromolecules*, **25**, 1743 (1992).

Alward, D. B.; Kinning, D. J.; Thomas, E. L.; Fetters, L. J. "Effect of Arm Number and Arm Molecular Weight on the Solid-State Morphology of Poly(styrene-isoprene) Star Block Copolymers." *Macromolecules*, **19**, 215 (1986).

Amorim, M. C. V.; Oliveira, C. M. F.; Tavares, M. I. B. "Investigation of PMMA/Polyoxide Blends Containing Graft-Copolymer Compatibilizers by Using NMR, SEM, and Thermal Analysis." *J. Appl. Polym. Sci.*, **61**, 2245 (1996).

Avgeropoulos, A.; Poulos, Y.; Hadjichristidis, N.; Roovers, J. "Synthesis of 16-Arm Vergina Star Block Copolymers." *Macromolecles*, **29**, 6076 (1996).

Balsara, N. P.; Perahia, D.; Safinya, C. R.; Tirrell, M.; Lodge, T. P. "Birefringence Detection of the Order-Disorder Transition in Block Copolymer Liquids." *Macromolecules*, **25**, 3896 (1992).

Bareiss, R. E. "Polymolecularity Correction Formulae for the Claculation of Weight and Number Average Mean Squared Radii of Gyration from Experimentally Determined Z-Average Mean Squared Radius of Gyration. *Eur. Polym. J.*, **19**, 847 (1983).

Barton, A. F. M., Ed. *Handbook of Polymer-Liquid Interaction Parameters & Solubility Parameters*; CRC Press: Boston, 1990.

Bates, F. S. "Block Copolymers." *Science*, **251**, 845 (1991).

Bates, F. S.; Berney, C. V.; Cohen, R. E. "Microphase Structure of Solvent-Cast Diblock Copolymers and Copolymer/Homopolymer Blends Containing Spherical Microdomains." *Macromolecules*, **16**, 1101 (1983).

Bates, F. S.; Frederickson, G. H. "Block Copolymer Thermodynamics: Theory and Experiment." *Annu. Rev. Phys. Chem.*, **41**, 525 (1990).

Bates, F. S.; Fredrickson, G. H. "Conformational Asymmetry and Polymer-Polymer Thermodynamics." *Macromolecules*, **27**, 1065 (1994).

Bates, F. S.; Schulz, M. F.; Khandpur, A. K.; Førster, S.; Rosedale, J. H.; Almdal, K.; Mortensen, K. "Fluctuations, Conformational Asymmetry, and Block Copolymer Phase Behavior." *Faraday Discuss. Chem. Soc.*, **98**, 7 (1994).

Bates, F. S.; Schulz, M. F.; Rosedale, J. H.; Almdal, K "Correlation of Binary Polyolefin Phase Behavior with Statistical Segment Length Asymmetry. *Macromolecules*, **25**, 5547 (1992).

Benoit, H.; Hadziioannou, G. "Scattering Theory and Properties of Block Copolymers with Various Architectures in the Homogeneous Bulk State." *Macromolecules*, **21**, 1449 (1988).

Beyer, F. L.; Gido, S. P.; Hadjichristidis, N. "Microphase-Separated Morphologies of Comb-Block Copolymers" *Macromolecules*, in preparation (1997).

Beyer, F. L.; Gido, S. P.; Poulos, Y.; Hadjichristidis, N. "Morphology of Vergina Star 16-Arm Block Copolymers and Scaling Behavior of Interfacial Area with Graft Point Functionality." *Macromolecules*, **30**, 2373 (1997).

Brandrup, J., Immergut, E. H., Eds. *Polymer Handbook*, 3rd ed.; John Wiley & Sons: New York, 1989.

Bras, W.; Derbyshire, G. E.; Ryan, A. J.; Mant, G. R.; Felton, R. A.; Lewis, R. A; Hall, C. J.; Greaves, G. N. "Synchrotron X-Ray Camera for Simultaneous Wide-Angle and Small-Angle Scattering." *Nucl. Instrum. Methods Phys. Res.*, **A326**, 587 (1993).

Braun, D.; Fischer, M.; Hellmann, G. P. "Block-Graft Copolymers as Compatibilizers in Polymer Blends." *Polymer*, **37**, 3871 (1996).

Chen, J. T.; Thomas, E. L.; Ober, C. K.; Mao, G.-p. "Self-Assembled Semectic Phases in Rod-Coil Block Copolymers." *Science*, **273**, 343 (1996).

Cohen, R. E.; Cheng, P. L.; Douzinas, K.; Kofinas, P.; Berney, C. V. "Path Dependent Morphologies of a Diblock Copolymer of Polystyrene and Hydrogenated Polybutadiene." *Macromolecules*, **23**, 324 (1990).

Cowie, J. M. G. In: *Comprehensive Polymer Science: The Synthesis, Characterization, Reactions, and Applications of Polymers. Chain Polymerization I*; C. J. Eastmond, A. Ledwith, S. Russo, P. Sigwalt, Eds.; Pergamon: Oxford, 1989; Vol. 3; 33.

David, J.; Pochan, D. J.; Gido, S. P.; Zhou, J.; Mays, J. W. "Morphological Behavior of a Poly(styrene-*b*-cyclohexadiene) Block Copolymer with Tunable Conformational Asymmetry." in preparation.

Disko, M. M.; Liang, K. S.; Behal, S. K.; Roe, R. J.; Jeon, K. J. "Catenoid-Lamellar Phase in Blends of Styrene-Butadiene Diblock Copolymer and Homopolymer." *Macromolecules*, **26**, 2783 (1993).

Dreyfuss, P.; Quirk, R. P. In: *Encyclopedia of Polymer Science and Engineering*; H. F. Mark, N. M. Bikales, C. G. Overberger, G. Menges and J. I. Kroschwitz, Eds.; Wiley-Interscience: New York, 1987; Vol. 7; 551.

Feng, H.; Tian, J.; Ye, C. "Compatibilization Effect of Graft Copolymer on Immiscible Polymer Blends. II. LLDPE/PS/LLDPE-*g*-PS Systems." *J. Appl. Polym. Sci.*, **61**, 2265 (1996).

Flory, P. J. *Statistical Mechanics of Chain Molecules*; Wiley-Interscience: New York, 1969.

Floudas, G.; Hadjichristidis, N.; Iatrou, H.; Pakula, T.; Fischer, E. W. "Microphase Separation in Model 3-Miktoarm Star Copolymers (Simple Graft) and Terpolymers. 1. Statics and Kinetics." *Macromolecules*, **27**, 7735 (1994).

Fogden, A.; Hyde, S. T.; Lundberg, G. "Bending Energy of Surfactant Films." *Journal of the Chemical Society. Faraday Transactions*, **87**, 949 (1991).

Folkes, M. J.; Keller, A. "The Birefringence and Mechanical Properties of a 'Single Crystal' from a Three Block Copolymer." *Polymer*, **12**, 222 (1971).

Fox Jr., T. G.; Flory, P. J. "Unperturbed Coil Dimensions from Dilute Solution Viscometry." *J. Phys. Colloid Chem.*, **53**, 197 (1949).

Frederickson, G. H.; Bates, F. S. "Dynamics of Block Copolymers: Theory and Experiment." *Annu. Rev. Mater. Sci.*, **26**, 501 (1996). (4)

Fredrickson, G. H.; Liu, A. J.; Bates, F. S. "Entropic Corrections to the Flory-Huggins Theory of Polymer Blends: Architectural and Conformational Effects." *Macromolecules*, **27**, 2503 (1994).

Fujii, Y.; Tamai, Y.; Konishi, T.; Yamakawa, H. "Intrinsic Viscosities of Oligo and Poly(methylmethacrylates." *Macromolecules*, **24**, 1608 (1991).

Gehlsen, M. D.; Bates, F. S. "Conformational Asymmetry in Poly(vinylcyclohexane) Containing Diblock Copolymers." *Macromolecules*, **27**, 3611 (1994).

Gido, S. P.; Lee, C.; Pochan, D. J.; Pispas, S.; Mays, J. W.; Hadjichristidis, N. "Synthesis, Characterization, and Morphology of Model Graft Copolymers with Trifunctional Branch Points." *Macromolecules*, **29**, 7022 (1996).

Goodman, I., Ed. *Developments in Block Copolymers*; Applied Science: New York, 1982; Vol. 1.

Hadjichristidis, N.; Iatrou, H.; Behal, S. K.; Chludzinski, J. J.; Disko, M. M.; Garner, R. T.; Liang, K. S.; Lohse, D. J.; Milner, S. T. "Morphology and Miscibility of Miktoarm Styrene-Diene Copolymers and Terpolymers." *Macromolecules*, **26**, 5812 (1993).

Hajduk, D. A.; Gruner, S. M.; Rangarajan, P.; Register, R. A.; Fetters, L. J.; Honeker, C.; Albalak, R. J.; Thomas, E. L. "Observation of a Thermotropic Order-Order Transition in a Diblock Copolymer." *Macromolecules*, **27**, 490 (1994).

Hasegawa, H.; Hashimoto, T.; Hyde, S. T. "Microdomain Structures with Hyberbolic Interfaces in Block and Graft Copolymer Systems." *Polymer*, **37**, 3825 (1996).

Hashimoto, T.; Koizumi, S.; Hasegawa, H. "Ordered Structure in Blends of Block Copolymers. 2. Self-Assembly for Immiscible Lamella-Forming Copolymers." *Macromolecules*, **27**, 1562 (1994).

Hashimoto, T.; Koizumi, S.; Hasegawa, H.; Izumitani, T.; Hyde, S.T. "Observation of 'Mesh' and 'Strut' Structures in Block Copolymer/Homopolymer Mixtures." *Macromolecules*, **25**, 1433 (1992).

Hashimoto, T.; Nagatoshi, K.; Todo, A.; Hasegawa, H.; Kawai, H. "Domain-Boundary Structure of Styrene-Isoprene Block Copolymer Films Cast from Toluene Solutions." *Macromolecules*, 7, 364 (1974).

Hashimoto, T.; Sakamoto, N.; Koga, T. "Nucleation and Growth of Anisotropic Grain in Block Copolymers Near the Order-Disorder Transition." *Phys. Rev. E*, **54**, 5832 (1996).

Hashimoto, T.; Todo, A.; Itoi, H.; Kawai, H. "Domain-Boundary Structure of Styrene-Isoprene Block Copolymer Films Cast from Soutions. 2. Quantitative Estimation of the Interfacial Thickness of Lamellar Microphase Systems." *Macromolecules*, **10**, 384 (1977).

Helfand, E.; Sapse, A. M. "Theory of Unsymmetric Polymer-Polymer Interfaces." *The Journal of Chemical Physics*, **62**, 1327 (1975).

Helfand, E.; Wasserman, Z. R. "Block Copolymers." In: *Developments in Block Copolymers*; I. Goodman, Ed.; Elsevier: New York, 1982; Vol. 1.

Helfand, E.; Wasserman, Z. R. "Block Copolymer Theory. 6. Cylindrical Domains." *Macromolecules*, **13**, 994 (1980 ).

Helfand, E.; Wasserman, Z. R. "Strong-Segregation Theory of Microphase Separated Block Copolymers." *Macromolecules*, **9**, 879 (1976).

Holmberg, A.; Piculell, L.; Wesslén, B. "Viscosity Effects of a Graft Copolymer with a Hydrophobic Backbone and Hydrophilic Side Chains in a Water/Cyclohexane Oil-Continuous Microemulsion." *J. Phys. Chem.*, **100**, 462, (1996).

Huynh, B.-G.; Jérome, R.; Teyssié, P. "Star-Shaped Block Copolymers. I. Synthesis of New A(B)2 Starshaped Block Copolymers Based on Vinyl or Diene Hydrocarbons (A) and Oxirane (B)*J. Polym. Sci., Polym. Chem. Ed.*, **18**, 3483 (1980).

Hyde, S. T. "Curvature and the Global Structure of Interfaces in Surfactant-Water Systems." *Colloque de Physique*, ***C7***, 209 (1990).

Iatrou, H.; Hadjichristidis, N. "Synthesis of a Model Three-Miktoarm Star Terpolymer." *Macromolecules*, **25**, 4649 (1992).

Iatrou, H.; Siakali-Kioulafa, E.; Hadjichristidis, N.; Roovers, J.; Mays, J. W. "Hydrodynamic Properties of Model Three-Miktoarm Star Copolymers." *J. Polym, Sci., Polym. Phys.*, **33**, 1925 (1995).

Israelachvili, J. N. *Intermolecular and Surface Forces*, 2nd ed.; Academic Press: New York, 1992.

Jung, K.; Abetz, V.; Stadler, R. "Thermodynamically Controlled Morphological Disorder in a Mircophase-Separated Cylindrical Block Copolymer." *Macromolecules*, **29,** 1076 (1996).

Karandinos, A.; Nan, S.; Mays, J. W.; Hadjichristidis, N. "Solution Properties and Unperturbed Dimensions of Stereoregular Poly(*t*-butylmethacrylates)." *Macromolecules*, **24**, 2007 (1991).

Khandpur, A. K.; Foerster, S.; Bates, F. S.; Hamley, I. W.; Ryan, A. J.; Bras, W.; Almdal, K.; Mortensen, K. "Polyisoprene-Polystyrene Diblock Copolymer Phase Diagram near the Order-Disorder Transition." *Macromolecules*, **28**, 8796 (1995).

Khandpur, A. K.; Macosko, C. W.; Bates, F. S. "Transmission Electron Microscopy of Saturated Hydrocarbon Block Copolymers." *J. Polym. Sci., B: Polym. Phys.*, **33**, 247 (1995).

Kinning, D. J.; Winey, K. I.; Thomas, E. L. "Structural Transitions from Spherical to Nonspherical Micelles in Blends of Poly(styrene-butadiene) Diblock Copolymer and Polystyrene Homopolymers." *Macromolecules*, **21**, 3502 (1988).

Konishi, T.; Yoshizaki, T.; Yamakawa, H. "On the 'Universal Constants' ρ and ϕ of Flexible Polymers." *Macromolecules*, **24**, 5614 (1991).

Kozhokaryu, M.; Skazka, V. S.; Berdnikova, K. G. "The Chain Statistics of Poly(*t*-butylmethacrylate)." *Vysokomol. Soedin.*, **8**, 1063 (1967).

Lee, C.; Gido, S. P.; Pitsikalis, M.; Mays, J. W.; Tan, N. B.; Trevino, S.; Hadjichristidis, N. "Synthesis, Characterization, and Morphology of Asymmetric Simple Graft Block Copolymers." *Macromolecules*, in press (1997).

Lee, C.; Gido, S. P.; Poulos, Y.; Mays, J. W.; Tan, N. B.; Trevino, S.; Hadjichristidis, N. "H ($S_2IS_2$) Double Graft Copolymers: Effect of Molecular Architecture on Morphology." *J. Chem. Phys.*, in press (1997).

Lee, C.; Gido, S. P.; Poulos, Y.; Mays, J. W.; Tan, N. B.; Trevino, S.; Hadjichristidis, N. "π (SI)I(SI) Double Graft Copolymers: Effect of Molecular Architecture on Morphology." in preparation.

Lee, C.; Pochan, D. J.; Gido, S. P.; Mays, J. W.; Hadjichristidis, N. "Morphologies of Simple Graft/Homopolymer Blends." in preparation.

Leibler, L. "Theory of Microphase Separation in Block Copolymers." *Macromolecules*, **13**, 1602 (1980).

Lescanec, R. L.; Hajduk, D. A.; Kim, G. Y.; Gan, Y.; Yin, R.; Gruner, S. M.; Hogen-Esch, T. E.; Thomas, E. L. "Comparison of the Lamellar Morphology of Microphase-Separated Cyclic Block Copolymers and Their Linear Precursors." *Macromolecules*, **28**, 3485 (1995).

Lewis, P. R.; Price, C. "The Morphology of $(Styrene)_x$ $Isoprene)_y$ $(Styrene)_x$ Block Copolymers." *Polymer*, **12**, 258 (1972).

Li, J.; Wan, Y.; Xu, Z.; Mays, J. W. "Third Virial Coefficients of Polystyrene in Different Theta Solvents." *Macromolecules*, **28**, 5347 (1995).

Lin, C. C.; Jonnalagadda, S. V.; Kesani, P. K.; Dai, H. J.; Balsara, N. P. "Effect of Molecular Structure on the Thermodynamics of Block Copolymer Melts." *Macromolecules*, **27**, 7769 (1994).

Long, T. E.; Broske, A. D.; Bradley, D. J.; McGrath, J. E. "Synthesis and Characterization of Poly(*t*-butylmethacrylate-*b*-isoprene-*b*-*t*-butylmethacrylate) Block Copolymers by Anionic Techniques." *J. Polym. Sci., Polym. Chem. Ed.*, **27**, 4001 (1989).

Löwenhaupt, B.; Steurer, A.; Hellmann, G. P.; Gallot, Y. "Microphases and Macrophases in Polymer Blends with a Diblock Copolymer." *Macromolecules*, **27**, 908 (1994).

Lyatskaya, Y.; Jacobson, S. H.; Balazs, A. C. "Effect of Composition on the Compatibilizing Activity of Comb Copolymers." *Macromolecules*, **29**, (1996).

Matsen, M. W.; Bates, F. S. "Conformationally Asymmetric Block Copolymers." *J. Polym, Sci., Polym. Phys*. **35**, 945 (1997).

Matsen, M. W.; Schick, M. "Self-Assembly of Block Copolymers." *Current Opinion in Colloid and Interface Science*, **1**, 329 (1996).

Matsen, M. W.; Schick, M. "Stable and Unstable Phases of a Diblock Copolymer Melt." *Phys. Rev. Lett*., 72, 2660 (1994).

Matsen, M. W.; Whitmore, M. D. "Accurate Diblock Copolymer Phase Boundaries At Strong Segregations Using SCFT." *J. Chem. Phys*., **105**, 9698 (1996).

Matsushita, Y.; Choshi, H.; Fujimoto, T.; Hasagawa, N. "Preparation and Morphological Properties of a Triblock Copolymer of the ABC Type." *Macromolecules*, **13**, 1053 (1980).

Mays, J. W. "Synthesis of 'Simple Graft' Poly(isoprene-*g*-styrene) by Anionic Polymerization." *Polym. Bull*., **23**, 247 (1990).

Milner, S. T. "Chain Architecture and Asymmetry in Copolymer Microphases." *Macromolecules*, **27**, 2333 (1994).

Milner, S. T.; Witten, T. A.; Cates, M. E. "Theory of the Grafted Polymer Brush." *Macromolecules*, **21**, 2610 (1988).

Miyata, T.; Takagi, T.; Uragami, T. "Microphase Separation in Graft Copolymer Membranes with Pendant Oligodimethylsiloxanes and Their Permselectivity for Aqueous Ethanol Solutions." *Macromolecules*, **29**, 7787 (1996).

Mogi, Y.; Mori, K.; Kotsuyi, H.; Matsushita, Y.; Noda, I. "Molecular Weight Dependence of the Lamellar Domain Spacing of ABC Triblock Copolymers and Their Chain Conformations in Lamellar Domains." *Macromolecules*, **26**, 5169 (1993).

Molau, G. E., Ed. *Colloidal and Morphological Behavior of Block and Graft Copolymers*; Plenum Press: New York, 1971.

Mori, K.; Hasegawa, H.; Hashimoto, T. "Small-Angle X-Ray Scattering from Bulk Block Polymers in Disordered State. Estimation of $\chi$ Values from Accidental Thermal Fluctuations." *Polymer Journal*, **17**, 799 (1985).

Morton, M.; Fetters, L. J. "Anionic Polymerization of Vinyl Monomers." *Rubber Chemistry and Technology*, **48**, 359 (1975).

Olmsted, P. D; Milner, S. T. "Strong-Segregation Theory of Bicontinuous Phases in Block Copolymers." *Physical Review Letters*, **72**, 936 (1994).

Olvera de la Cruz; Sanchez, I. C. "Theory of Microphase Separation in Graft and Star Copolymers." *Macromolecules*, **19**, 2501 (1986).

Owens, J. N.; Gancarz, I. S.; Koberstein, J. T.; Russell, T. P. "Investigation of the Microphase Separation Transition in Low Molecular Weight Diblock Copolymers." *Macromolecules*, **22**, 3380 (1989).

Pennisi, R. W.; Fetters, L. J. "Preparation of Asymmetric Three-Arm Polybutadiene and Polystyrene Stars." *Macromolecules*, **21**, 1094 (1988).

Pitsikalis, M.; Pispas, S.; Mays, J. W.; Hadjichristidis, N. "Nonlinear Block Copolymer Architectures." *Adv. Polym. Sci.*, in press (1997).

Pochan, D. J.; Gido, S. P.; Pispas, S.; Mays, J. W. "Morphological Transitions in an $I_2S$ Simple Graft Block Copolymer: From Folded Sheets to Folded Lace to Randomly Oriented Worms at Equilibrium." *Macromolecules*, **29**, 5099 (1996)

Pochan, D. J.; Gido, S. P.; Pispas, S.; Mays, J. W.; Ryan, A. J.; Fairclough, J. P. A.; Hamley, I. W.; Terrill, N. J. "Morphologies of Microphase-Separated $A_2B$ Simple Graft Copolymers." *Macromolecules*, **29**, 5091 (1996).

Pochan, D. J.; Gido, S. P.; Zhou, J.; Mays, J. W.; Whitmore, M. D.; Ryan, A. J. "Microphase Separated Morphology of a Conformationally Asymmetric Block Copolymer." *J. Polym. Sci. Polym. Phys.*, in press, (1997).

Pochan, D. J.; Lee, C.; Gido, S. P.; Mays, J. W.; Hadjichristidis, N. "Morphologies of Simple Graft Binary Blends." in preparation.

Quirk, R. P.; Ignatz-Hoover, F. "Living Coupling Agents. Rational Synthesis of Heteroarm Star-Branched Polymers." In: *Recent Advances in Anionic Polymerization*; T. E. Hogen-Esch and J. Smid, Eds.; Elsevier: New York, 1987; 393.

Quirk, R. P.; Kinning, D. J.; Fetters, L. J. In: *Comprehensive Polymer Science: The Synthesis, Characterization, Reactions, and Applications of Polymers. Specialty Polymers & Polymer Processing*; S. L. Aggarwal, Ed.; Pergamon: Oxford, 1989; Vol. 7; 1.

Radzilowski, L. H.; Wu, J. L.; Stupp, S. I. "Self-Assembly of Rod-Coil Diblock Copolymers." *Macromolecules*, **26**, 879 (1993).

Rangarajan, P.; Register, R. A.; Fetters, L. J.; Bras, W.; Naylor, S.; Ryan, A. J. "Crystallization of a Weakly Segregated Polyolefin Diblock Copolymer." *Macromolecules*, **28**, 4932 (1995).

Riess, G.; Schlienger, M.; Marti, S. "New Morphologies in Rubber Modified Polymers." *J. Macromol. Sci., Phys.*, **B17**, 355 (1980).

Roovers, J.; Toporowski, P. "Synthesis of High Molecular Weight Ring Polystyrenes." *Macromolecules*, **16**, 843 (1983).

Rounds, N. A. University of Akron: Ph.D. Dissertation, 1970.

Ryan, A. J.; Hamley, I. W.; Bras, W.; Bates, F. S. "Structure Development in Semicrystalline Diblock Copolymers Crystallizing from the Melt." *Macromolecules*, **28**, 3860 (1995).

Sakurai, S.; Kawada, H.; Hashimoto, T.; Fetters, L. J. "Thermoreversible Morphology Transition between Spherical and Cylindrical Microdomains of Block Copolymers." *Macromolecules*, 26, 5796 (1993).

Semenov, A. N. "Contribution to the Theory of Microphase Layering in Block Copolymer Melts." *Sov. Phys. JETP*, **61**, 7331 (1985).

Shibayama, M.; Hasegawa, H.; Hashimoto, T.; Kawai, H. "Microdomain Structure of an ABC Type Triblock Polymer of Polystyrene-Poly-(4-vinylbenzyl)-di-methylamine-)-Polyisoprene Cast from Solutions." *Macromolecules*, **15**, 274 (1982).

Shinozaki, A.; Jasnow, D.; Balazs, A. C. "Microphase Separation in Comb Copolymers." *Macromolecules*, **27**, 2496 (1994).

Stickler, M.; Panke, D.; Wunderlich, W. "Solution Properties of Poly(methylmethacrylate) in Methyl Methacrylate. 1. Viscosities from the Dilute to the Concentrated Regimes." *Makromol.* Chem., **188**, 2651 (1987).

Stockmayer, W. H. "Some Remarks on Excluded Volume and on Intrinsic Viscosity Plots" *Br. Polym. J.*, 9, 89 (1977).

Storey, R. F.; Chisholm, B. J.; Masse, M. A. "Morphology and Physical Properties of Poly(styrene-*b*-isobutylene-*b*-styrene) Block Copolymers." *Polymer*, **37**, 2925 (1996).

Thomas, E. L.; Alward, D. B.; Kinning, D. J.; Martin, D. C.; Handlin Jr., D. L.; Fetters, L. J. "Ordered Bicontinuous Double-Diamond Structure of Star Block Copolymers: A New Equilibrium Microdomain Morphology." *Macromolecules*, **19**, 2197 (1986).

Thomas, E. L.; Kinning, D. J.; Alward, D. B.; Henkee, C. S. "Ordered Packing Arrangements of Spherical Micelles of Diblock Copolymers in Two and Three Dimensions." *Macromolecules*, **20**, 2934 (1987).

Tselikas, Y.; Iatrou, H.; Hadjichristidis, N.; Liang, K. S.; Mohanty, K.; Lohse, D. J. "Morphology of Miktoarm Star Block Copolymers of Styrene and Isoprene." *J. Chem. Phys.*, **105**, 2456 (1996).

Tsitsilianis, C.; Ghaumont, P.; Rempp, P. "Synthesis and Characterization of Hetero-Arm Star Copolymers." *Makromol. Chem.*, 191, 2319 (1990).

Vavasour, J. D.; Whitmore, M. D. "Self-Consistent Mean Field Theory of the Microphases of Diblock Copolymers." *Macromolecules*, **25**, 5477 (1992).

Vavasour, J. D.; Whitmore, M. D. "Self-Consistent Field Theory of Block Copolymers with Conformational Asymmetry." *Macromolecules*, **26**, 7070 (1993).

Vlahos, C.; Horta, A.; Hadjichristidis, N.; Freire, J. "Monte Carlo Simulations of the Conformations of $A_2B$ and $A_3B$ Miktoarm Star Copolymers in Dilute Solution." *Macromolecules*, **28**, 1500 (1995).

Vlahos, C.; Tselikas, Y.; Hadjichristidis, N.; Roovers, J.; Rey, A.; Freire, J. "Conformation of $A_2B$ and $A_3B$ Miktoarm Star Copolymers in Dilute Solutions." *Macromolecules*, **29**, 5599 (1996).

Winey, K. I.; Thomas, E. L.; Fetters, L. J. "Isothermal Morphology Diagrams for Binary Blends of Diblock Copolymer and Homoploymer." *Macromolecules*, **25**, 2645 (1992).

Winey, K. I.; Thomas, E. L.; Fetters, L. J. "Swelling a Lamellar Diblock Copolymer with Homopolymer: Influences of Homopolymer Concentration and Molecular Weight." *Macromolecules*, **24**, 6182 (1991).

Yamakawa, H. *Modern Theory of Polymer Solutions*; Harper and Row: New York, 1971; Ch. 7.

Yanagase, A.; Ito, M.; Yamamoto, N.; Ishikawa, M. "Mechanism of Enhanced Impact Strength of Poly(vinylchloride) Modified by Acrylic Graft Copolymer." *J. Appl. Polym. Sci.*, **60**, 87 (1996).

Zhao, J.; Majumdar, B.; Schulz, M. F.; Bates, F. S.; Almdal, K.; Mortensen, K.; Hajduk, D. A.; Gruner, S. M. "Phase Behavior of Pure Diblocks and Binary Diblock Blends of Poly(ethylene)-poly(ethylethylene)." *Macromolecules*, **29**, 1204 (1996).

Zhong, X. F.; François, B. "Soluble Polystyrene-*b*-Poly(*p*-Phenylene) Block Copolymers Prepared from Polystyrene-*b*-Poly(1,3-Cyclohexadiene) Precursors. Study of the Aromatization Process. *Makromol. Chem.*, **192**, 2277 (1991).

Zimm, B. H. "Chain Molecule Hydrodynamics by the Monte-Carlo Method and the Validity of the Kirkwood-Riseman Approximation." *Macromolecules*, **13**, 592 (1980).